STUDIES ON NATURAL RAMAN OPTICAL ACTIVITY

by

Angelo Raymond Gargaro

A Thesis presented in

partial fulfilment for

the degree of Doctor of Philosophy

in the

Faculty of Science

of the

University of Glasgow

Chemistry Department

October 1991

ProQuest LLC.
789 East Eisenhower Parkway
P.O. Box 1346
Ann Arbor, MI 48106 – 1346

ACKNOWLEDGEMENTS

I am indebted to my supervisor Prof. L. D. Barron for his continual advice, help and encouragement throughout the course of this Ph.D. research.

I am also grateful to Dr. L. Hecht for his advice and help with both the theoretical and experimental aspects of Raman optical activity during the period of this research.

I would also like to thank Prof. P. L. Polavarapu and Mr. Z. Q. Wen for helpful discussions during the course of this research.

I am grateful to my family for putting up with me over the period of this research.

I also extend my gratitude to my many friends both inside and outside university who have made my Ph.D such a memorable experience.

Finally I wish to thank the Science and Engineering Research Council for financial support during the period of research.

CONTENTS

PREFACE

Vibrational optical activity (VOA) associated with the vibrational transitions of chiral molecules can be studied by two distinct experimental techniques: vibrational circular dichroism (VCD), the long wavelength extension of circular dichroism into the infrared, and Raman optical activity (ROA), the differential scattering of right and left circularly polarized electromagnetic radiation. No theoretical description exists to relate these two methods. Each technique therefore probes the stereochemistry of chiral molecules uniquely, hence they must be considered as complementary. In fact, vibrational bands which exhibit strong VCD intensity tend to show weak ROA intensity and vice versa.

Chapter one contains a brief historical review of VOA describing the two experimental techniques and their advantages and disadvantages with respect to one another. The most recent theoretical analysis of ROA is then reviewed and its relationship to the original theoretical description of ROA noted. The final section of chapter one deals with *ab initio* calculations of Raman and ROA intensities. The theory is described and practical aspects of its implementation are discussed.

In chapter two we describe the design of an entirely new instrument for the measurement of ROA spectra of biological molecules. The various components and their use are discussed and improvements over those used previously noted. The performance of this instrument is then compared with our previous ROA instruments and with the most recently reported ROA instrument from another laboratory.

The first experimental observations of forward scattered ROA are reported for trans-pinane and β-pinene in chapter three. The origin of the unexpected ROA intensity in the spectrum of β-pinene is ascribed by

general group theoretical arguments to isotropic scattering, which was previously thought to make a negligible contribution to the total ROA intensity.

The ROA of alanine as a function of pH is discussed in chapter four. A vibrational analysis is presented and origins of the ROA intensity suggested. This is compared with an *ab initio* calculation of the Raman and ROA intensities of alanine at neutral pH. Finally a vibrational analysis of alaninol is attempted based on the corresponding analysis for alanine.

Chapter five contains a vibrational analysis for serine, cysteine, valine and threonine derived from comparisons between their ROA spectra and other previously reported vibrational analyses based primarily on isotopic substitution data. The situation is more complex than in alanine due to possible contributions to the ROA intensity from different rotamers. The results are then used to explain the lack of ROA intensity in the spectrum of isoleucine.

In the final chapter we discuss the Raman and ROA spectra of proline and 4-hydroxyproline. These differ from the amino acids discussed previously on account of their five membered ring structure and their lack of an NH_3^+ group which we have identified as generating large ROA intensity in the spectra of the other amino acids we have studied. The use of proline and 4-hydroxyproline as a probe of peptide and protein structure is also discussed.

1 INTRODUCTION

1.1 Historical review of vibrational optical activity

A system is considered to exhibit natural optical activity if it responds differently to right and left circularly polarized electromagnetic radiation in the absence of external electromagnetic fields. A common manifestation of this phenomenon is a rotation of the plane of polarization of linearly polarized incident light; the optical rotation of the system [1]. All substances show induced optical activity in the presence of an externally applied magnetic field [2] and in special situations an electric field [3]. The microscopic origin of natural optical activity for optically active samples is molecular chirality (from the Greek *chir* meaning hand).

Natural optical activity has typically been associated with molecular *electronic* transitions that can be studied by optical rotatory dispersion (ORD) [4], the wavelength dependence of the rotation of linearly polarized electromagnetic radiation, and circular dichroism (CD) [4], the difference in the absorption for left and right circularly polarized electromagnetic radiation. CD is now preferred over ORD as a result of its more direct relationship to the properties of the specific states being excited in the transition and the development of high-sensitivity CD instrumentation [5].

However, both these techniques are limited to certain molecular situations: some hydrocarbons exhibit little optical rotation at certain wavelengths [6], thus restricting ORD measurements, while CD requires that a chromophoric transition, such as the $n \rightarrow \pi^*$ transition of a carbonyl group, for instance, exists in the region ~ 185-700 nm currently obtainable using commercial instrumentation and also shows a *Cotton*

effect, which is not always the case [7]. A Cotton effect is defined as the CD (together with the anomalous ORD which accompanies it) in the absorption region as shown in fig. 1.1 (adapted from ref. 8).

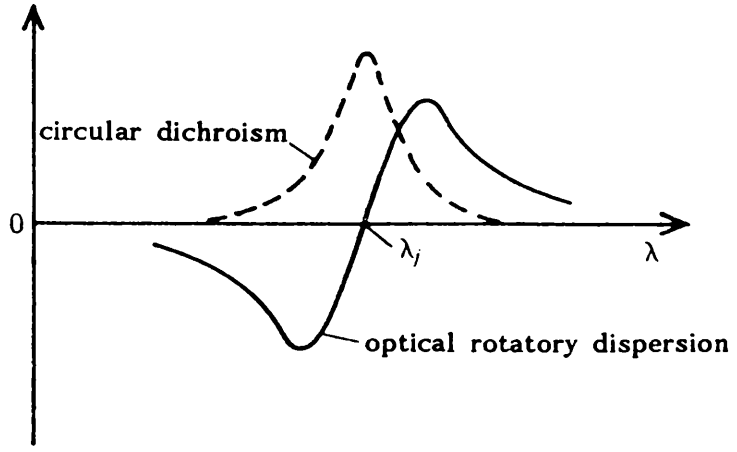

Fig. 1.1. Circular dichroism and anomalous optical rotatory dispersion in the region of an electronic absorption wavelength λ_j. The signs shown correspond to a positive Cotton effect.

The major constraint on the use of these chromophores is that by themselves they are inherently symmetric but become dissymmetric by a small chiral perturbation of their molecular environment. The chirality of the system therefore is probed only indirectly so that great care has to be exercised in the interpretation of CD spectra.

If a manifestation of optical activity existed for vibrational spectroscopy most of the above problems could be overcome since a vibrational spectrum contains bands associated with all parts of the molecule with better resolution and more straightforward methods of assignment (via group frequencies and normal coordinate analysis for example), and should thus provide more complete stereochemical information than either ORD or CD. Happily not one but two such phenomena can be measured experimentally: vibrational circular dichroism

(VCD), the long wavelength extension of CD into the infrared [5,9]; and natural Raman optical activity (ROA), the differential scattering of right and left circularly polarized radiation [8,10,11]. Both were observed in the solution phase at approximately the same time [12-15] and are complementary at the moment since ROA is best in the region 100-1800 cm^{-1} while VCD cannot, at present, be extended below ~ 650 cm^{-1} [16,17].

There are two possible experimental approaches to VCD. Historically it has been measured in the CH, OH and CD stretching regions (2600-3500 cm^{-1}) with dispersive spectrographs. However, the use of this type of instrument for the measurement of low frequency (800-1800 cm^{-1}) vibrations has been severely restricted by the necessity of completely changing the optics, detector, etc... several times in order to achieve complete spectral coverage and optimum instrument response. Fourier-transform (FT) VCD instruments, on the other hand, enable collection of the entire mid-infrared spectral region (800-1800 cm^{-1}) in one experiment. To date, only one FT-VCD spectrum has been reported in the CH stretching region due to artefact problems [18]. Therefore, at present, dispersive instruments are employed in the region 2600-3500 cm^{-1} while FT instruments are used for the region 800-1800 cm^{-1}.

ROA, by comparison, has given birth to a plethora of possible experimental strategies based on the use and measurement of circularly polarized radiation. The first, and until recently only, ROA experiment to be performed involved modulating the incident laser radiation between right and left circular polarization states [8,10-13]; this has been termed incident circular polarization (ICP) ROA. The experimentally observed ICP quantity is a dimensionless circular intensity difference (CID):

$$\Delta_\alpha = (I_\alpha^R - I_\alpha^L)/(I_\alpha^R + I_\alpha^L). \qquad (1.1)$$

The intensities I refer to the scattered radiation, the superscripts (R,L) denote corresponding states of circular polarization of the incident laser radiation and the subscript (α) refers to the state of linear polarization of the scattered radiation. An alternative experimental approach is to measure the intensity of the circularly polarized component of the scattered radiation. This experiment has been called scattered circularly polarized (SCP) ROA [8,19-24] with CID

$$\Delta^{\alpha} = (I_R^{\alpha} - I_L^{\alpha})/(I_R^{\alpha} + I_L^{\alpha}). \qquad (1.2)$$

The superscript (α) here refers to the state of linear polarization of the incident radiation. The possibility also arises of measuring both ICP and SCP ROA simultaneously. This has been termed dual circular polarization (DCP) ROA [21,24-27]. Two forms of DCP ROA are measurable: DCP_I where the measurement is of $I_R^R - I_L^L$, the in-phase combination of ICP and SCP; and DCP_{II} the out-of-phase combination of ICP and SCP where the measurement is of $I_R^L - I_L^R$. An analysis based on Stokes-Mueller calculus, within the original theory of ROA, suggested that ICP measured in a backscattering (180^0) geometry is the most favourable ROA experiment [26]. However, recent work has suggested that, within a more general theory of ROA [28], DCP_I measured in a backscattering geometry might be equally favourable since there is no isotropic contribution to the Raman intensity. Experimental results [24] appear to support this argument in terms of the quality of the ROA measured but not in terms of the speed of data acquisition. Polavarapu has proposed both ICP and SCP ROA measurements using an FT instrument [29,30] while Hecht and Nafie [31] have theoretically described experiments which involve the modulation of linearly polarized radiation, called linearly polarized (LP) ROA.

Originally the only ICP ROA measurement to be performed utilized a depolarized right-angle (90^0) scattering geometry [12,13] (achieved by setting the transmission axis of a polaroid analyser parallel to the scattering plane). Instrumental advances enabled the routine recording of total (without an analyser in the scattered beam) [32] and polarized (with the transmission axis of the analyser set perpendicular to the scattering plane) [33] 90^0 ROA spectra. Hecht and Barron [34] identified another possible experimental strategy based on 90^0 scattering termed 'magic-angle' ROA in which the transmission axis of the analyser is set at $\pm \sin^{-1}(\sqrt{2}/\sqrt{3}) \approx \pm 54.74^0$ to the scattering plane. In this experiment the contribution from the electric dipole-electric quadrupole ROA mechanism vanishes so that pure electric dipole-magnetic dipole ROA spectra can be measured (but leaving the isotropic part). Several years ago Hug [35] measured the first ICP ROA spectra using a backscattering (180^0) geometry, but unfortunately the preliminary data were destroyed by fire. Hecht *et al.* [36] subsequently remeasured backward scattered ICP ROA, using Hug's original experimental arrangement, based on the realization that higher signal-to-noise ratios (SNRs) can be achieved with a backscattering geometry. This scattering configuration is essential for the measurement of ROA of samples with high backgrounds such as aqueous solutions of biologically significant molecules. The optical arrangement employed for backscattering was easily modified to allow the collection of forward scattered ICP ROA [37]. Forward scattered ROA is the optimum experimental strategy for measuring isotropic ROA (*vide infra*).

Recently it has become possible, using sophisticated quantum chemical computer programs, to calculate from first principles both the VCD and ROA spectra of small molecules of small molecules, typically

with less than 50 electrons [38-40]. This opens up the possibility of determining the absolute configuration of chiral molecules without resort to semi-empirical methods, since the absolute configuration follows automatically with a high degree of confidence if there is extensive correlation between the theoretical and experimental spectra.

Rotational optical activity has been postulated by Salzman [41], Polavarapu [42] and Barron and Johnston [43]. However, it is expected that rotational optical activity will provide less stereochemical information than VOA since rotational transitions are associated with motions of the entire molecule rather than motions of specific parts of the molecule as in VOA.

I was directly involved in many aspects of the new era of backward scattered ICP ROA experiments on biologically relevant molecules [44-52] and also in the first forward ROA measurements [37]. This thesis concentrates primarily on Raman and ROA studies of amino acids, the molecular building blocks of peptides and proteins. Comparisons between the spectra are used to suggest a plausible vibrational analysis for the amino acids studied and to illuminate the origin of the ROA intensity in some of the observed Raman bands and to assist the interpretation of future detailed ROA spectroscopic investigations of peptides and proteins.

1.2 Theory

ROA was originally described theoretically by Barron and Buckingham [53]. The most widely employed version of this theory [54] uses a set of four Stokes parameters to characterize the intensity and polarization state of the scattered radiation. Attempts to use this theory for a systematic analysis of the artefacts which plague the ROA experiment (especially in 90^0), using the method of Stokes parameters, were restricted to the

effect of the cone of collection since the theory contained no information about the other optical components used in the experiment [55,56]. Subsequently Hecht *et al.* [26,57] developed the theory of ROA in terms of the phenomenological Stokes-Mueller calculus [58] which enabled the analysis to be extended to the complete optical train. An analysis of ICP ROA in terms of its dependence on the polar scattering angle has been performed for particular analyser orientations by Andrews [59]. His work suggests that it would be possible to separate the magnetic dipole and electric quadrupole contributions to the CID for measurements at different scattering angles. Hecht and Barron [26] then provided a more comprehensive analysis which lead to the discovery of 'magic-angle' ICP ROA [34]. Recently a general theory of ROA, which allows the direct calculation of the ROA intensities for all possible circularly polarized ROA experiments, has been presented [28]. This theory formulates the ROA intensities for isotropically averaged samples with explict dependence on unit polarization and propagation vectors for the detected and incident radiation, as well as in terms of the Stokes-Mueller calculus.

1.2.1 *Molecular scattering of polarized radiation*

The scattered electric field detected in the wave zone at a point d, at a distance R from the molecular origin which is large compared with the wavelength of the incident radiation, is given, within a semi-classical formalism [8,20], by

$$\tilde{E}^{d}_{\alpha} = \frac{\omega^2 \mu_0}{4\pi R} e^{i\omega(R/c-t)} (\tilde{a}_{\alpha\beta})_{mn} \tilde{E}^{i}_{\beta}, \qquad (1.3)$$

where μ_0, ω and c denote the magnetic permeability, the angular

frequency of the exciting radiation and the speed of light, respectively. A tilde (~) denotes a complex quantity and the superscripts d and i on the complex electric vector $\tilde{E}$ refer to the detected and incident radiation. The quantity $(\tilde{a}_{\alpha\beta})_{mn}$ is a general scattering tensor for a particular transition m←n between initial and final molecular states $|n\rangle$ and $|m\rangle$, with particular propagation directions for the incident and detected radiation characterized by the unit vectors $\underset{\sim}{n}^{i}$ and $\underset{\sim}{n}^{d}$:

$$(\tilde{a}_{\alpha\beta})_{mn} = (\tilde{\alpha}_{\alpha\beta})_{mn} + \frac{1}{c}\left\{\varepsilon_{\gamma\delta\beta} n^{i}_{\delta} (\tilde{G}_{\alpha\gamma})_{mn} + \varepsilon_{\gamma\delta\alpha} n^{d}_{\delta} (\tilde{\mathcal{G}}_{\gamma\beta})_{mn}\right.$$

$$\left. + \frac{1}{3} i\omega [\, n^{i}_{\gamma} (\tilde{A}_{\alpha\gamma\beta})_{mn} - n^{d}_{\gamma} (\tilde{\mathcal{A}}_{\beta\gamma\alpha})_{mn}]\right\}, \qquad (1.4)$$

with $\varepsilon_{\alpha\beta\gamma}$ denoting the third-rank antisymmetric unit tensor (Levi-Cività). $(\tilde{\alpha}_{\alpha\beta})_{mn}$ is the complex electric dipole-electric dipole transition polarizability (Raman) tensor, $(\tilde{G}_{\alpha\gamma})_{mn}$ and $(\tilde{\mathcal{G}}_{\gamma\beta})_{mn}$ are complex electric dipole-magnetic dipole transition optical activity (gyration) tensors, while $(\tilde{A}_{\alpha\gamma\beta})_{mn}$ and $(\tilde{\mathcal{A}}_{\beta\gamma\alpha})_{mn}$ are complex electric dipole-electric quadrupole transition optical activity tensors. The Roman ROA tensors above refer to oscillations of the induced electric dipole moment originating from magnetic dipole and electric quadrupole transitions of the molecules, while the script ROA tensors are associated with oscillations of the induced magnetic dipole and the electric quadrupole, respectively, arising from initial electric dipole transitions of the molecule.

The time-averaged intensity I of the scattered radiation is given by [28]

$$I(\tilde{e}^{d*}, \tilde{e}^{i}) \propto |\tilde{e}^{d*}_{\alpha} \tilde{E}^{d}_{\alpha}|^2 = 90K |\tilde{e}^{d*}_{\alpha} (\tilde{a}_{\alpha\beta})_{mn} \tilde{e}^{i}_{\beta}|^2, \qquad (1.5a)$$

with

$$K = \frac{1}{90}\left(\frac{\omega^2 \mu_0 \tilde{E}^{(0)}}{4\pi R}\right)^2, \qquad (1.5b)$$

where $\tilde{E}^{(0)}$ represents the magnitude of the electric field evaluated at the molecular origin and $\tilde{e}$ is a unit vector characterizing the polarization of the light wave.

Inserting eq. (1.4) into eq. (1.5a) and performing some mathematical manipulations yields [28]

$$I(\tilde{e}^{d*}, \tilde{e}^{i}) = 90K \{ \tilde{e}^{d*}_A \tilde{e}^{i}_B \tilde{e}^{d}_C \tilde{e}^{i*}_D l_{A\alpha} l_{B\beta} l_{C\gamma} l_{D\delta} \tilde{\alpha}_{\alpha\beta} \tilde{\alpha}^*_{\gamma\delta}$$

$$+ \frac{2}{c} \mathrm{Im}(\tilde{e}^{d*}_A \tilde{e}^{i}_B \tilde{e}^{d}_C \tilde{e}^{i*}_E \tilde{\alpha}_{\alpha\beta} [n^{i}_D (i\varepsilon_{\rho\delta\varepsilon} \tilde{G}^*_{\gamma\rho} + \frac{1}{3} \omega \tilde{A}^*_{\gamma\delta\varepsilon})$$

$$+ n^{d}_D (i\varepsilon_{\rho\delta\gamma} \tilde{G}^*_{\rho\varepsilon} - \frac{1}{3} \omega \tilde{A}^*_{\varepsilon\gamma\delta})]) l_{A\alpha} l_{B\beta} l_{C\gamma} l_{D\delta} l_{E\varepsilon} \}, \qquad (1.6)$$

where small Greek subscripts are used for molecule-fixed axes and capital Latin subscripts for space-fixed axes. $l_{A\alpha}$ are direction cosines from the space-fixed axes to the molecule-fixed axes. $(\tilde{\alpha}_{\alpha\beta})_{mn}$ etc... have been written as $\tilde{\alpha}_{\alpha\beta}$ etc... for economy in eq. (1.6). The Einstein summation convention is implied [8].

1.2.2 *Molecular property tensors*

Quantum mechanical expressions for the complex transition polarizability and optical activity tensors can be obtained from second-order time-dependent perturbation theory [20]. The complex transition polarizability is of the form [28]

$$(\tilde{\alpha}_{\alpha\beta})_{mn} = \frac{1}{\hbar} \sum_{j \neq n,m} \left(\frac{\langle m|\hat{\mu}_\alpha|j\rangle\langle j|\hat{\mu}_\beta|n\rangle}{\omega_{jn} - \omega + i\Gamma_j} + \frac{\langle m|\hat{\mu}_\beta|j\rangle\langle j|\hat{\mu}_\alpha|n\rangle}{\omega_{jm} + \omega + i\Gamma_j} \right), \qquad (1.7)$$

where a circumflex (^) denotes an operator, $|j\rangle$ represents a complex manifold of intermediate excited states, ω_{jn} is the angular transition frequency between molecular states j and n, Γ_j is the bandwidth of the jth excited state, $\hat{\mu}_\alpha$ is the electric dipole operator and Greek subscripts are used to refer to Cartesian directions in the molecular frame. The corresponding optical activity transition tensors can be defined by appropriate substitution of $\hat{\mu}_\alpha$ with $\hat{m}_\alpha$, the magnetic dipole operator, or $\hat{\Theta}_{\alpha\beta}$, the electric quadrupole operator, by means of the following conversion relations:

$$(\tilde{G}_{\alpha\beta})_{mn} \qquad \hat{\mu}_\beta \rightarrow \hat{m}_\beta \,, \tag{1.8a}$$

$$(\tilde{\mathcal{G}}_{\alpha\beta})_{mn} \qquad \hat{\mu}_\alpha \rightarrow \hat{m}_\alpha \,, \tag{1.8b}$$

$(\tilde{\alpha}_{\alpha\beta})_{mn}$ = by

$$(\tilde{A}_{\alpha\beta\gamma})_{mn} \qquad \hat{\mu}_\beta \rightarrow \hat{\Theta}_{\beta\gamma} \,, \tag{1.8c}$$

$$(\tilde{\mathcal{A}}_{\gamma\alpha\beta})_{mn} \qquad \hat{\mu}_\alpha \rightarrow \hat{\Theta}_{\alpha\beta} \text{ and } \hat{\mu}_\beta \rightarrow \hat{\mu}_\gamma \,. \tag{1.8d}$$

The electric dipole, magnetic dipole and electric quadrupole operators are defined as the following sums over all molecular particles i with mass m_i and electric charge e_i [8]:

$$\hat{\mu}_\alpha = \sum_i e_i r_{i\alpha} \,, \tag{1.9a}$$

$$\hat{m}_\alpha = \frac{1}{2} \sum_i \frac{e_i}{m_i} \varepsilon_{\alpha\beta\gamma} r_{i\beta} p_{i\gamma} \,, \tag{1.9b}$$

$$\hat{\Theta}_{\alpha\beta} = \frac{1}{2} \sum_i e_i (3 r_{i\alpha} r_{i\beta} - r_i^2 \delta_{\alpha\beta}) \,, \tag{1.9c}$$

where r_i and p_i are the position and linear momentum vectors of the ith charged particle, respectively and $\delta_{\alpha\beta}$ denotes the second rank unit

symmetric tensor (Kronecker delta).

1.2.3 *Circular intensity differences*

The ROA observable is the difference in the intensity of scattered radiation in right versus left circular polarization states in both the incident and scattered radiation fields [28]:

$$\Delta I = I\left(\tilde{e}^{d*}, \tilde{e}^{i}\right) - I\left(\tilde{e}^{d}, \tilde{e}^{i*}\right), \tag{1.10}$$

which, using eq. (1.6), can be written as

$$\Delta I = \frac{360K}{c}\,\mathrm{Im}\left\{ \tilde{\alpha}_{\alpha\beta}\left(\tfrac{1}{3}i\omega\tilde{A}^{*}_{\gamma\delta\varepsilon} - \varepsilon_{\rho\delta\varepsilon}\tilde{G}^{*}_{\gamma\rho}\right)\mathrm{Im}\left(\tilde{e}^{d*}_{A}\tilde{e}^{i}_{B}\tilde{e}^{d}_{C}n^{i}_{D}\tilde{e}^{i*}_{E}\right)\right.$$

$$\left. - \tilde{\alpha}_{\alpha\beta}\left(\tfrac{1}{3}i\omega\tilde{A}^{*}_{\varepsilon\gamma\delta} + \varepsilon_{\rho\delta\gamma}\tilde{G}^{*}_{\rho\varepsilon}\right)\mathrm{Im}\left(\tilde{e}^{d*}_{A}\tilde{e}^{i}_{B}\tilde{e}^{d}_{C}n^{d}_{D}\tilde{e}^{i*}_{E}\right)\right\}\langle 1_{A\alpha}1_{B\beta}1_{C\gamma}1_{D\delta}1_{E\varepsilon}\rangle, \tag{1.11}$$

where the angular brackets indicate isotropic averaging. $(\tilde{\alpha}_{\alpha\beta})_{mn}$ etc ... have been written as $\tilde{\alpha}_{\alpha\beta}$ etc ... for simplicity in eq. (1.11) and all following equations. Using the relationships given on pages 448 and 464 of ref. 28 eq. (1.11) can be written in terms of isotropic and anisotropic tensor invariants as follows

$$\begin{aligned}
\Delta I = \frac{8K}{c}\Big\{ & \mathrm{Im}\left(\tilde{P}_1 - 2\tilde{P}_5\right)\left[\, 9\alpha G + 2\beta_s(\tilde{G})^2 + 2\beta_a(\tilde{G})^2 \,\right] \\
& + \mathrm{Im}\left(\tilde{P}_3 + \tilde{P}_5\right)\left[\, -9\alpha G + \beta_s(\tilde{G})^2 + 3\beta_a(\tilde{G})^2 - \beta_s(\tilde{A})^2 + \beta_a(\tilde{A})^2 \,\right] \\
& + \mathrm{Im}\left(\tilde{P}_4 + \tilde{P}_5\right)\left[\, -9\alpha G + 4\beta_s(\tilde{G})^2 - 2\beta_a(\tilde{G})^2 + 4\beta_a(\tilde{A})^2 \,\right] \\
& + \mathrm{Im}\left(\tilde{P}_8 - 2\tilde{P}_{13}\right)\left[\, -9\alpha\tilde{G} - 2\beta_s(\tilde{G})^2 - 2\beta_a(\tilde{G})^2 \,\right] \\
& + \mathrm{Im}\left(\tilde{P}_{10} + \tilde{P}_{13}\right)\left[\, 9\alpha\tilde{G} - \beta_s(\tilde{G})^2 - 3\beta_a(\tilde{G})^2 - \beta_s(\tilde{A})^2 - \beta_a(\tilde{A})^2 \,\right] \\
& + \mathrm{Im}\left(\tilde{P}_{13} + \tilde{P}_{14}\right)\left[\, 9\alpha\tilde{G} - 4\beta_s(\tilde{G})^2 + 2\beta_s(\tilde{G})^2 - 2\beta_s(\tilde{A}) \,\right]\Big\},
\end{aligned} \tag{1.12}$$

where αG and $\alpha\tilde{G}$, $\beta_s(\tilde{G})^2$ etc ... , $\beta_a(\tilde{G})^2$ etc ... refer to isotropic, symmetric anisotropic and antisymmetric anisotropic tensor invariants, respectively. Explicit expressions for these and the common polarization factors $\tilde{P}_k$ are given in ref. 28. These polarization factors are dependent on the polarization state of the radiation and the scattering geometry.

1.2.4 *Circular intensity sums*

A similar treatment to that given above for the CID yields the circular intensity sum (CIS) [28]

$$I = I\left(\tilde{e}^{d*}, \tilde{e}^{i}\right) + I\left(\tilde{e}^{d}, \tilde{e}^{i*}\right), \tag{1.13}$$

$$I = 4K\Big\{ 3\beta_s(\tilde{\alpha})^2 + 5\beta_a(\tilde{\alpha})^2 + P_{15}\left[3\beta_s(\tilde{\alpha})^2 - 5\beta_a(\tilde{\alpha})^2 \right] + P_{16}\left[45\alpha^2 - 2\beta_s(\tilde{\alpha})^2 \right] \Big\}, \tag{1.14}$$

where α^2, $\beta_s(\tilde{\alpha})^2$ and $\beta_a(\tilde{\alpha})^2$ are isotropic, symmetric anisotropic and antisymmetric anisotropic tensor invariants. Explicit expressions for these tensors are given in ref. 28.

1.2.5 *ICP ROA measurements in backscattering*

The circular intensity difference and circular intensity sum given above by eqs. (1.12) and (1.14) are completely general in the sense that by appropriate substitution for $\tilde{P}_k$ they apply to all possible CP ROA modulation techniques and scattering geometries. For the purpose of this work we will refer to ICP in a backscattering geometry, since most of the spectra shown here were recorded using this experimental configuration, and so only this result will be given in detail here:

$$I_u^R(180^0) - I_u^L(180^0) = \frac{8K}{c}\Big\{ 45\alpha G + 7\beta_s(\tilde{G})^2 + 5\beta_a(\tilde{G})^2 + \beta_s(\tilde{A}) - \beta_a(\tilde{A})^2 + 45\alpha\tilde{G} - 5\beta_s(\tilde{G})^2 + 5\beta_a(\tilde{G})^2 + 3\beta_s(\tilde{A})^2 - \beta_a(\tilde{A})^2\Big\}, \quad (1.15a)$$

and

$$I_u^R(180^0) + I_u^L(180^0) = 4K\Big\{ 45\alpha^2 + 7\beta_s(\tilde{\alpha})^2 + 5\beta_a(\tilde{\alpha})^2 \Big\}, \quad (1.15b)$$

where u denotes unpolarized scattering radiation. The interested reader is referred to ref. 28 for the results at other scattering geometries.

1.2.6 *Approximations-the Rayleigh limit*

In the limit of non-resonant ($\Gamma_j \to 0$) Rayleigh scattering (m=n) the following approximate relationships can be deduced from eqs. (1.7) and (1.8) [20]:

$$\tilde{\alpha}_{\alpha\beta} \approx \tilde{\alpha}^*_{\beta\alpha}, \quad (1.16a)$$

$$\tilde{G}_{\alpha\beta} \approx \tilde{G}^*_{\beta\alpha} \text{ and } \tilde{G}_{\alpha\beta} \approx \tilde{G}^*_{\beta\alpha}, \quad (1.16b)$$

$$\tilde{A}_{\alpha\beta\gamma} \approx \tilde{A}^*_{\alpha\beta\gamma} \text{ and } \tilde{A}_{\alpha\beta\gamma} \approx \tilde{A}^*_{\alpha\beta\gamma}. \quad (1.16c)$$

Since in this limit the polarizability is real it becomes symmetric on account of eq. (1.16a). The antisymmetric contribution to the CIS as given by eq. (1.15b) therefore vanishes identically. The antisymmetric optical activity tensor invariants $\beta_a(\tilde{G})^2$ etc ... also vanish since they all contain contributions from $(\tilde{\alpha}_{\alpha\beta})^a_{nn}$. The following relationships are also valid [27], omitting the subscript s since a distinction between symmetric and

antisymmetric parts becomes meaningless:

$$\alpha G = - \alpha G , \tag{1.17a}$$

$$\beta(\tilde{G})^2 = - \beta(\tilde{G})^2 , \tag{1.17b}$$

$$\beta(\tilde{A})^2 = \beta(\tilde{A})^2. \tag{1.17c}$$

Consequently the CID and CIS given by eqs. (1.15a) and (1.15b) reduce to

$$I_u^R(180^0) - I_u^L(180^0) = \frac{32K}{c} \left\{ 3\beta(\tilde{G})^2 + \beta(\tilde{A})^2 \right\}, \tag{1.18a}$$

$$I_u^R(180^0) + I_u^L(180^0) = 4K \left\{ 45\alpha^2 + 7\beta(\tilde{\alpha})^2 \right\}. \tag{1.18b}$$

The superscript tildes may be dropped from the tensors since only the imaginary part of G (designated by a prime) and the real parts of α and A are non-zero. Eqs. (1.18a) and (1.18b) may now be written as

$$I_u^R(180^0) - I_u^L(180^0) = \frac{32K}{c} \left\{ 3\beta(G')^2 + \beta(A)^2 \right\} , \tag{1.19a}$$

$$I_u^R(180^0) + I_u^L(180^0) = 4K \left\{ 45\alpha^2 + 7\beta(\alpha)^2 \right\} , \tag{1.19b}$$

which is an equivalent result to that obtained using the original formulation of ROA by Barron and Buckingham [8]. Explicit expressions for the tensor invariants are, within the original theory:

$$\alpha = \frac{1}{3} \alpha_{\alpha\alpha} = \frac{1}{3} (\alpha_{XX} + \alpha_{YY} + \alpha_{ZZ}) , \tag{1.20a}$$

$$\beta(\alpha)^2 = \frac{1}{2} (3\alpha_{\alpha\beta}\alpha_{\alpha\beta} - \alpha_{\alpha\alpha}\alpha_{\beta\beta})$$

$$= \frac{1}{2}[(\alpha_{XX} - \alpha_{YY})^2 + (\alpha_{XX} - \alpha_{ZZ})^2 + (\alpha_{YY} - \alpha_{ZZ})^2 + 6(\alpha_{XY}^2 + \alpha_{XZ}^2 + \alpha_{YZ}^2)], \quad (1.20b)$$

$$G' = \frac{1}{3} G'_{\alpha\alpha} = \frac{1}{3} (G'_{XX} + G'_{YY} + G'_{ZZ}), \quad (1.20c)$$

$$\beta(G')^2 = \frac{1}{2} (3\alpha_{\alpha\beta} G'_{\alpha\beta} - \alpha_{\alpha\alpha} G'_{\beta\beta})$$
$$= \frac{1}{2} \{(\alpha_{XX} - \alpha_{YY})(G'_{XX} - G'_{YY}) + (\alpha_{XX} - \alpha_{ZZ})(G'_{XX} - G'_{ZZ})$$
$$+ (\alpha_{YY} - \alpha_{ZZ})(G'_{YY} - G'_{ZZ}) + 3[\alpha_{XY}(G'_{XY} + G'_{YX}) + \alpha_{XZ}(G'_{XZ} + G'_{ZX})$$
$$+ (\alpha_{YZ}(G'_{YZ} + G'_{ZY})]\}, \quad (1.20d)$$

$$\beta(A)^2 = \omega\alpha_{\alpha\beta}\varepsilon_{\alpha\gamma\delta}A_{\gamma\delta\beta}$$
$$= \frac{1}{2} \omega\{(\alpha_{YY} - \alpha_{XX})A_{ZXY} + (\alpha_{XX} - \alpha_{ZZ})A_{YZX} + (\alpha_{ZZ} - \alpha_{YY})A_{XYZ}$$
$$+ \alpha_{XY}(A_{YYZ} - A_{ZYY} + A_{ZXX} - A_{XXZ})$$
$$+ \alpha_{XZ}(A_{YZZ} - A_{ZZY} + A_{XXY} - A_{YXX})$$
$$+ \alpha_{YZ}(A_{ZZX} - A_{XZZ} + A_{XYY} - A_{YYX})\}. \quad (1.20e)$$

These differ from the expressions given in ref. 8 where some of the terms listed above were inadvertently left out.

1.3 *Ab initio* Raman optical activity

1.3.1 *Introduction*

Quantum mechanical methods for the calculation of vibrational Raman spectra are now routinely implemented by evaluating the polarizability derivatives $(\partial\alpha_{\alpha\beta}/\partial Q)_0$ using the analytical expressions given in refs. 60 and 61, where Q refers to the normal coordinates . Calculations of ROA intensities, however, also require evaluation of the electric dipole-magnetic dipole optical activity tensor $G'_{\alpha\beta}$ and the electric

dipole-electric quadrupole optical activity tensor $A_{\alpha\beta\gamma}$ and their derivatives with respect to normal coordinates. Amos [62,63] has theoretically described and implemented a procedure for calculating these tensors and their derivatives in the CADPAC program. However, since it is not possible to evaluate $G'_{\alpha\beta}$ (and $A_{\alpha\beta\gamma}$ *vide infra*) analytically at the present time, they must be calculated numerically. This places restrictions on the basis set size and on the size of molecules for which *ab initio* ROA calculations can be currently performed [40]. Several calculations [40,49,51,64-66] of the Raman and ROA intensities of small molecules are now available with encouraging preliminary results.

1.3.2 *Theory of ab initio ROA*

The quantum mechanical expression for the polarizability has been given by eq. (1.7). However, we will use the notation of ref. 40 in the following sections since this conforms to the original notation used by Amos [62]. The polarizability is therefore [40]

$$\alpha_{\alpha\beta} = \frac{2}{\hbar} \sum_{j\neq 0} \frac{\omega_{j0}}{\omega_{j0}^2 - \omega^2} \mathrm{Re}\left(\langle 0|\mu_\alpha|j\rangle\langle j|\mu_\beta|0\rangle\right), \tag{1.21}$$

where $\omega_{j0} = (E_j - E_0)/\hbar$ with E_j and E_0 denoting the energies of the jth and ground state respectively. In the non-resonant case, $\omega_{j0} >> \omega$, eq. (1.21) reduces to

$$\alpha_{\alpha\beta} = 2 \sum_{j\neq 0} \frac{\langle 0|\mu_\alpha|j\rangle\langle j|\mu_\beta|0\rangle}{E_j - E_0} . \tag{1.22}$$

Eq. (1.22) can be evaluated using unperturbed molecular orbitals φ_k^0 and their first order changes in the presence of an electric field $\varphi'_k(F_\alpha)$ as follows [62]:

$$\alpha_{\alpha\beta} = 4 \sum_{k} \langle \varphi_k^0 | \mu_\alpha | \varphi_k'(F_\beta) \rangle . \qquad (1.23)$$

The required derivatives with respect to normal coodinates can then be evaluated using the expressions given in refs. 60 and 61. The electric dipole-electric quadrupole optical activity tensor $A_{\alpha\beta\gamma}$ is, after simplification in the non-resonant limit

$$A_{\alpha\beta\gamma} = 2 \sum_{j \neq 0} \frac{\langle 0|\mu_\alpha|j\rangle\langle j|\Theta_{\beta\gamma}|0\rangle}{E_j - E_0} , \qquad (1.24)$$

and is evaluated [62] as

$$A_{\alpha\beta\gamma} = 4 \sum_{k} \langle \varphi_k^0 | \Theta_{\beta\gamma} | \varphi_k'(F_\alpha) \rangle . \qquad (1.25)$$

This follows directly from the conversion relations given in eqs. (1.8). In principle, since the evaluation procedure is similar, $(\partial A_{\alpha\beta\gamma}/\partial Q)_0$ can be evaluated using the same analytical methods as $(\partial \alpha_{\alpha\beta}/\partial Q)_0$; however, no commercial software to implement this calculation exists at the present time.

Similarly, the electric dipole-magnetic dipole optical activity tensor $G'_{\alpha\beta}$ can be written as [62]

$$\omega^{-1} G'_{\alpha\beta} = -2\hbar \sum_{j=0} \frac{\mathrm{Im}(\langle 0|\mu_\alpha|j\rangle\langle j|m_\beta|0\rangle)}{E_j - E_0} . \qquad (1.26)$$

It has been shown [62], that in the static limit $\omega \to 0$, eq. (1.26) can be evaluated to give

$$\omega^{-1} G'_{\alpha\beta} = -4\hbar \sum_{k} \mathrm{Im}(\langle \varphi_k'(F_\alpha) | \varphi_k'(B_\beta) \rangle), \qquad (1.27)$$

where $\varphi'_k(B_\beta)$ are the first order changes of the molecular orbitals in the presence of a magnetic field perturbation. Analytical methods for evaluating $(\partial G'_{\alpha\beta}/\partial Q)_0$ are not yet available and it must be obtained numerically by computing $G'_{\alpha\beta}$ at the equilibrium and displaced geometries, in the static limit.

1.3.3 *Ab initio calculations of ICP ROA in a backscattering geometry*

The normalised CID in a backscattering geometry is, within the original theory of ROA [8], given by:

$$\Delta(180^0) = \frac{48\left[\beta(G')^2 + \frac{1}{3}\beta(A)^2\right]}{2c\left[45\alpha^2 + 7\beta(\alpha)^2\right]} . \qquad (1.28)$$

This is necessary since the only *ab initio* calculations so far performed have been within the original theory. It is the transition tensor versions of these polarizability and optical activity tensors that must be used in Raman and ROA intensity calculations. At transparent frequencies Raman scattering is normally formulated using Placzek's approximation, in which quantities such as $(\hbar/2\omega_p)(\partial\alpha_{\alpha\beta}/\partial Q)_0$ must be evaluated to give the transition polarizability for a fundamental vibrational transition associated with the normal coordinate Q [8]. The *ab initio* ROA parameters are obtained by evaluating $\alpha_{\alpha\beta}$, $G'_{\alpha\beta}$ and $A_{\alpha\beta\gamma}$ at their equlibrium geometry and at geometries displaced by 0.005 Å along each atomic coordinate using the CADPAC program [63]. Comparisons can then be made with respect to the intensity and sign of the theoretical and experimental ROA bands. Such a procedure will be illustrated for alanine in chapter 4.

2 THE ROA INSTRUMENT

2.1 Introduction

It has been known for over a decade [35] that multichannel ROA instruments offer superior performance, in terms of the speed of data acquisition, than the conventional scanning spectrometers which were first used to measure ROA. The normal detectors employed in these scanning instruments were photo-multiplier tubes. The multichannel instruments, on the other hand, were typically equipped with intensified photo-diode arrays as light detectors [10,11,21,22,32,67,68]. These intensified photo-diode arrays are in the process of being replaced by spectroscopic grade cooled charge-coupled devices (CCDs), which have been identified as almost ideal Raman detectors for low-light level applications [69,70] due to their high quantum efficiency (ca. 80% for a backthinned back illuminated CCD compared with ~ 8% for an intensified photo-diode array) and their extremely low read-out noise and dark current at lower temperatures. These excellent performance characteristics make them also very attractive for use in ROA spectroscopy. It has been demonstrated that a CCD coupled to a high-efficiency monochromator plus an electro-optic modulator in the incident laser beam comprises an almost ideal ROA instrument [37,44-52,71]. Another ROA instrument equipped with a CCD but with a different modulation technique has also been reported [23,24,27]. At the same time recent analyses based on either the general ROA theory [28] or the original ROA theory [26], of all possible CP ROA experiments have indicated that ICP in a backscattering geometry is a particularly favourable experiment for measuring ROA. We therefore decided to design and construct a completely new instrument, optimized for the measurement of backscattered ICP ROA, especially of biologically

significant molecules, comprising a high luminosity f/4.1 single stage spectrograph and a backthinned CCD [52].

2.2 Optical layout

The optical layout of the instrument is shown in fig. 2.1. The incident laser radiation from a continuous wave Argon ion laser (L) operating at 514.5 nm (Spectra-Physics, model 2016-045 *stabilite*®) passes through a calcite Glan-Taylor polarizer (GTP) (Leysop, model GT12) which ensures that the input laser radiation is almost completely linearly polarized.

Following this polarizer is an electro-optic modulator (EOM), discussed separately later, which switches the incident laser radiation between right and left circular polarization states. The incident laser beam is then focused directly into the sample by a 150 mm focal length plano-convex synthetic fused silica lens (L1) (Melles Griot, model 01 LQP 013). The sample is held in a spectrosil quartz cell (Optiglass) (SC), with an internal cross-section of 5×5 mm, by a table type YZΘyΘz mount (Micro-Controle).

The backscattering arrangement is based on the usual mirror 'with a hole' idea (an alternative approach using a right-angle prism to reflect the laser light to the sample along the backscattering axis has also been implemented [24,27]). The cone of backscattered Raman light passes through a Lyot depolarizer (LD) (Leysop), consisting of two linearly birefringent calcite crystals of 2:1 thickness ratio whose optic axes are orientated at 45^0 to each other, and is then collimated by a 25 mm focal length symmetric-convex synthetic fused silica lens (L2) (Melles Griot, model 01 LQD 001) onto an elliptical mirror (EM) orientated at 45^0 to the incident laser beam. The presence of the Lyot, which depolarizes the

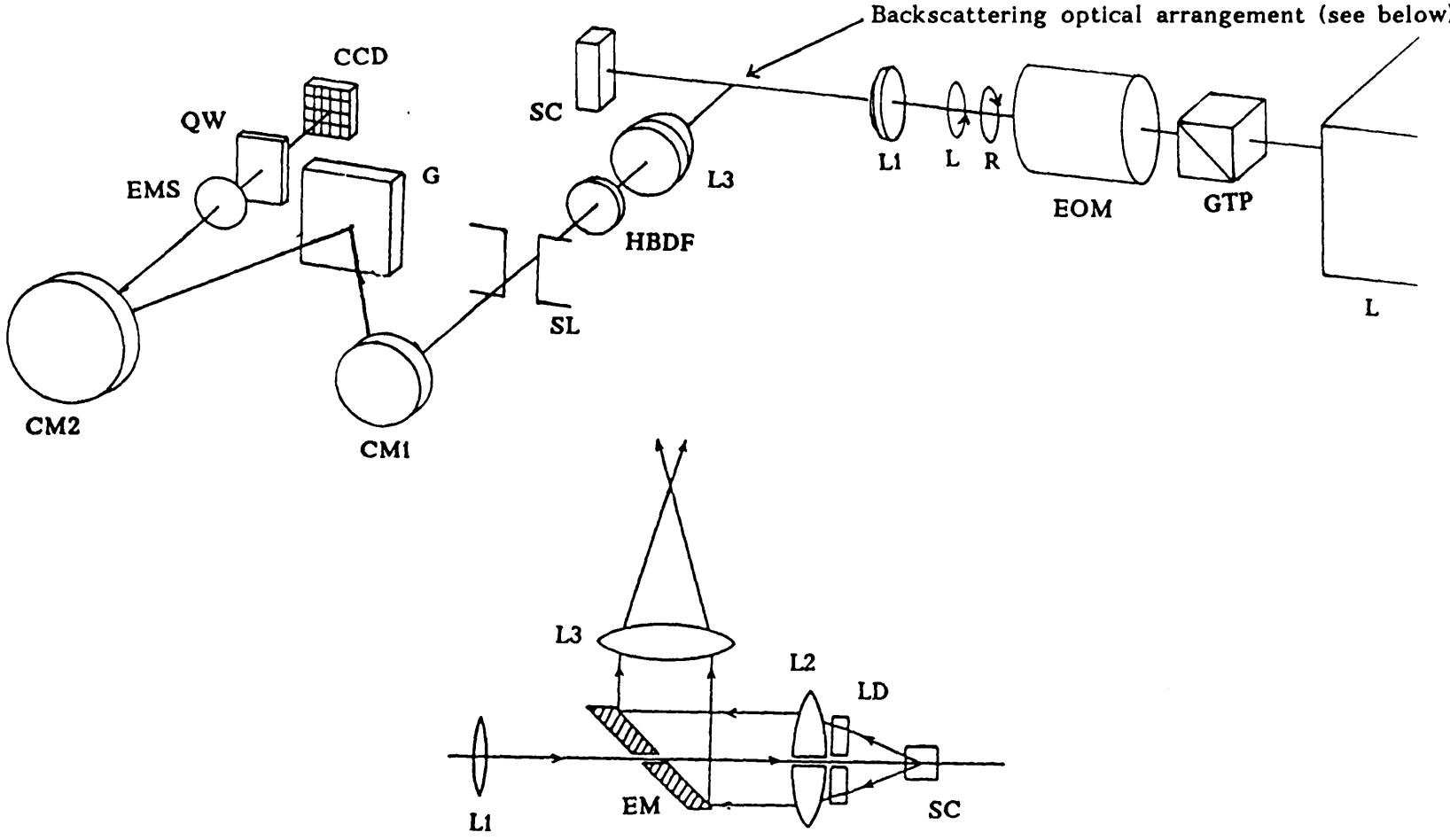

Fig. 2.1. The optical layout of the Glasgow ROA instrument.

backscattered Raman light, is essential in this arrangement if ROA spectra are to be obtained since the mirror would otherwise introduce polarization artefacts. The reflected light from this mirror is focused to a point by a 38 mm focal length fused silica lens (L3) (Optical Works Limited) and collected by a high quality 84.8 mm, focal length f/4.1, camera lens (CL) (Carl Zeiss Planar T). This light is then focused through a holographic Bragg diffraction filter (HBDF) (Physical Optics Corporation) [72,73]. This reduces the intensity of the unshifted Rayleigh band and allows measurement of Raman spectra to about 150 cm^{-1} in neat organic liquids and ~ 500 cm^{-1} in aqueous solutions. The light then passes through the vertical axial entrance slit (SL) of a 246.7 mm focal length f/4.1 single-stage in-plane assymmetric Czerny-Turner spectrograph (Jobin Yvon HR 250S).

Inside the spectrograph the Raman light is collected by a concave circular collimating mirror (CM1), 60 mm in diameter, which deflects the Raman light onto a quadratic (58×58 mm^2) holographic 1200 grooves/mm ion etched grating (G) blazed at 630 nm. The efficiency of this grating is approximately 58% at 525 nm for non polarized light. The dispersed light is then collected by a 85 mm diameter concave camera mirror (CM2) which focuses the dispersed light through an electro-mechanical shutter (EMS) and a quartz window (QW) onto the CCD chip (CCD). The CCD camera is placed such that the chip is directly in the focal plane of the instrument by means of a mounting flange at the axial exit port of the spectrograph.

2.3 The polarization modulation system

As mentioned earlier, the polarization state of the incident laser beam is switched between right and left circular by a specially modified

Electro Optic Developments (EOD) model 850-16 electro-optic modulator. The major changes between this modulator and the standard 850-16 version are: (i) the modulator was assembled in such a way as to minimise strain on the crystal, (ii) the separation of the electrodes has been decreased to improve the electric field uniformity, (iii) a larger crystal apperture of 16 mm was used and (iv) the tolerances on parallelism between the optic (z) axis and the electrodes has been decreased. These changes have led to the following change in specification: extinction ratio 2700±200:1 for the modified 850-16 as compared with 800±1 for the standard 850-16 version. The modulator has a longitudinal electric field generated by gold ring electrodes mounted on the end faces of a potassium dideuterium phosphate (KD^*P) crystal. It is driven by a Leysop 5000 series high voltage differential amplifier. This unit features individually adjustable positive and negative voltage limits and, when driven by a TTL pulse, generates an ultra-stable bipolar high voltage square wave for switching the initially linearly polarized laser beam alternately between right and left circular polarization states. The crystal is temperature stabilised to within $\pm$ 0.1^0 by an EOD model TC 150 temperature controller. This is necessary to avoid any drift effects caused by external temperature changes since the voltage required to switch between the right and left circular polarization states is dependent on the refractive index of the crystal which is a temperature dependent property. A custom built electronics box ensures that the polarization modulation sequence begins in the right phase by timing out the modulation sequence if no pulse is applied after a time which is greater than the normal acquisition time.

While the realization of the modulation scheme mentioned above is fine for ICP ROA measurements it cannot be used for SCP or DCP ROA

measurements [23,26]. In an attempt to overcome difficulties in the alignment of the electro-optic modulator used in traditional ICP experiments Zimba *et al.* [74] employed a Soleil-Babinet compensator to manually switch the polarization state of the incident laser beam between right and left circular polarization states in order to measure ICP ROA. Spencer and co-workers [21] employed a manually operated quarter wave plate to measure the circularly polarized component of the scattered radiation in their pioneering experiments on SCP ROA. Hecht *et al.* [23,27] subsequently used a similar experimental set-up (with the quarter wave plate attached to a motorized 360^0 rotator) to measure ICP, SCP and DCP_I ROA. This system is perhaps the most flexible in that it allows all possible CP ROA experiments to be performed but it suffers from serious problems with respect to dead time in the aquisition sequence since it has to be mechanically switched between the right and left circular polarization states.

2.4 Detector and electronics

Our detection system is based on a Wright Instruments Peltier cooled CCD camera system which consists of a camera head, a camera electronics unit and a computer interface board. The camera head is fitted with an EEV P86231/T (385×578 pixel, each pixel measuring 22×22 μm) CCD which is thinned and back illuminated. It is cooled by a 4 stage Peltier cooler to give a CCD operating temperature of around 200 K, where the dark current is normally below 0.1 electrons/pixel/second. Waste heat from the camera head is removed by air cooling assisted by a fan. The camera head is operated in the full frame mode with the exposure time defined by opening and closing the mechanical shutter. The charges from adjacent CCD pixels are added together on chip via a

process called binning [75]; our CCD uses serial binning which is illustrated in fig. 2.2. This is necessary because of the 2D nature of the

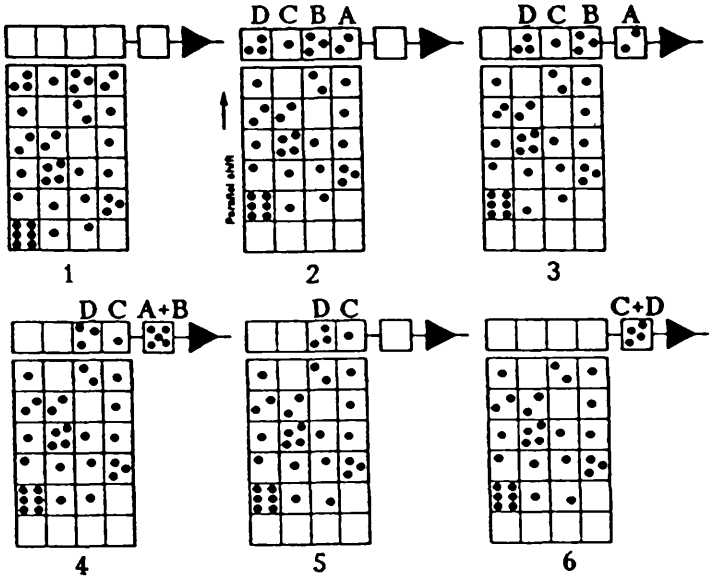

Fig. 2.2. Diagram of serial binning, adapted from ref. 75. (1) Photogenerated electrons are integrated in the parallel register. (2) Charge in the parallel register is shifted upwards by one row, causing charge from the top row of the parallel register to transfer into the serial register. (3) Charge packet A is transferred into the output mode potential well. (4) Charge packet B is transferred to the output mode and combined with charge packet A. (5) The combined charge packets are sensed by the on-chip amplifier and the output mode potential well is reset. (6) Steps 3 and 4 are repeated to bin charge packets C and D.

CCD relative to a diode array detector where the height of the Raman spectrum is covered by only one detector element. In our instrument a typical Raman band is dispersed over ~ 75 CCD pixels (at saturation on the strongest Raman band). Reading out this signal without binning would generate 75 sets of read-out noise and significantly increase the

aquisition time; binning reduces this to one set of read-out noise and is essential if ROA spectra with a high SNR are to be obtained. The CCD is aligned with its short axis along the slit axis of the spectrograph and its long axis parallel to the direction of dispersion which gives the maximum possible coverage of ~ 1200 cm^{-1} with 1200 g/mm grating and 514.5 excitation.

The camera electronics module contains three circuit boards. The main board contains power supplies and circuitry to handle the serial data links to the computer interface. An auxiliary board contains the power supply and temperature regulating control circuitry for the Peltier cooler and circuitry to control the shutter. The CCD board contains all the circuitry to bias and clock the CCD and to amplify, sample and digitize the output signals. Basic signal processing is accomplished by a variable gain 15-bit analog-to-digital converter that assigns numerical values ranging from 0 to approximately 32000 to each pixel. These values are referred to as ADC units. The system gain, defined as the ratio of electron counts (e^-) per ADC unit, scales the full well capacity of the CCD to the limits of the ADC. We use minimum amplifer gain (g=1) corresponding to 29.6 e^- per ADC unit, generating a noise of 7.7 e^- per readout cycle.

2.5 Computer control and software

A Dell system 325D AT computer equipped with a 80386 processor, a 80387 maths co-processor, a Wright Instruments interface board and a VGA moniter is used to synchronize the acquisition of Raman and ROA spectra with the electro-optic modulation system and the ROA box as depicted in fig. 2.3. This supports a customized version of the Lab Calc (Galactic Industries) spectral acquisition and manipulation program. The

standard Raman acquisition program has been modified by Wright Instruments in order to measure ROA. This package allows all the normal spectral manipulations, such as smoothing, to be performed in a real time environment.

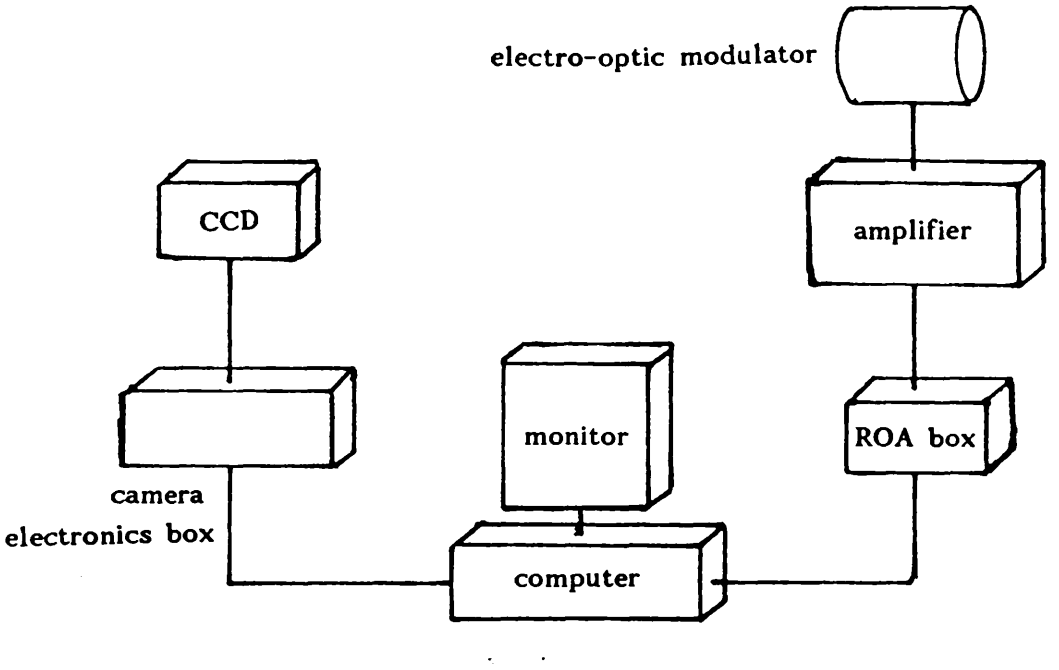

Fig. 2.3. The electronic layout of the Glasgow ROA instrument.

The wavenumber calibration for Stokes Raman shifts across the chip is given by:

$$\Delta\bar{\nu} = 10^7 \left(\frac{1}{\lambda_0} - \frac{1}{(c-a)d + \lambda_c} \right), \qquad (2.1)$$

where λ_0 is the exciting wavelength, λ_c is the wavelength reading of the spectrograph, c is the pixel corresponding to the λ_c reading, a is the actual pixel and d is the dispersion in nm/pixel across the chip, calculated by taking the difference in wavelength between two bands of known frequency and the difference of their corresponding pixel

positions. This procedure is accurate to within ± 2 cm^{-1} for α-pinene which we use as an ROA standard and is equivalent to the virtual channel method for calibrating multichannel Raman instruments as described by Hamaguchi [76].

2.6 The ROA acquisition sequence

The acquisition sequence is as follows: the ROA box ensures that the amplifier is ready to receive the TTL pulse from the computer. The computer then triggers the modulator to switch the incident laser beam from a linear polarization state to a right circular polarization state, simultaneously the CCD shutter opens and the CCD stores the right circularly polarized Raman spectrum. The shutter closes, the chip is read out and the data sent to a Lab Calc memory (1). The chip is cleared and the computer then instructs the modulator to switch to the corresponding left circular polarization state and also tells the CCD shutter to open. Data are acquired as before and stored in a separate Lab Calc memory (2). The CID $I_u^R - I_u^L$ between these spectra is calculated, simply (1) - (2), and stored in memory (3). Memories (1) and (2) are cleared and the process is repeated, with the CIDs being added together in memory (3), until an adequate SNR is achieved. The CIS is just the sum of the last two data sets in memories (1) and (2) multiplied by the number of acquisitions. The resultant raw $I_u^R - I_u^L$ and $I_u^R + I_u^L$ (we employ no smoothing or enantiomeric subtraction [27]) spectra are then incorporated into a special template where all the information about the acquisition is displayed, and then plotted, using a Hewlett Packard laser printer.

2.7 Sample preparation

Sample preparation constitutes a very important element of a successful ROA study. Impurities can cause fluorescence which obscures the Raman spectrum, dust can upset ROA measurements by causing variations in the intensity of the Raman spectrum and dirt on the cell walls can cause bright spots to form which may also lead to variations in the intensity of the Raman spectra particularly at low frequency due to stray light from Rayleigh scattering. Crystalline samples were either recrystallised or treated with activated charcoal and the solution then filtered through a Millipore filter (0.22 μm), to remove dust, into the sample cell. The cell would normally have been cleaned with chromic acid and then washed several times with filtered methanol. Liquids were normally distilled and then transferred directly into the cell. Any residual fluorescence left after this treatment could normally be "burned off" by exposure to the laser beam for a short period of time.

2.8 Control of artefacts

Experimental artefacts have plagued ROA measurements from their conception and indeed the first genuine observations of ROA were only achieved [12] after the origin of the major sources of artefacts were understood in terms of the polarization dependence of the isotropic and anisotropic molecular polarizability contributions to the scattering intensity as a function of scattering angle. Over the years several attempts have been made [26,55-57] to systematically analyse the main sources of ROA artefacts; however, they are still minimized using empirical trial and error procedures (*vide infra*).

Initially the electro-optic modulator is very carefully aligned and the quarter-wave voltages established accurately using a Soleil-Babinet

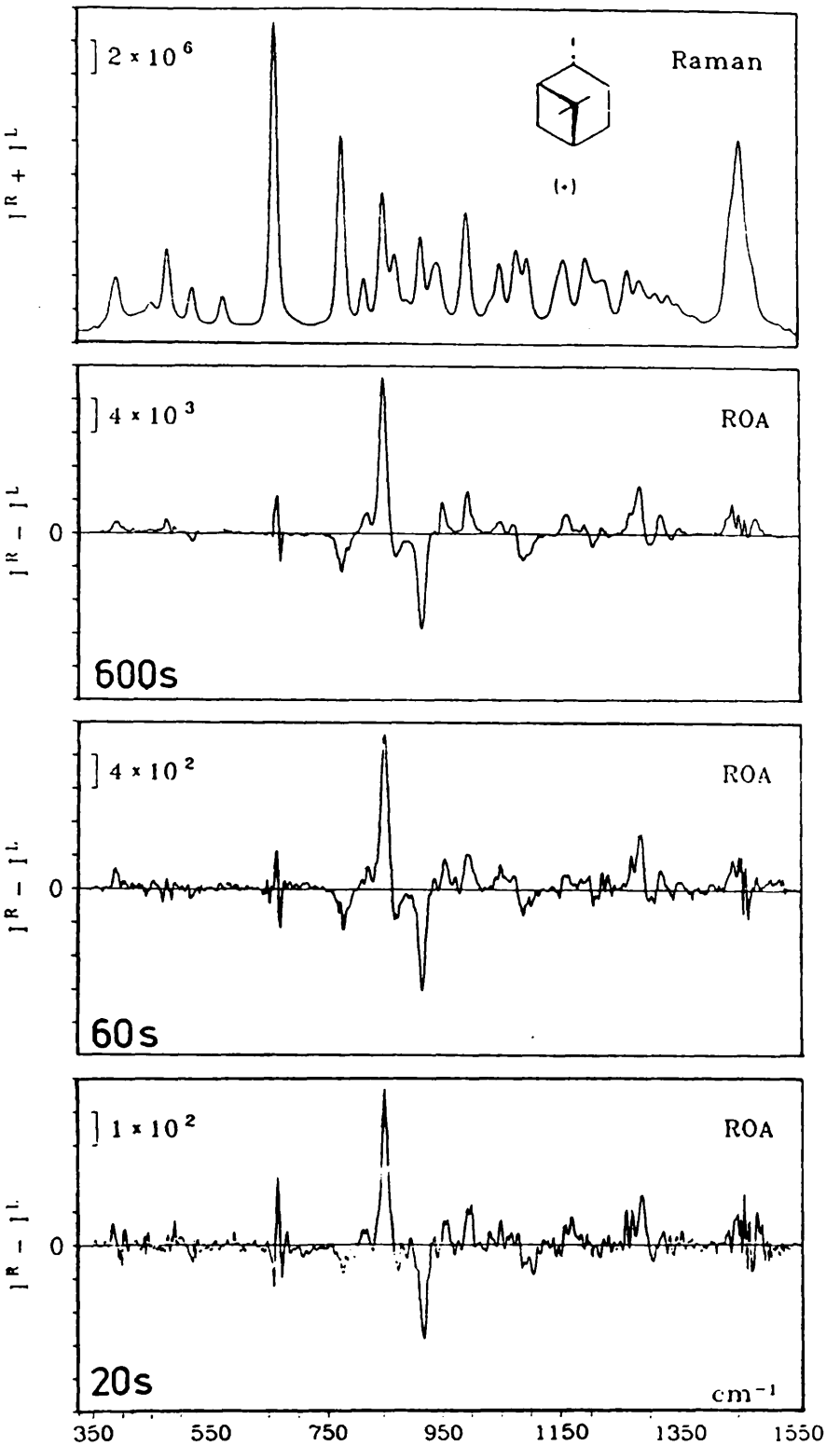

Fig. 2.4. Backscattered Raman and ROA spectra of (+)-trans-pinane recorded on the Glasgow ROA instrument described in this chapter. The Raman spectrum at the top corresponds to the 600 s ROA spectrum

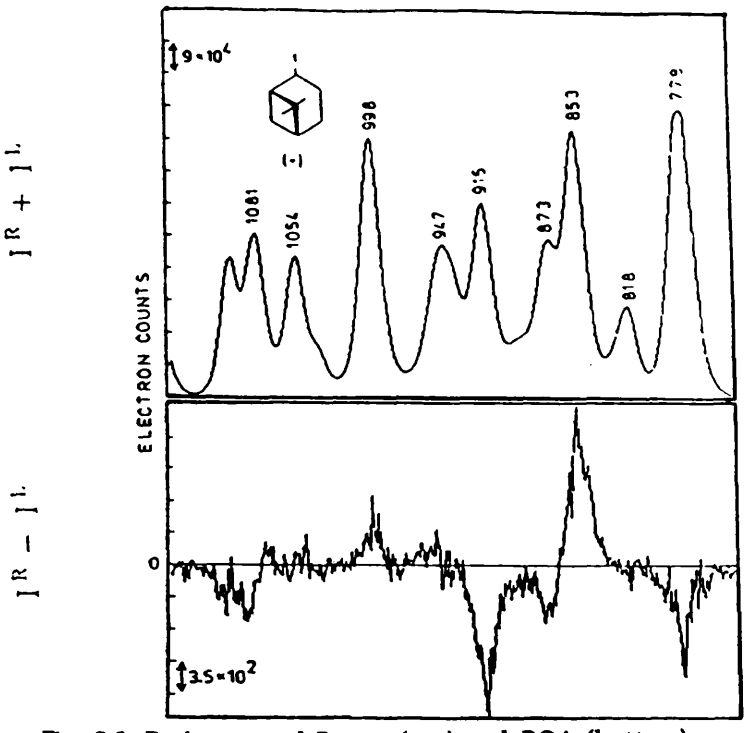

Fig. 2.5. Backscattered Raman (top) and ROA (bottom) spectra of (+)–trans-pinane recorded on the old Glasgow ROA instrument equipped with a CCD. Adapted from ref. 71.

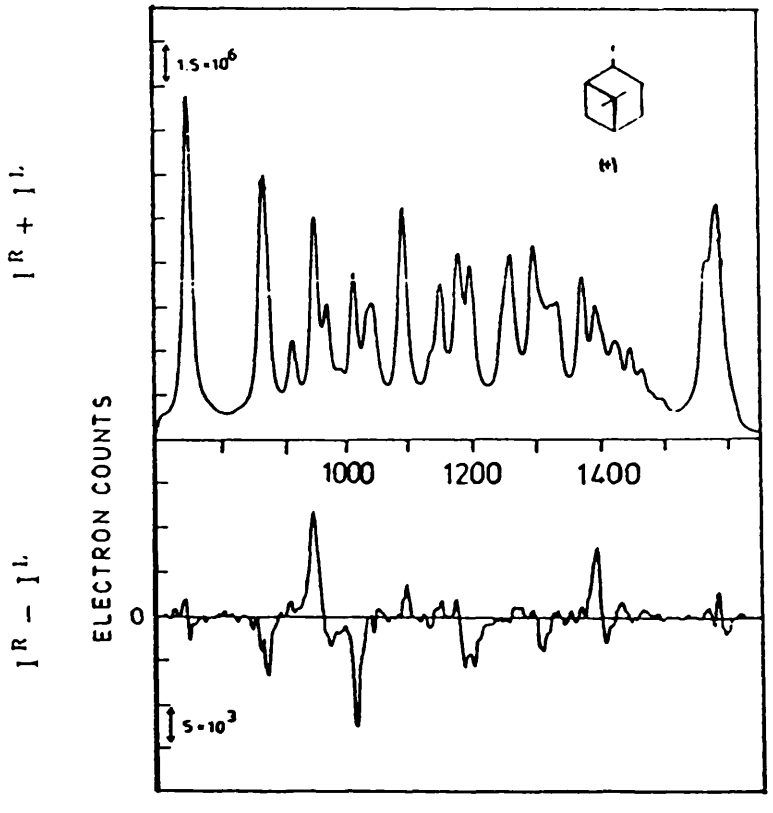

Fig. 2.6. Backscattered Raman (top) and ROA (bottom) spectra of (+)-trans-pinane recorded on the old Glasgow ROA instrument equipped with an intensified diode array. Adapted from ref. 36.

compensator. ROA spectra of α-pinene were recorded and the Lyot depolarizer rotated until any artefact on the strongly polarized band at 667 cm^{-1} was minimized. Also all optical components, with the exception of the camera lens, are constructed from high quality strain-free fused quartz to minimise birefringence artefacts in the optical train.

2.9 Instrumental performance

The backscattered ROA spectra of trans-pinane after 20, 60 and 600 seconds are shown in fig. 2.4. These are compared with earlier backscattered ROA spectra of trans-pinane (figs. 2.5 and 2.6) one of which was recorded on a double-grating spectrograph [67] equipped with a CCD [71] and the other on the same spectrograph but with a diode array detector [36]. It is apparent that our spectra are significantly superior to both of these earlier spectra in terms of SNR and speed of acquisition. We would estimate that we have achieved a factor of ~ 30 in terms of speed over the best previous ROA instruments based on diode array detectors. Another CCD based ROA instrument has recently been reported by Nafie and co-workers [23,24,27]. Comparison of the ROA spectra of alanine [24,49] reported for both these instruments leads us to suggest that our instrument with an unthinned CCD [49] would still be a factor of 2-3 times faster than this other backscattering CCD instrument.

3 ROA IN FORWARD SCATTERING

3.1 Introduction

In this chapter the very first solution phase ROA spectra using a forward scattering geometry are reported [37]. The normalised CIDs for backward (180^0), forward (0^0) and polarized (x), depolarized (z) and magic angle (*) right-angle (90^0) scattered ICP ROA are given, within the original formulation of Barron and Buckingham, by eqs. (3.1a-e) [8,34]

$$\Delta(0^0) = \frac{8\left[45\alpha G' + \beta(G')^2 - \beta(A)^2\right]}{2c\left[45\alpha^2 + 7\beta(\alpha)^2\right]}, \tag{3.1a}$$

$$\Delta(180^0) = \frac{48\left[\beta(G')^2 + \frac{1}{3}\beta(A)^2\right]}{2c\left[45\alpha^2 + 7\beta(\alpha)^2\right]}, \tag{3.1b}$$

$$\Delta_x(90^0) = \frac{2\left[45\alpha G' + 7\beta(G')^2 + \beta(A)^2\right]}{c\left[45\alpha^2 + 7\beta(\alpha)^2\right]}, \tag{3.1c}$$

$$\Delta_z(90^0) = \frac{12\left[\beta(G')^2 - \frac{1}{3}\beta(A)^2\right]}{6c\beta(\alpha)^2}, \tag{3.1d}$$

$$\Delta_*(90^0) = \frac{\frac{20}{3}\left[9\alpha G' + 2\beta(G')^2\right]}{\frac{10}{3}\left[9\alpha^2 + 2\beta(\alpha)^2\right]}, \tag{3.1e}$$

where $\alpha G'$, $\beta(G')^2$, $\beta(A)^2$, α^2 and $\beta(\alpha)^2$ are defined as previously by eq. (1.20). Common factors in the numerators and denominators of eq. (3.1) have not been cancelled so that the relative sum and difference intensities can be directly compared.

Since these equations contain three different variables three linearly independent ROA measurements are necessary in order to extract information regarding the relative contributions of $\alpha G'$, $\beta(G')^2$ and $\beta(A)^2$ to the generation of ROA in a particular Raman band. In principle the measurement of backscattered ROA together with polarized and

depolarized 90^0 scattering constitutes a minimum set for the extraction of this information (these are the three scattering configurations which most ROA spectra have been recorded with). However, as will become clear from the following discussion, the measurement of forward scattered ROA is important in helping to clarify certain ROA scattering mechanisms. It is also apparent, from the complexity of eq. (3.1), that theories which lead to any further simplification of these CIDs and that interpret ROA spectra in terms of simple models would be extremely attractive. Several theories have been proposed [11] but we will only consider the bond polarizability theory [8].

3.2 The bond polarizability theory

The bond polarizability theory of ROA intensities [77] predicts that for a molecule composed entirely of idealised axially symmetric bonds the following relations are valid: $\beta(G')^2 = \beta(A)^2$ and $\alpha G' = 0$. In this limit eq. (3.1) reduces to:

$$\Delta(0^0) = 0, \tag{3.2a}$$

$$\Delta(180^0) = \frac{64\beta(G')^2}{2c\left[45\alpha^2 + 7\beta(\alpha)^2\right]}, \tag{3.2b}$$

$$\Delta_x(90^0) = \frac{16\beta(G')^2}{c\left[45\alpha^2 + 7\beta(\alpha)^2\right]}, \tag{3.2c}$$

$$\Delta_z(90^0) = \frac{8\beta(G')^2}{6c\beta(\alpha)^2}, \tag{3.2d}$$

$$\Delta_*(90^0) = \frac{\frac{40}{3}\beta(G')^2}{\frac{10}{3}\left[9\alpha^2 + 2\beta(\alpha)^2\right]}. \tag{3.2e}$$

Within this approximation, the ROA intensity in backward scattering is

four times that for polarized 90^0 scattering, a result which has been confirmed experimentally for trans-pinane [36]. Similarly trans-pinane also shows the predicted ratio of 2:1 for the polarized-to-depolarized 90^0 intensities [78]. A crucial test therefore is to discover if trans-pinane shows zero ROA intensity in forward scattering as predicted by eq. (3.2a).

The bond polarizability theory is of course not expected to hold for molecules that contain non-axially symmetric bonds such as C=O and C=C, a typical example being β-pinene. However, it has been found that molecules containing oxygen or sulphur heteroatoms can also show large deviations from the predicted ratio of 2:1 for the polarized-to-depolarized ROA intensities despite having axial symmetry in all the bonds. In the case of arylethanes [79] the presence of the non-axially symmetric aromatic ring is probably the main source of the observed deviation from the predicted 2:1 ratio. For chiral three-membered ring compounds such as substituted oxiranes and thiiranes [80], even though the C–X (X= O or S) is formally axially symmetric, examination of an electron density map for these molecules shows that the bonds are in fact bent with most of the electron density lying off a straight line between the carbon and X atoms. For menthol and neothiomenthol [81] the deviation from the predicted 2:1 ratio is less easy to explain in simple terms but may result from isotropic scattering (*vide infra*).

3.3 Trans-pinane and the bond polarizability theory

The Raman circular intensity sum and difference spectra of (+)-trans-pinane in forward scattering (top pair) and backward scattering (bottom pair) in the frequency range from 630 to 1070 cm^{-1} are shown in fig. 3.1. These spectra were recorded on an earlier ROA instrument [67] in which the intensified diode array detector had been replaced by an

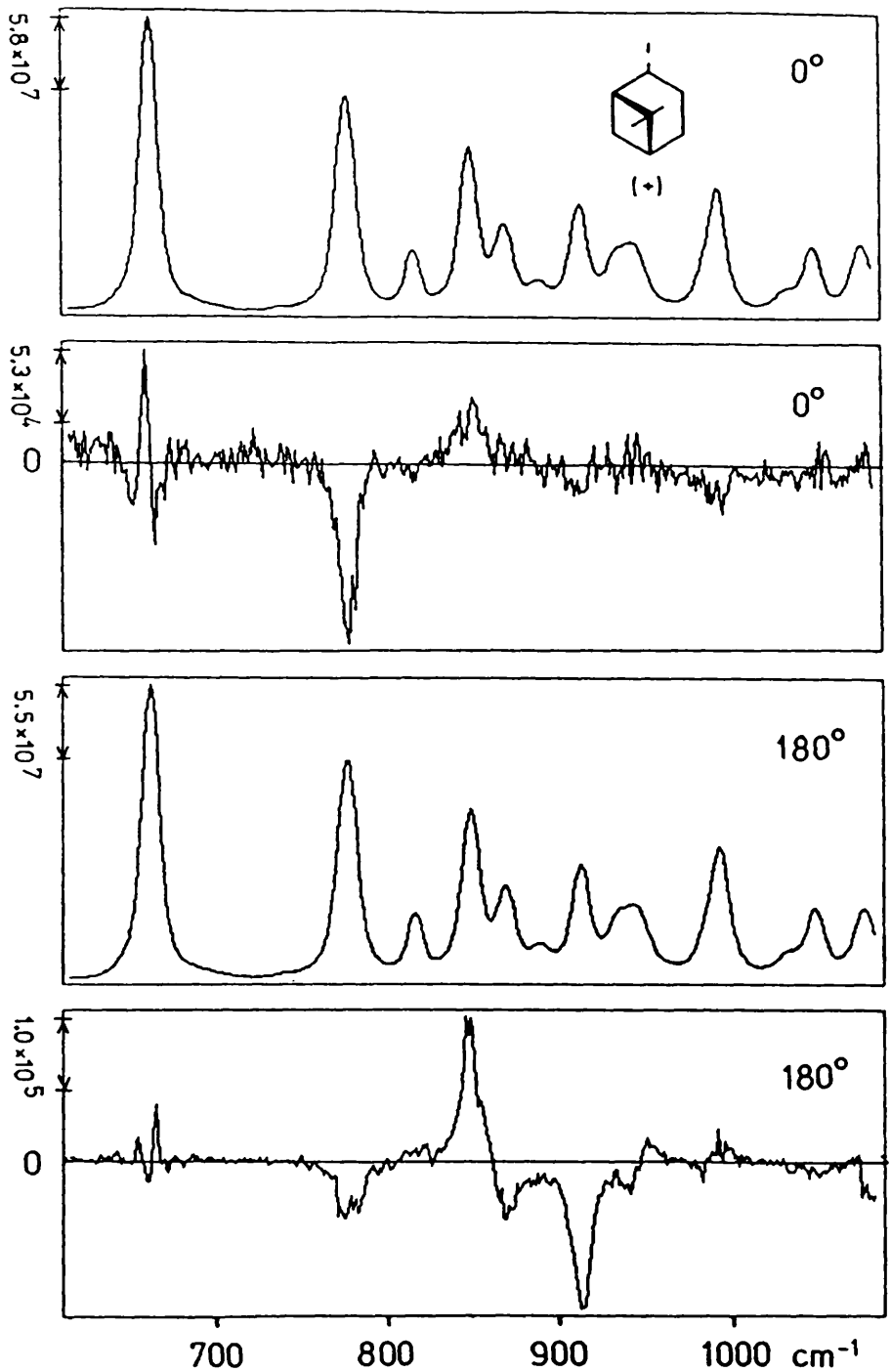

Fig. 3.1. The forward scattered (upper pair) and backward scattered (lower pair) Raman and ROA spectra of neat (+)-trans-pinane. These spectra were recorded on the old Glasgow multichannel ROA instrument [67] equipped with a front illuminated unthinned CCD. The experimental conditions are given in ref. 37.

unthinned front illuminated CCD. Firstly, as predicted by the denominators of eqs. (3.1a) and (3.1b), the CIS spectra are virtually identical in forward and backward scattering. The ROA spectra, however, are dramatically different in accordance with the result predicted by the bond polarizability theory. Few signals are observed in the forward scattered ROA spectrum apart from the ROA band at 775 cm^{-1} which is similar in both forward and backward scattering with $\Delta(0^0) \approx \Delta(180^0) \approx -7\times10^{-4}$. The ROA observed in backward scattering is large and similar in appearance as compared to the ROA measured in 90^0 scattering [78], but much more intense [36] as predicted by the bond polarizability theory. The band at 775 cm^{-1} is of particular interest since it probably originates from isotropic scattering, via $\alpha G'$, associated with a characteristic pinane-type skeletal mode, and shows a correlation with the equivalent band in β-pinene (*vide infra*).

3.4 β-pinene: isotropic scattering associated with the methylene twist

The Raman circular intensity sum and difference spectra of (-)-β-pinene in forward scattering (top pair) and backward scattering (bottom pair) in the frequency range from 630 to 1070 cm^{-1} are shown in fig. 3.2. The CIS in forward and backward scattering are, as expected from the previous discussion, almost identical. The backscattered CID is virtually identical to the corresponding depolarized 90^0 spectrum [34,82] while the forward scattered spectrum is completely different. Most of the ROA signals in the backscattered spectrum have either disappeared or are much reduced in the forward scattered spectrum. This is a not an unexpected result since only if the normal mode contained significant contributions from the C=C group would significant ROA be expected in forward scattering within the bond polarizability theory. However, a large

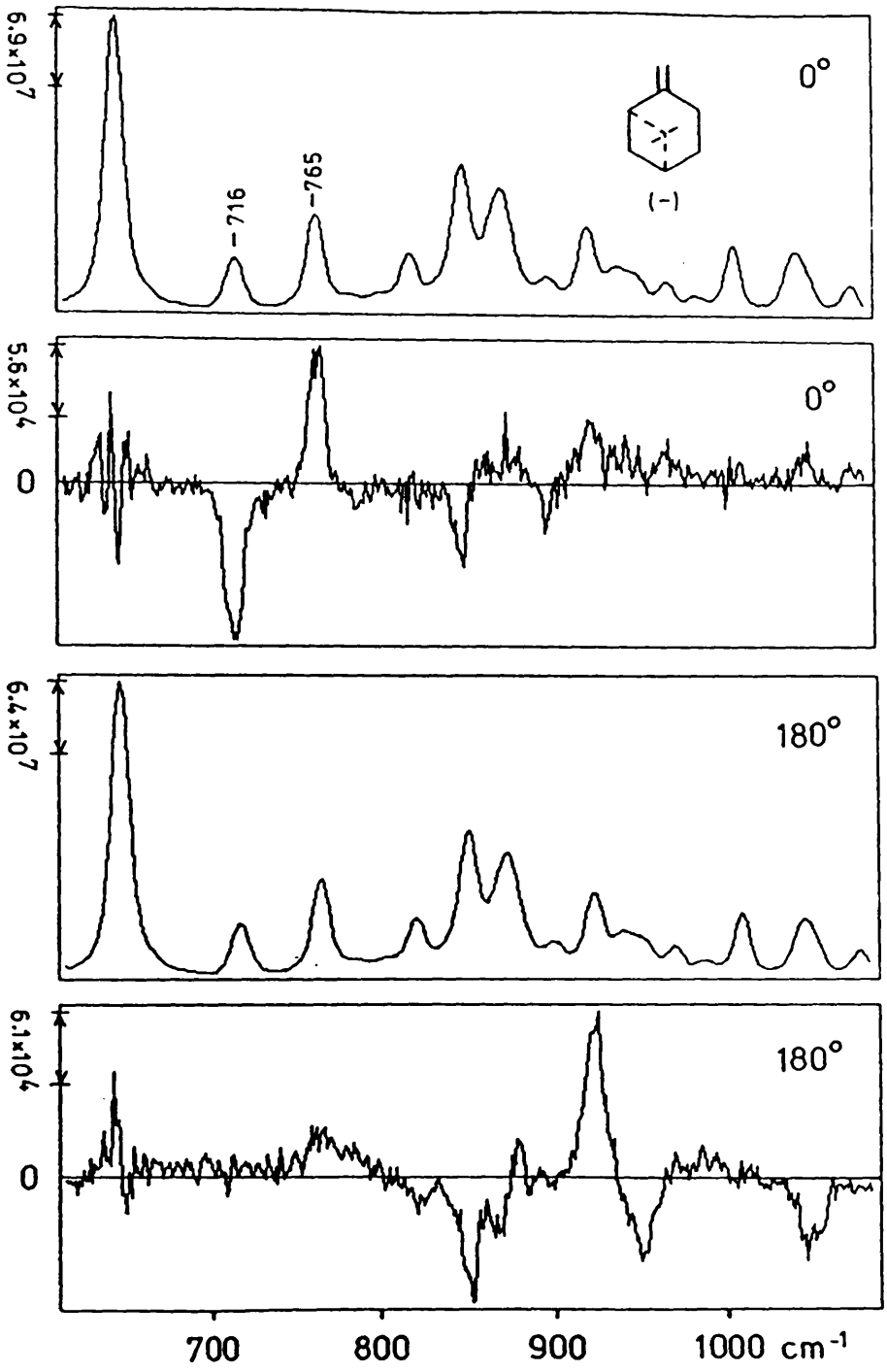

Fig. 3.2. The forward scattered (upper pair) and backward scattered (lower pair) Raman and ROA spectra of neat (-)-β-pinene. These spectra were recorded on the old Glasgow multichannel ROA instrument [67] equipped with a front illuminated unthinned CCD. The experimental conditions are given in ref. 37.

ROA couplet with $\Delta(0^0) \approx \pm 2\times10^{-3}$ appears in the bands at 716 and 765 cm^{-1} in the forward scattered spectrum that is completely absent in the backward scattered spectrum. The polarized and magic angle 90^0 scattered ROA spectra of β-pinene also show this couplet. Its absence in the corresponding depolarized ROA spectrum was explained by Barron and Escribano [82] in terms of a large electric quadrupole contribution, with $\beta(A)^2 = 3\beta(G')^2$, associated with olefinic deformations. This conclusion was based on the assumption that the isotropic term, $\alpha G'$, makes negligible contributions to the polarized ROA. This assumption was justified at the time because there was no direct experimental evidence for any significant isotropic contributions in other polarized ROA spectra and $\alpha G'$ does vanish identically within the bond polarizability theory. Barron and Escribano [82] did, however, emphasize that isotropic scattering could not be ruled out as the source of this ROA couplet and that measurements at other scattering angles would be necessary to provide further experimental evidence to distinguish between these two possibilities. The results given above can only be reconciled with the earlier 90^0 measurements if this couplet originates in almost pure isotropic scattering. This conclusion is reinforced by the CID Δ-values which are predicted by eqs. (3.1a) and (3.1c) to be twice as big in forward scattering as they are in polarized 90^0 scattering if the ROA originates from pure isotropic scattering. This is what is found, within experimental error, if the $\Delta(0^0)$ given above is compared with the $\Delta_x(90^0)$ values which can be estimated from fig. 1 of ref. 82 to be $\pm 1\times10^{-3}$.

A vibrational assignment for these two Raman bands was proposed by Hecht and Barron [34]. They suggested that the olefinic methylene twist makes a significant contribution to the Raman band at 716 cm^{-1} and as discussed previously the Raman band at 765 cm^{-1} can be assigned to a

characteristic pinane-type skeletal mode. They therefore ascribed the origin of this ROA couplet to interactions between this twist and the skeletal mode. In the D_{2h} point group of ethene (table 3.1) the methylene

C_{2v}	E	C_2	$\sigma_v(xy)$	$\sigma_v(yz)$		
A_1	1	1	1	1	z	x^2, y^2, z^2
A_2	1	1	-1	-1	R_z	$xy, G'_{\alpha\alpha}$
B_1	1	-1	1	-1	x, R_y	xz
B_2	1	-1	-1	1	y, R_x	yz

$\alpha\alpha$ = xx, yy or zz

D_{2h}	E	$C_2(z)$	$C_2(y)$	$C_2(x)$	i	$\sigma(xy)$	$\sigma(xz)$	$\sigma(yz)$		
A_g	1	1	1	1	1	1	1	1		x^2, y^2, z^2
B_{1g}	1	1	-1	-1	1	1	-1	-1	R_z	xy
B_{2g}	1	-1	1	-1	1	-1	1	-1	R_y	xz
B_{3g}	1	-1	-1	1	1	-1	-1	1	R_x	yz
A_u	1	1	1	1	-1	-1	-1	-1		$G'_{\alpha\alpha}$
B_{1u}	1	1	-1	-1	-1	-1	1	1	z	
B_{2u}	1	-1	1	-1	-1	1	-1	1	y	
B_{3u}	1	-1	-1	1	-1	1	1	-1	x	

$\alpha\alpha$ = xx, yy or zz

Table 3.1. Character tables for the point groups C_{2v} (top) and D_{2h}(bottom).

twist transforms as A_u while in a structure of C_{2v} symmetry (table 3.1) it transforms as A_2. Both these irreducible representations are spanned by the tensor components G'_{XX}, G'_{YY} and G'_{ZZ} (*vide* table 3.1). A fundamental Raman scattering transition associated with the methylene twist is therefore allowed through G', the isotropic part of the axial

electric dipole-magnetic dipole optical activity tensor, even in the parent structure of highest symmetry (D_{2h}). Hence, significant isotropic ROA, via $\alpha G'$, might be expected if the effective symmetry of the olefinic group is reduced to that of a chiral point group as in β-pinene so that α, the isotropic part of the polar polarizability tensor, can also contribute to Raman scattering in the methylene twist. This condition (a Raman transition allowed through G' in a high-symmetry parent structure but only through α owing to chiral perturbations) is a particularly favourable experimental situation because large ROA intensity could be generated in association with a weak Raman band. An analogous situation exists in conventional electronic CD studies where a magnetic dipole allowed transition is present in a high-symmetry chromophore and the parallel electric dipole transition is induced by the chiral environment so that the CD is associated with a weak absorption band, the classic example being the $n \rightarrow \pi^*$ transition of the carbonyl chromophore [8].

As discussed earlier, the Raman band at 775 cm^{-1} in the Raman spectrum of trans-pinane arises from a pinane-type skeletal mode in a similar fashion to the 765 cm^{-1} band in β-pinene. It is gratifying therefore that the isotropic ROA associated with this band in the forward scattered spectrum of (+)-trans-pinane has the opposite sign to that observed for the similar band in (-)-β-pinene, since the pinane skeletons have opposite absolute configurations in these two molecules.

3.5 Conclusions

The experimental results for trans-pinane indicate that the bond polarizability theory of ROA intensities appears to be a justified approximation for pure saturated hydrocrabons within the original theory of ROA. The small effects observed in the forward scattered ROA

spectrum probably originate from isotropic scattering.

Large isotropic ROA contributions in forward scattering have been unequivocally identified for β-pinene. If they are associated with the methylene twist we would expect to find significant isotropic ROA in twist and torsion modes of other molecules if the mode transforms the same as the isotropic optical activity tensor invariant G' in a parent structure of higher symmetry. Polarized and depolarized ROA data are available [83] for (-)-caryophyllene, (-)-methylene menthane and (-)-3-methylmethylenecyclohexane. Each of these molecules, like β-pinene, contains an exocylcic double bond. The first two of these molecules exhibit an ROA couplet which disappears on going from polarized to depolarized ROA whereas the last one does not. Since this behaviour closely resembles that of β-pinene we would expect significant forward scattered ROA intensity for caryophyllene and methylene menthane.

Fig. 3.3. The structures of (-)-methylene menthone (left) and (-)-3-methylmethylenecyclohexane (right).

However, since the structures of methylene menthane and 3-methylmethylenecyclohexane are so closely related (fig. 3.3) it may be that isotropic ROA is generated by a more complex mechanism than that described above.

It has been suggested that ROA measurements could be obtained

using coherent Raman techniques [84-90]. Only one attempt has been reported, that of Schneider *et al.* [87,90], who failed to detect any ROA in a coherent anti-Stokes Raman (CARS) experiment on the 1002 cm^{-1} breathing mode of (+) and (-)-1-phenylethylamine. Since the CARS experiment essentially measures ROA in forward scattering this is not an unexpected result since our studies have shown that forward scattered incoherent ROA measurements are the least favourable of all the possible ROA experiments unless there is a significant isotropic contribution. It has also been shown theoretically [84] that coherent ROA vanishes within the bond polarizability (two-group) model. We therefore suggest that future attempts to observe CARS ROA be concentrated initially on the 716 and 765 cm^{-1} bands in β-pinene, which are highly favourable on account of the large isotropic contribution to the ROA exhibited by these two bands.

4 ROA OF ALANINE

4.1 Introduction

The word protein is taken from the Greek *proteios*, meaning first, which reflects the view that they probably form the most important class of chemical compounds. They are found in all living cells and are the principal material of skin, muscles, tendons, nerves, and many hormones. Proteins are derived from 23 naturally occuring α-amino carboxylic acids of general structure:

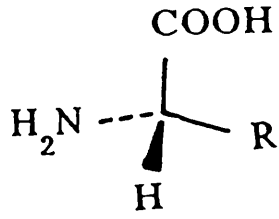

Only two exceptions to this structure exist, namely proline and 4-hydroxyproline, where the side chain is bonded to the nitrogen atom to give an imino acid:

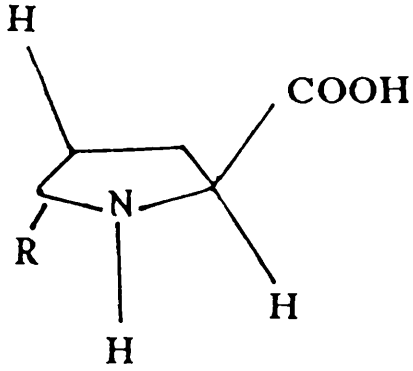

R=H or OH

Neutral amino acids are known to exist as zwitterions in aqueous solution in which there has been proton exchange between the COOH and NH_2 groups. Stereochemical studies of these naturally occuring amino

acids have shown that they all have the same absolute configuration about the carbon atom carrying the alpha amino (imino) group, and that this configuration is the same as that in L-(-)-glyceraldehyde (fig. 4.1). Within the Cahn-Ingold-Prelog convention the group R always happens to have a lower priority than COOH; thus all naturally occuring amino acids exhibit the *S* configuration.

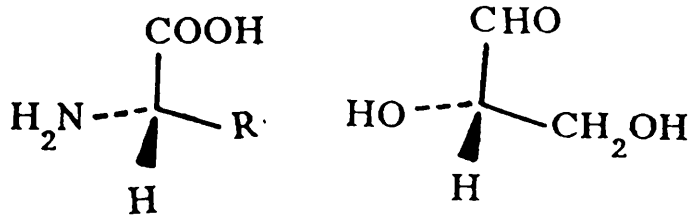

Fig. 4.1. Absolute stereochemistry of amino acids (left) in relation to L-(-)-glyceraldehyde (right).

When linked together these amino acids offer an enormous number of possible structural permutations. The solution conformation adopted by these amino acids both individually and when joined is of extreme chemical significance since it determines the secondary structure of proteins. For example, alanine and leucine have been found to stabilise the α-helix structure, which is one of the prominent secondary conformations available to proteins, the others being β-sheet and random coil, whereas glycine and proline destabilise it [91].

The simplest chiral amino acid, alanine (2-aminopropionic acid) has been the subject of extensive vibrational studies, mainly in the solid state, which makes it an almost ideal molecule for ROA studies since a complete vibrational analysis, which is necessary to deduce the origins of the ROA, is available. For our purposes the most important articles are one by Diem *et al.* [92] who performed a detailed vibrational analysis of alanine based primarily on solution-phase Raman spectra and a

Urey-Bradley normal coordinate analysis; one on intermolecular vibrational coupling in crystals of DL-alanine by Kettle and co-workers [93]; two mid-infrared VCD studies of alanine in H_2O and D_2O by Diem [94] and by Freedman *et al.* [95]; a VCD study by Zuk *et al.* in the CH stretching region of α-amino acids as a function of pH [96]; an infrared and Raman study by Byler and Susi [97] which identifies the C^*-H deformation (bending) modes; a normal coordinate analysis by Susi and Byler [98] based on the Raman spectra of several polycrystalline alanine isotopomers and an infrared study by Percy and Stenton [99] which investigated the effects of N^{15} and O^{18} substitution on the spectrum of alanine. It should also be mentioned that ROA data (acquired in depolarized 90^0 scattering) for several bands of alanine in water is presented in a doctoral thesis by Hohmann [100], but the instrumental sensitivity was marginal. Nafie *et al.* [24] have recently presented a backscattered DCP_I CCD spectrum of alanine in the frequency range discussed in this work but only attempted an analysis of the origin of ROA in two bands. This chapter contains a full vibrational analysis of L-alanine based on comparisons between the experimental Raman and ROA spectra measured over a range of pH values and theoretical Raman and ROA spectra of alanine at pH=7.0.

4.2 Vibrational analysis of alanine

The vibrational analysis of alanine, which exists as a zwitterion in neutral solution, has provoked extensive disussion in the literature. Although the spectra of almost every possible isotopomer have been carefully studied the vibrational assignments for some bands still remain unsatisfactory. The effect of selected isotopic substitutions on the Raman and infrared frequencies of the parent molecule is summarised in table 4.1. In an attempt to clarify the situation Prof. P. L. Polavarapu, at

Table 4.1 Effect of isotopic substitution on the vibrational frequencies of alanine

mode assignment[a]	Ala-d_0[a]	Ala-C^*-d_1[a]	Ala-C-d_3[a]	Ala-N-d_3[a]	Ala[e]	Ala-N^{15}[e]	Ala-O^{18}[e]
$\delta^a NH_3^+$	1645[b]	1645[b]	1645[b]	1190[b]			
$\delta^a NH_3^+$	1625[b]	1625[b]	1625[d]	1180[b]	1621	1619	1611
$\nu^a COO^-$	1607[c]	1607[c]	1607[c]	1607	1590	1590	1577
$\delta^s NH_3^+$	1498[b]	1498[b]	1498[b]	1145[b]	1505	1502	1505
$\delta^a CH_3$	1459	1456	1038	1461	1455	1455	1455
$\delta^a CH_3$	1459	1456	1038	1461	1455	1455	1455
$\nu^s COO^-$	1410	1407	1402	1409	1412	1412	1402
$\delta^s CH_3$	1375	1373	1050	1375			
δC^*-H	1351	959	1347	1337	1362	1362	1354
δC^*-H	1301	880[d]	1291	1291	1307	1307	1296
ζNH_3^+	1220	1211	1220	874	1237	1234	1237
ζNH_3^+	1145	1158	1165	840	1152	1148	1150
$\nu^a CCN$	1110	1079	1109	1148	1114	1112	1111
$\nu CC(O_2)$	1001[b]	1010	941	1097	1014	1011	1014
ζCH_3	995[b]	1000sh	820	1055			
ζCH_3	922	899[d]	758	920	919	916	911
$\nu^s CCN$	850	823	921	812	850	847	835
γCOO^-	775	747		778	772	772	767
δCOO^-	640	635	610	613	649	649	634

δ^a antisym. bend, ν^a antisym. stretch, δ^s sym. bend, ζ rocking, γ wagging, a Solution phase Raman frequencies from ref. 92, b Solid-state or infrared frequencies from ref. 92, c Solution frequency of alanine-N-d_3 in D_2O from ref. 92, d These modes are accidentally degenerate in solution but clearly split in the soild phase see ref. 92, e Infrared frequencies from ref. 99.

Vanderbilt University, has performed an *ab initio* vibrational analysis and ROA intensity calculation at the self consistant field (SCF) [40] level with both the 6-31G and 6-31G* basis sets. Only the combination of his numerical results with the experimental data yields plausible vibrational assignments for zwitterionic alanine [49,50].

It is well known that *ab initio* vibrational frequencies at the SCF level are approximately ten to twenty percent higher than the corresponding experimental frequencies [101]. They can be brought into closer correspondence with the experimental frequencies in a number of ways: the most satisfactory is to perform a more sophisticated version of the *ab initio* calculation with the inclusion of the effects of configuration interaction [101]; others involve the use of scaling factors on the *ab initio* force constants. There are two possible procedures for doing this: (i) a constant scaling factor which does not affect the predicted vibrational intensities or more importantly the normal mode compositions or (ii) multiple scaling factors which do affect the predicted vibrational intensities and normal mode compositions. We do not comment on the validity of either scaling method [102,103] but base our correlations on the comparison of the calculated and observed relative intensity patterns and limit our discussion to the region 700-1700 cm^{-1} for which we have reliable ROA data. Our suggested correlations between the experimental band frequencies and the frequencies of the 6-31G* theoretical values are listed in table 4.2.

In the ~ 750-1250 cm^{-1} region of the experimental Raman spectrum of alanine in water (pH ≈ 7)(fig. 4.2), the band at 850 cm^{-1} is intense while those at 775, 922, 995, 1001, 1110, 1145 and 1220 cm^{-1} are relatively weak with similar intensities. This same pattern is also found in both the 6-31G [49] and 6-31G* theoretical Raman spectra of alanine (fig. 4.3). We

Table 4.2 Comparison of the experimental and *ab initio* theoretical ROA parameters for alanine[a]

Experimental		*Ab initio* 6-31G*		Assignments	
Frequency (cm^{-1})	$\Delta(180^0)\times10^4$	Frequency (cm^{-1})	$\Delta(180^0)\times10^4$	6-31G*	This work
775	-11.7	838	-0.7	COO^- wag+sym COO^- bend	COO^- wag
850	-2.4	881	-2.6	C^*-N stretch+sym COO^- bend	see text
922	+17.7	942	+6.5	C^*-C(O) stretch+ COO^- bend+ C^*-N stretch	C^*-$C(O_2)$ stretch
995	-7.0	1060	-0.4	NH_3^+ rock+ CH_3 rock	NH_3^+ rock /CH_3 rock
1001		1080	-9.8	NH_3^+ rock+ CH_3 rock+ C^*-$C(H_3)$ stretch	NH_3^+ rock /CH_3 rock
1110	+4.1	1164	+14.3	NH_3^+ rock+ CH_3 rock+ C^*-N stretch +C^*-$C(H_3)$ stretch	NH_3^+ rock
1145	+14.8	1205	+2.7	C^*H bend+ CH_3 rock +NH_3^+ rock	CCN stretch
1220	-3.4	1314	-18.0	NH_3^+ rock+ CH_3 rock +C^*-$C(H_3)$ stretch	NH_3^+ rock
1301	+4.0	1395	+11.2	sym NH_3^+ bend+ C-O stretch+ C^*H bend	C^*H bend
1351	-2.6	1447	-21.7	C^*H bend+ NH_3^+ rock	C^*H bend
1375	-0.6	1568	-3.5	sym CH_3 bend	sym CH_3 bend
1410	-2.4	1501	-12.5	C^*H bend+ COO^- torsion	sym COO^- stretch
1459	-0.7	1639	-2.7	asym CH_3 bend	asym CH_3 bend
1459	+3.0	1641	+4.1	asym CH_3 bend	asym CH_3 bend

a adapted from ref. 49.

notice that the predicted 881 cm^{-1} mode in the 6-31G* spectrum exhibits the largest intensity with those predicted at 838, 942, 1060, 1080, 1164, 1205 and 1314 cm^{-1} relatively weak with similar intensity (this same pattern is also observed in the 6-31G theoretical spectrum [49]). We therefore have confidence in the correlation of the experimental band at 850 cm^{-1} with the 6-31G* mode at 881 cm^{-1}. The remaining experimental bands can then be correlated with the remaining theoretical modes in their corresponding order of frequency. However, some uncertainity exists in this procedure since the theoretical ordering of modes does not always need to match that of the experimental spectra, but the relative intensities are too similar to use as a reliable criterion for correlation. The ROA spectrum can play an important role here since the sign of the ROA bands provides an additional criterion for the correlation. We shall see that a comparison of the experimental and predicted ROA signs suggests that our predicted ordering of this set of modes is correct for both basis sets.

Correlations of the experimental bands in the region ~ 1250–1700 cm^{-1} at neutral pH with the *ab initio* results is not as satisfactory as in the lower frequency region, and it is useful to invoke the assignments of Diem *et al.* [92], Kettle and co-workers [93], Byler and Susi [97] and Percy and Stenton [99] in this region since they all make use of valuable isotopic data.

The experimental Raman bands at 1301 and 1351 cm^{-1} have been assigned by Diem *et al.* [92] and by Byler and Susi [97] to orthogonal C^*-H deformation (bending) modes. However, the isotopic substitution data suggests significant contributions from NH_3^+ bending motions since these bands shift to 1291 and 1337 cm^{-1} (*vide* table 4.1) in the Raman spectra of alanine in D_2O where the NH_3^+ group has been replaced by the

ND_3^+ group [92]. A similar shift to lower frequency upon NH_3^+ deuteration has also been observed for the corresponding bands in DL-alanine crystals [93]. The lower frequency band must also contain contributions from the methyl group since it shifts to 1291 cm^{-1} (*vide* table 4.1) upon deuteration of the methyl group. The infrared spectra of O^{18} labelled alanine in the region 150-1700 cm^{-1} [99] suggests that both these bands are also coupled to the symmetric COO^- stretching vibration. It should be noted that Percy and Stenton [99] have misassigned the 1362 cm^{-1} infrared band of alanine to a methyl symmetric deformation (bending) mode, which is a fairly weak infrared band, rather than correctly to the C^*-H deformation (bending) mode (see Byler and Susi [97] for a discussion of the assignment of this band). These extensive vibrational couplings are in disagreement with the conclusion of Diem *et al.* [92] that the Raman spectra of alanine can be interpreted well in terms of group frequencies and predominantly local modes (*vide infra*). Correlation of these modes with the 6-31G* theroetical modes is difficult and will be discussed later.

The experimental Raman bands at 1375 and 1459 cm^{-1} were assigned by Diem *et al.* [92] and by Byler and Susi [97,98] to methyl deformation (bending) modes, again using isotopic data. This is supported by the assignments of Kettle and co-workers for the corresponding bands in crystalline DL-alanine [93]. The 1375 cm^{-1} band is due to the symmetric methyl deformation (bending) mode and correlates with the 6-31G* mode at 1563 cm^{-1}. The 1459 cm^{-1} band is due to the nearly degenerate pair of antisymmetric methyl deformation (bending) modes and correlates with the 6-31G* modes at 1639 and 1641 cm^{-1}, respectively.

The experimental Raman band at 1410 cm^{-1} has been assigned by Diem *et al.* [92] and by Kettle and co-workers [93] to the symmetric

COO^- stretching vibration, while Percy and Stenton [99] and Susi and Byler [98] have postulated extensive vibrational mixing of this mode with the orthogonal C^*-H deformation (bending) modes. It is perhaps worth noting that previously Byler and Susi [97] also assigned this mode to a group frequency of the carboxylate group (their normal coordinate analysis may therefore be flawed in its interpretation of the origin of this band). The isotopic data of Diem *et al.* [92] (*vide* table 4.1) suggest that this mode is also slightly coupled to a vibration of the methyl group (probably the symmetric deformation (bending) mode) since it shifts 8 cm^{-1} to lower frequency upon deuteration of the methyl group and also to a lesser extent to the orthogonal C^*-H deformation (bending) modes. The ratio of the frequencies of the symmetric COO^- stretch to the antisymmetric COO^- stretch, ν_s/ν_a, exhibits the value 0.88 in crystalline alanine and glycine [104]. If this value were to change upon isotopic substitution as in nitromethane (0.90 in the d_0 species and 0.88 in the d_3 species [105]), for example, then two possible explanations can be invoked [106]: either coupling of the COO^- symmetric stretch with the stretching modes of the attaching bonds, i.e. C-COO^-, or non symmetric hydrogen bonding. The agreement for glycine and alanine of this ratio is not unexpected for crystals where packing considerations predominate but would suggest that the symmetric COO^- stretching mode is not coupled to the stretching modes of the adjacent bonds. In alanine-N-d_3 one would expect non symmetric hydrogen bonding between the ND_3^+ and COO^- groups according to the arguments of Zuk *et al.* [96] and hence $\nu_s/\nu_a \neq 0.88$: however, $\nu_s/\nu_a = 0.88$ (*vide* table 4.1), which would tend to cast doubt on the ring current mechanism of VCD intensities (*vide infra*). Unfortunately, lack of data for the other isotopomers, where the antisymmetric COO^- mode is difficult to identify

in the Raman spectrum due to its weakness, rules out any definite comment on the nature of hydrogen bonding in solution for alanine, but based on the above discussion and the Raman data for alanine in >6N-HCL (*vide infra*) it is highly probable that this mode is indeed an islolated COO^- symmetric stretch. The 6-31G* theoretical calculation does not help much here since although the modes at 1523 and 1501 cm^{-1} contain vibrational contributions from the COO^- group, in neither of them does the COO^- symmetric stretch dominate. The combined Raman intensity of these two theoretical modes would correlate with the large Raman intensity observed in the experimental 1410 cm^{-1} band, but it is not sufficiently large to supress the intensity of the antisymmetric methyl deformation (bending) modes, which is in conflict with the experimental observations. The Raman band observed at 1410 cm^{-1} exhibits significantly larger intensity than the one at 1459 cm^{-1}. It should also be noted that, while the experimental bands due to the methyl symmetric and antisymmetric deformations (bends) are separated by the 1410 cm^{-1} band, the 6-31G* theoretical methyl deformation (bending) modes are adjacent. Hence the predicted ordering of these modes is not correct. They have to be re-arranged in order to achieve a satisfactory correlation with the experimental Raman bands.

Substitution of the COO^- group in L-alanine by a CH_2OH group formally yields L-alaninol. The Raman spectrum of neat L-alaninol (*vide* fig. 4.8 in section 4.5) shows no band at ~ 1410 cm^{-1}. This observation supports our assignment of this band in alanine to a normal mode associated with the COO^- group. Significantly the antisymmetric methyl deformation (bending) mode is the most intense band in the Raman spectrum of alaninol but this may arise from interactions between this mode and an adjacent CH_2 bending mode. Another possible explanation is

Fermi resonance of the alanine antisymmetric methyl deformation (bending) mode with either an overtone or combination mode. A similar situation may occur in arylethanes where the antisymmetric methyl deformation (bending) mode interacts with an aromatic ring mode to generate an ROA couplet [79]. Analysis of the data for alanine, however, suggests that an overtone cannot be involved since none would occur in the correct spectral region, while the lack of a frequency shift upon isotopic substitution suggest either a skeletal mode or one involving the COO^- group. Two plausible possibilities are the combination mode γ COO^- + δ COO^- (using the notation of Diem *et al.* [92] and table 4.1) which would occur at 1415 cm^{-1} or the difference mode ν_s COO^- - τ COO^- which would exhibit a frequency of 1423 cm^{-1}. Either of these modes could then interact with the antisymmetric methyl deformation (bending) mode at 1459 cm^{-1} because there are no symmetry restrictions in a C_1 symmetry molecule, reducing its intensity and boosting the intensity of the symmetric COO^- stretching vibration which would have a similar frequency to the other half of this Fermi resonance doublet.

4.3 ROA of alanine

The Raman (top) and ROA (bottom) spectra of L and D alanine in water (pH≈7) are shown in fig. 4.2. One point to note is the almost perfect reflection symmetry between these two spectra as would be expected for opposite enantiomers. The Raman (top) and ROA (bottom) spectra of alanine in >6N-HCl (pH≈0), >6N-NaOH (pH≈14) and 1N-HCl (pH≈3) and 1N-NaOH (pH≈9) are shown in figs. 4.4, 4.5 and 4.6, respectively.

Begining at the low frequency end of the experimental ROA spectrum of L-alanine in water (*vide* fig. 4.2) we observe small negative ROA

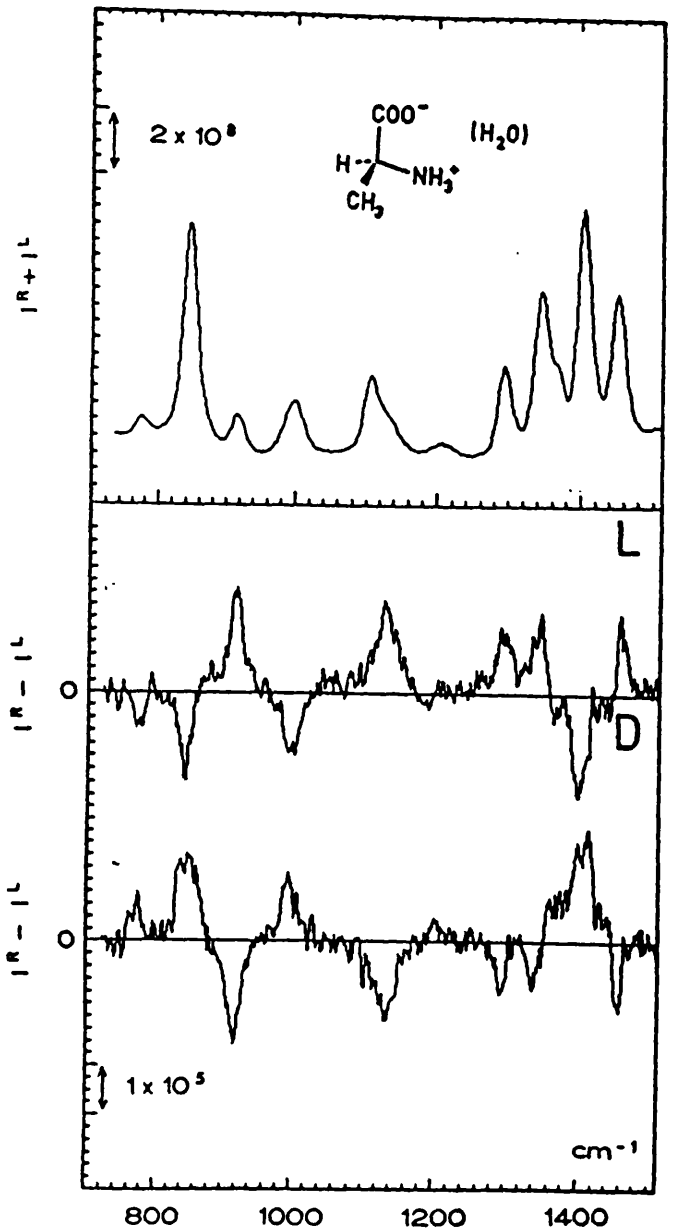

Fig. 4.2. Backscattered Raman (top) and ROA (bottom) spectra of L and D-alanine in H_2O. These spectra were recorded with a front illuminated unthinned CCD using the spectrograph described in chapter 2. The experimental conditions are given in ref. 49.

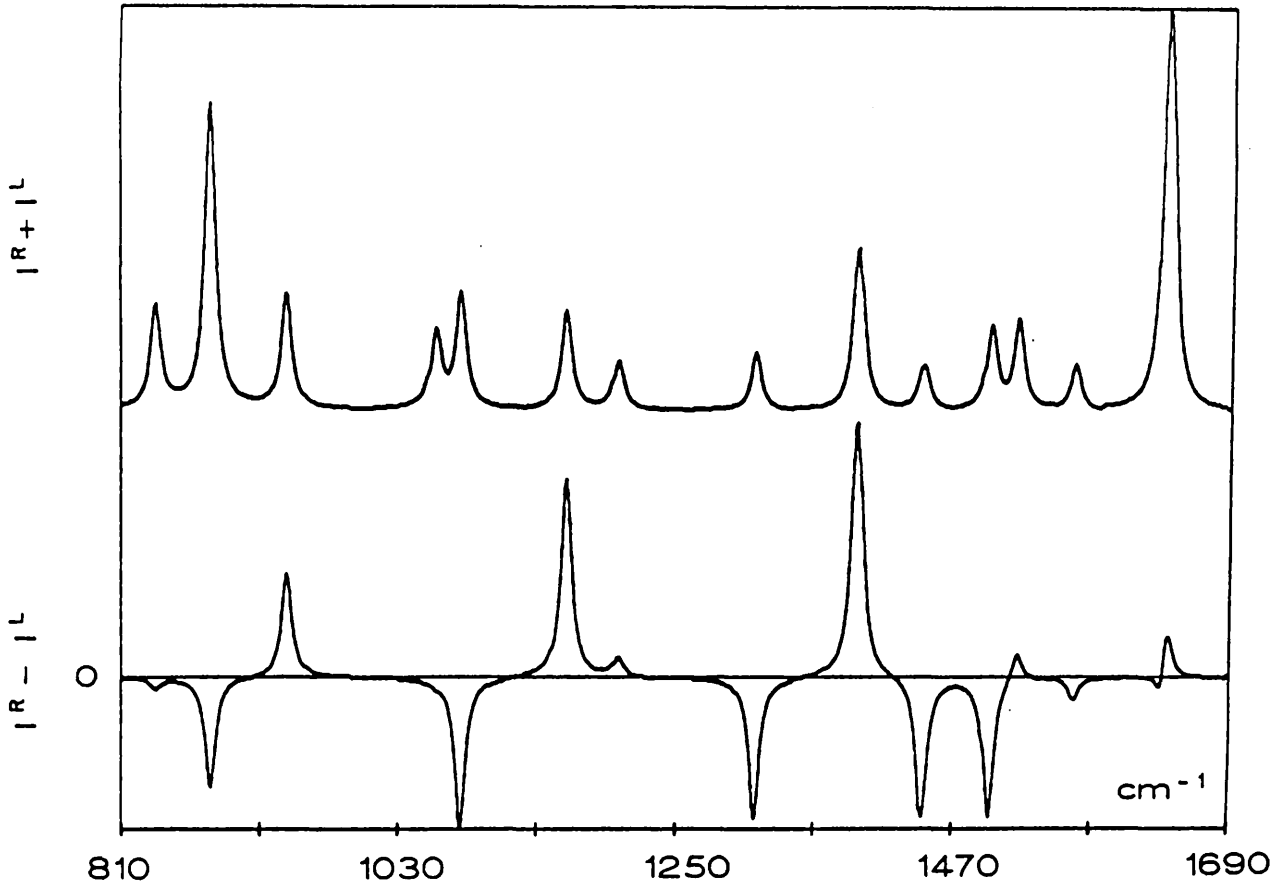

Fig. 4.3. *Ab initio* backscattered Raman (top) and ROA (bottom) spectra of zwitterionic L-alanine obtained with the 6-31G* basis set.

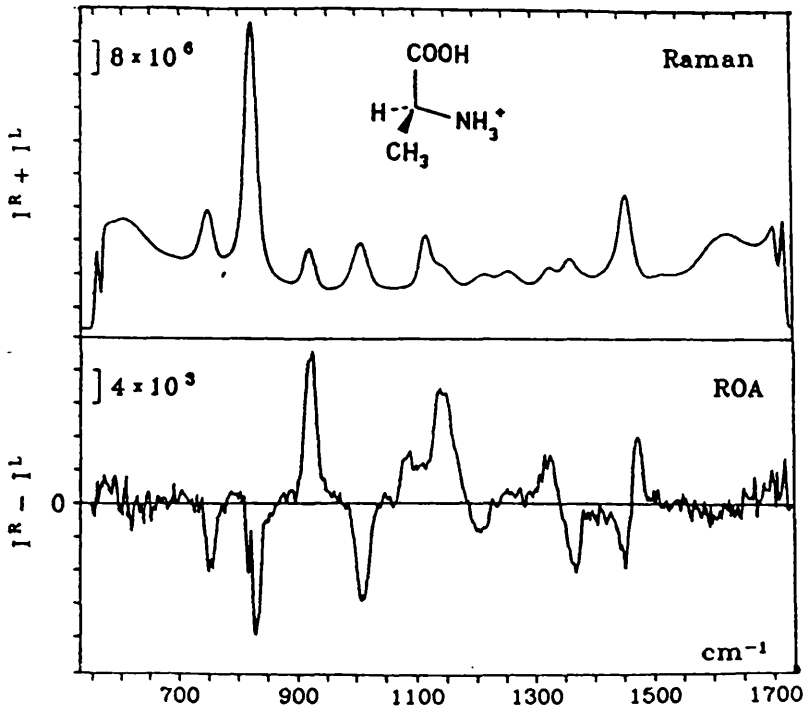

Fig. 4.4. Backscattered Raman (top) and ROA (bottom) spectra of L-alanine in >6N-HCl. These spectra were recorded on the instrument described in chapter 2. Experimental conditions: exposure time 2 s, laser power 650 mW, acquisition time 3 hours, slit width 0.12 mm.

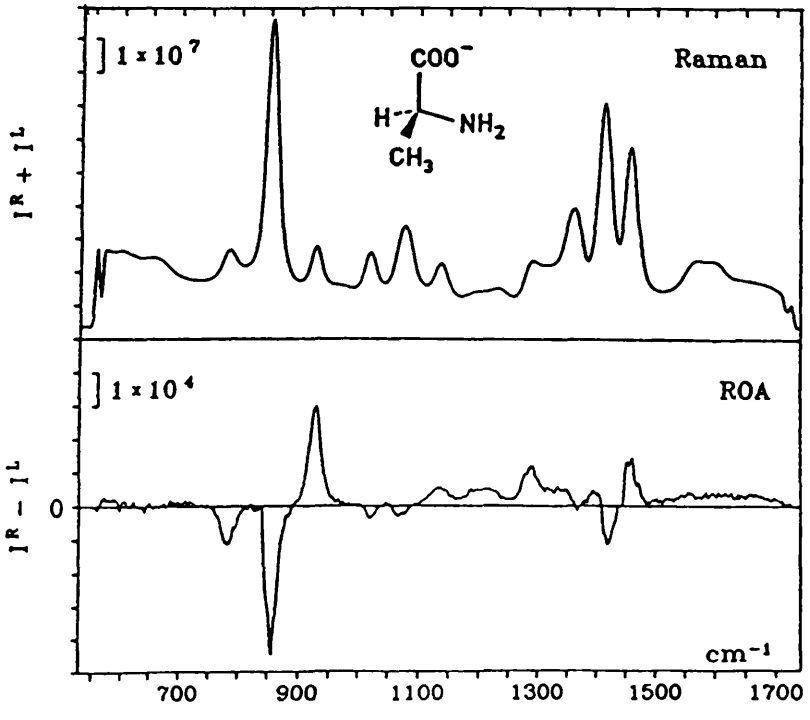

Fig. 4.5. Backscattered Raman (top) and ROA (bottom) spectra of L-alanine in >6N-NaOH. These spectra were recorded on the instrument described in chapter 2. Experimental conditions: exposure time 1.5 s, laser power 650 mW, acquisition time 3 hours, slit width 0.12 mm.

intensity in the band at ~ 650 cm^{-1} which has been assigned by Diem *et al.* [92] and by Susi and Byler [98] to a bending mode of the COO^- group, this disappears in the ROA spectrum in >6N-HCl where the COO^- group has been protonated (fig. 4.4) and also in the spectrum in >6N-NaOH (fig. 4.5) which suggests that the ROA arises from interactions between the COO^- and NH_3^+ groups.

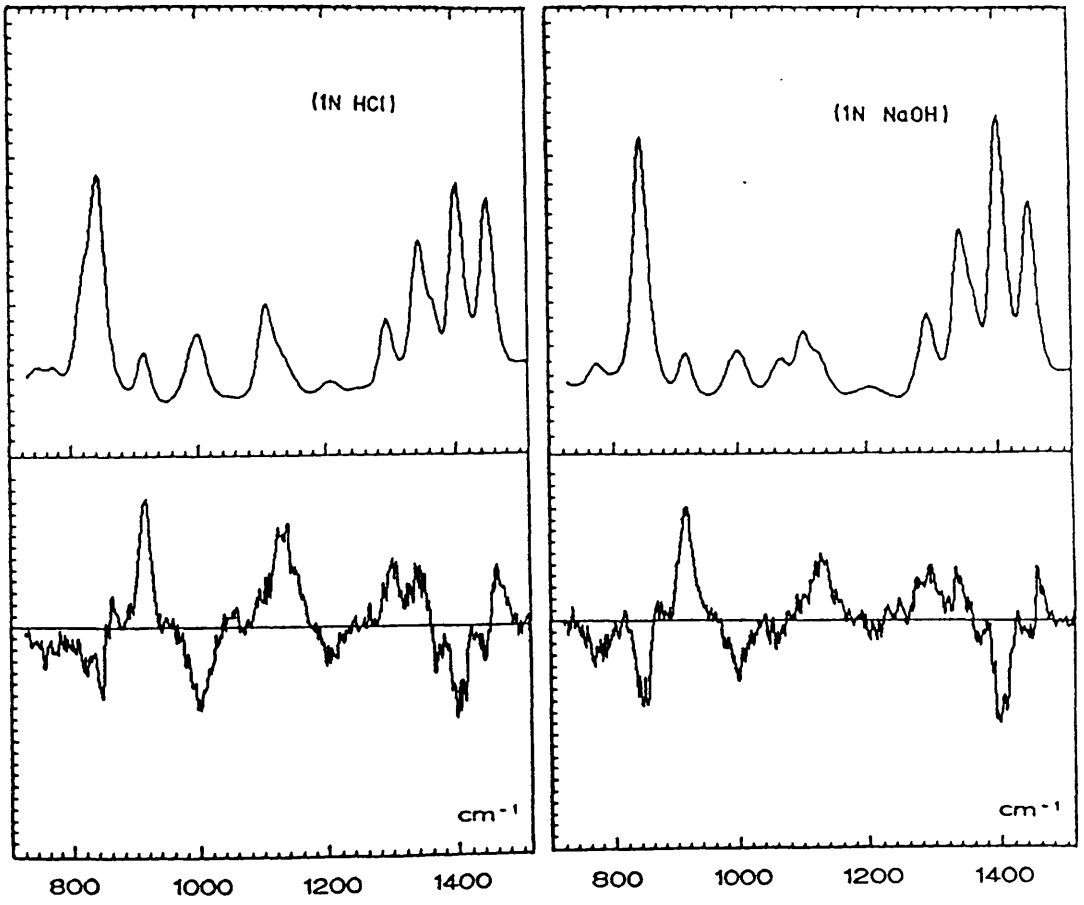

Fig. 4.6. Backscattered Raman (top) and ROA (bottom) spectra of L-alanine in 1N-HCl (left) and 1N-NaOH (right). These spectra were recorded with an unthinned front illuminated CCD using the spectrograph described in chapter 2. The experimental conditions are given in ref. 49.

The first Raman band for which we have a corresponding theoretical calculation occurs at 775 cm^{-1} and exhibits negative ROA intensity. It has

been assigned by Diem *et al.* [92] and by Susi and Byler [98] to the COO^- wagging mode. The corresponding band of crystalline DL-alanine has been identified as a COO^- bending rather than wagging mode [93]. The 6-31G* calculation supports both these assignments since both modes contribute to the theoretical mode at 838 cm^{-1}, and correctly predicts the negative ROA intensity. Perhaps equally important is the agreement between the theoretical calculation and the isotopic substitution data. This band shifts to 747 cm^{-1} upon deuteration of the CH group. The calculated normal mode has components associated with the C^*-H deformation (bend) and a symmetric C^* (where the * refers to the chiral carbon) bend (shown in fig. 4.7) which agrees with the isotopic data.

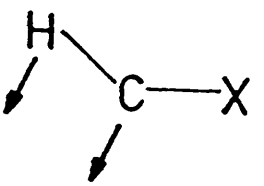

Fig. 4.7. Pictorial representation of the symmetric C^* bend. Adapted from ref. 106

Similar Raman and ROA features appear in the spectra of alanine in >6N-NaOH (fig. 4.5) which is consistent with the COO^- group remaining unprotonated with approximately the same conformation as at neutral pH. However, in the Raman spectrum of the >6N-HCl solution (fig. 4.4) this band shifts to a lower frequency, 746 cm^{-1}, but maintains the same negative ROA pattern. This suggests the normal mode now contains contributions from the COOH group, which is supported by an *ab initio* calculation on neutral alanine which predicts a band with negative ROA intensity in this region arising from the out-of-plane carbonyl deformation plus the O-H torsion.

The next band at 850 cm^{-1} exhibits negative ROA intensity and

appears based on corresponding isotopic data, to be a complex mixture of different normal modes. It has been assigned by Diem *et al.* [92] and by Kettle and co-workers [93] to the symmetric CCN stretch by analogy to its structural and mass equivalent the isopropyl group, whereas Susi and Byler [98] prefer an assignment to a methyl rocking mode. The 6-31G* calculation supports both these assignments, predicting the largest contribution (53%) from the symmetric CCN stretch with a 12% contribution from a methyl rocking mode. Again as with the band at 775 cm^{-1} the calculation supports the isotopic data, predicting additional contributions to the normal mode composition from a symmetric COO^- bending mode and the COO^- wagging mode. This band shifts by 15.5 cm^{-1} [99] in the O^{18} substituted alanine infrared spectrum and by 29 cm^{-1} in the Raman spectrum of alanine in >6N-HCl where the COO^- group is protonated, but still shows negative ROA intensity. This supports the hypothesis that the COO^- group does contribute to the normal mode at 850 cm^{-1}. The calculation on neutral alanine does predict a band with negative ROA intensity in this region arising from the out-of-plane carbonyl deformation plus the C^*-$C(O_2)$ stretch. A similar negative ROA band is observed in the >6N-NaOH solution which supports the assignments above.

The next two bands in the experimental Raman spectrum at 922 and 1000 cm^{-1} will be discussed together. Diem *et al.* [92] assign the first of these bands to a methyl rocking mode and the second to a methyl rock at 995 cm^{-1} plus a C^*-$C(O_2)$ stretch at 1001 cm^{-1} (two bands are observed at this frequency in the solid state Raman spectrum of alanine [92]). A well characterized ROA couplet, positive in the lower frequency band and negative in the higher, appears in the spectra of alanine in water and >6N-HCl solution. However in >6N-NaOH solution the negative

ROA signal is much reduced in intensity and the parent Raman band itself shifts to higher frequency. At first glance it would be tempting to think of this couplet as arising from symmetric and antisymmetric combinations of the two orthogonal methyl rocking coordinates. The 6-31G* calculation on the other hand predicts both signs correctly but suggests a different origin for the ROA. The theoretical band at 942 cm^{-1} is predicted to arise predominantly from the C^*-$C(O_2)$ stretching vibration with additional contributions from the COO^- bend and C^*-N stretch but little contribution from the methyl rocking modes. The next two theoretical modes at 1060 and 1080 cm^{-1}, respectively, corresponding to the experimental bands at 995 and 1001 cm^{-1} (solid state frequencies), are predicted to be essentially composed of NH_3^+ and methyl rocking modes. These theoretical assignments are reinforced by the assignment of the corresponding two bands in crystalline DL-alanine [93] to a C–C stretch and methyl rocking modes, respectively. The data for the >6N-NaOH solution suggest that the primary source of ROA in the solution Raman band at 1000 cm^{-1} is NH_3^+ rocking modes with a small contribution from the corresponding methyl rocking modes, while the band at 922 cm^{-1}, which exhibits similar ROA in all three solutions, arises from the C^*-$C(O_2)$ stretching vibration. Nafie *et al.* [24] have presented an analysis of the band at 922 cm^{-1} along with that at 850 cm^{-1} in terms of coupling of the in- and out-of-phase motions of the methyl C–C stretching mode and the (1,-1) component of the degenerate methyl rocking mode, where the (1,-1) indicates the two hydrogen atoms are adjacent to the hydrogen bonded to the chiral carbon (*vide* rotamer structures in section 4.5). However, the ROA spectrum of serine (*vide* fig. 5.3 in the next chapter), where the methyl group has been replaced by a CH_2OH group, also exhibits this couplet. Thus, it is impossible for the

higher frequency component to arise from a methyl rocking mode. We therefore favour the assignment given above for these two bands with the couplet arising from interactions between the symmetric CCN stretch and the C^{*}-$C(O_2)$ stretch. The above assignments can only be reconciled with those of Diem *et al.* [92] by reconsidering their band assignments for alanine C-d_3 as shown in table 4.3.

All the ROA features discussed so far are at frequencies below the reported mid-infrared VCD studies of alanine [94], so no ROA-VCD comparisons can be made. However, the next three bands at 1110, 1145 and 1210 cm^{-1} in water come within the range of these VCD studies. These bands were assigned by Diem *et al.* [92] to the antisymmetric CCN stretch and NH_3^+ rocking modes respectively, whereas Kettle and co-workers [93] assigned the corresponding bands in the spectrum of crystalline DL-alanine to the antisymmetric CCN stretch and methyl rocking modes. Susi and Byler [98] have assigned the last of these bands to a NH_3^+ rocking mode and suggested that the other two could not be assigned in terms of group frequencies. The broad band at 1145 cm^{-1} shows broad positive ROA intensity whereas the band at 1110 cm^{-1} has either negative (there is evidence of a dip where this band overlaps the 1145 cm^{-1} band) or zero ROA intensity, with the band at 1220 cm^{-1} exhibiting small negative ROA intensity. The ROA spectrum of the >6N-HCl solution is similar to that observed in water but the ROA is larger on the band at 1216 cm^{-1} corresponding to the band at 1220 cm^{-1} in aqueous solution. In >6N-NaOH this region is completely different. There are now four Raman bands at 1078, 1137, 1196 and 1231 cm^{-1}, respectively, which give rise to a negative, positive, positive, positive ROA intensity pattern. Of these the band at 1078 cm^{-1} presumably arises from a vibration of the NH_2 group (perhaps the twisting mode) since it is not

observed in the Raman spectra at other pH values, while the band at

Table 4.3 Revised assignments for alanine-C-d_3

assignment by Diem *et al.* [92]	Solution frequencies from ref. 92 Ala-d_0	Ala-d_3	our assignment Ala-d_3(rev.)	
$\nu CC(O_2)$	1001[a]	941	941	NH_3^+ rock+ CH_3 rock
ζCH_3	995[a]	820	941	NH_3^+ rock+ CH_3 rock
ζCH_3	922	758	921	$\nu CC(O_2)$
$\nu^s CCN$	850	921	820	$\nu^s CCN$
γCOO^-	775		758	γCOO^-

ν, ζ and γ are as defined in table 4.1, a solid state frequency

1137 cm^{-1} can be assigned to a C^*–N stretching mode. The analysis for the other two bands is difficult and will not be discussed further. The 6-31G* calculation correctly predicts the ROA sign for the aqueous bands at 1145 and 1220 cm^{-1} but not for that at 1100 cm^{-1} (assuming that the latter is indeed negative). With respect to normal mode composition the band at 1110 cm^{-1} is predicted to contain C^*-N stretching and C^*-$C(H_3)$ stretching modes (these combined give the antisymmetric CCN stretch) plus NH_3^+ and methyl rocking modes. The band at 1145 cm^{-1} comprises methyl rocking, C^*-H deformation (bending) and NH_3^+ rocking modes (in this order with respect to potential energy contributions). The band at 1220 cm^{-1} contains NH_3^+ and methyl rocking modes. Thus, the *ab initio* normal mode composition appears to be a mixture of that by Diem *et al.* [92] and Kettle and co-workers [93]. The ROA appears to be generated

by NH_3^+ rocking modes in the band at 1110 cm^{-1} since this band disappears in >6N-NaOH solution. The band at 1140 cm^{-1} remains the same in all three solutions which suggests that the ROA is generated by the antisymmetric CCN stretch probably via interaction with an NH_3^+ rocking mode since it appears to be smaller in the >6N-NaOH solution. The fact that the ROA changes sign on the band at ~ 1220 cm^{-1} in the >6N-NaOH solution would indicate that it is generated in zwitterionic alanine by primarily an NH_3^+ rocking mode.

The VCD spectrum of alanine in this spectral region [94] shows negative, negative, positive features, respectively, in infrared bands at 1117, 1139 and 1221 cm^{-1}. The second and third vibrations generate opposite signs in both ROA and VCD. Diem [94] has suggested that coupling between orthogonal NH_3^+ rock coordinates is a plausible mechanism for the generation of VCD in these bands but we favour the interpretation given above in terms of interaction between the antisymmetric CCN stretch and the NH_3^+ rock. The very weak band at 1259 cm^{-1} in the >6N-HCl solution is probably associated with O-H deformations from the intact COOH group (an interpretation supported by the neutral alanine calculation which predicts contributions from the O-H group in this region). It would appear therefore that most of the ROA in this region is generated from the NH_3^+ rocking modes which is supported by the *ab initio* calculation which predicts extensive coupling of the NH_3^+ rocking modes with a variety of other modes in this region.

It is in the next group of five bands that the *ab initio* calculation does not correctly predict the spectra measured experimentally. As mentioned earlier, the first two of these bands at 1301 and 1351 cm^{-1} have been assigned both by Diem *et al.* [92] and Byler and Susi [97] to the orthogonal C^*-H deformations (bends) although Kettle and

co-workers [93] favour the assignment of the second of these to a symmetric methyl deformation (bending) mode (as discussed earlier, we believe this assignment is incorrect). These two bands show very large VCD intensity in both water and D_2O [94,95], although the frequency is shifted slightly in D_2O solution, which suggests contributions to the normal modes from the NH_3^+ group, the VCD pattern remains the same (although the intensity changes) which would indicate that the NH_3^+ group is not the main source of the observed VCD. At high and low pH [95] no distinct features assignable to the methine deformation (bending) modes are observed and the VCD intensity is approximately zero. The VCD intensity in these two modes decreases as the pH is lowered or raised away from the neutral point [95]. It has been suggested by Freedman *et al.* [95] that this VCD feature and its dramatic pH dependence are associated with a ring current mechanism involving electron flow, which is induced by the C^*-H deformations (bends), in the ring closed by hydrogen bonding between the carboxylate and NH_3^+ groups, with an additional interaction between a β-CH and the carboxylate group to form a secondary ring. Recently, Diem [94] has expressed reservations about whether the ring current mechanism can be invoked in this situation and the whole concept of the ring current mechanism in general. His argument is supported in this by recent *ab initio* VCD computational results on methyl lactate and methyl glycolate by Stephens and co-workers [107,108] who demonstrated that the presence of a ring is not essential to generate large VCD intensity in the C^*-H stretching modes, where similar behaviour is observed as a function of pH and a ring current mechanism has also been invoked [96]. VCD signals of comparable magnitude have also been observed in D_2O solution [94] which would also suggest that the ring current mechanism is flawed

in this situation, since one would actually expect slightly stronger "hydrogen bonding" between the ND_3^+ and carboxylate groups and thus a further enhancement of the VCD intensity (which is not observed experimentally). The ROA also exhibits a strong pH dependence. In >6N-HCl (pH ≈ 0) only one band is observed at 1330 cm^{-1} with positive ROA intensity which suggests that vibrations of the COO^- group (probably the symmetric stretch) contribute to the observed ROA in water. This conclusion is also supported by corresponding isotopic data on O^{18} substituted alanine [99] where both these modes shift to lower frequency (*vide* table 4.1). In >6N-NaOH solution (pH ≈ 14) two bands occur at 1286 and ~ 1325 cm^{-1} which are probably due to these orthogonal C^*-H deformations (bends). Both give rise to positive ROA. This same behaviour is reflected in VCD studies in D_2O solution where the bands shift in frequency but the VCD pattern remains the same. This would suggest (*vide supra*) that the NH_3^+ group does contribute to the normal mode but has no significance for the generation of VOA. The 6-31G* calculation predicts that four modes at 1395, 1447, 1501 and 1523 cm^{-1} have significant contributions from the C^*-H deformation (bending) mode, and of these two at 1395 and 1523 cm^{-1} are predicted to have positive ROA intensity. It would be tempting to assign the experimental bands at 1301 and 1351 cm^{-1} to these theoretical modes. However, the theoretical band at 1523 cm^{-1} should be correlated with a theoretical band at 1552 cm^{-1} in the 6-31G calculation [49] which, in agreement with experiment, contains the symmetric NH_3^+ bend as the major component of the normal mode. This suggests a problem with the 6-31G* basis set which, instead of giving a plausible group frequency for this mode, mixes it into several other bands including the one at 1395 cm^{-1} (which we will correlate to the experimental band at 1301 cm^{-1}) and probably

contaminates the normal mode compositions in this spectral region. This may explain the lack of success of the *ab initio* calculation in predicting the ROA sign and normal mode composition for the C^*-H orthogonal deformations (bends). A similar effect is found for the C^*-H deformation (bending) modes in an *ab initio* calculation on tartaric acid [51] where hydrogen bonding causes major differences between the experimental and theoretical spectra.

The methyl symmetric deformation (bending) mode at 1375 cm^{-1} in aqueous solution gives rise to negative ROA intensity. A similar feature is observed in >6N-HCl solution (where it is more pronounced due to a frequency shift of the C^*-H deformation (bending) modes). In >6N-NaOH solution, however, it appears to exhibit no significant ROA intensity. This would suggest that the ROA is generated by interactions of the methyl group with the NH_3^+ group. The VCD on this band [94] appears to vanish in D_2O solution which would support our hypothesis that the VOA is generated by interactions of the methyl group with the NH_3^+ group. The 6-31G* calculation correctly predicts the ROA sign for this band.

The next experimental band at 1410 cm^{-1} is usually assigned to the symmetric stretch of the COO^- group [92,93,97]. Only a normal coordinate analysis of alanine by Susi and Byler [98] disagrees with this assignment (they suggest that the COO^- symmetric stretch is highly mixed with other modes). This band gives rise to a positive VCD signal in water but has little or no VCD intensity in D_2O solution. In water it gives rise to negative ROA intensity which disappears completely in >6N-HCl. This observation confirms the assignment of this band to the symmetric stretching vibration of the COO^- group. In >6N-NaOH there appears to be a couplet, positive on the lower frequency side and negative on the higher. This, together, with the VCD results, suggests

that the VOA may originate in interactions between the carboxylate and NH_3^+ groups. The 6-31G* calculation, as with the C*-H deformation (bending) modes, is not very helpful here. In neither of the two remaining unassigned theoretical modes at 1447 and 1505 cm^{-1} do contributions from the COO^- group dominate although both have negative ROA intensity. We favour the correlation of the 1447 cm^{-1} band with the other C*-H deformation (bending) mode (although it has the wrong ROA sign) and the 1505 cm^{-1} band with the experimental band at 1410 cm^{-1}. The neutral alanine calculation predicts strong mixing of the COO^- symmetric stretch with the C*-H deformations (bends) and the symmetric methyl deformation (bending). The mode at 1505 cm^{-1} is predicted to have a contribution from the C*-H deformation (bending) modes. It may be that the calculation fails here due to Fermi resonance (*vide supra*) since the intensity of the theoretical modes and experimental bands do not agree with each other.

The next band, at 1460 cm^{-1}, has been assigned to the degenerate pair of antisymmetric methyl deformations [92,93,97-99]. It exhibits an ROA couplet, negative on the lower frequency side and positive on the higher, at low, neutral and high pH. This band has no observable VCD intensity. The ROA in the two split antisymmetric methyl deformations (bends) is probably generated through coupling with other modes. This situation is similar to the much studied case of arylethanes [79] where ROA couplets are generated in the antisymmetric methyl deformations (bends) through coupling with an aromatic mode that coincides in frequency. If a similar situation applies here then the other band has to be either a combination or difference band, since only one of these modes would have a similar frequency as compared with the frequency of the antisymmetric methyl deformation (bend). The 6-31G* calculation

correctly predicts the sign of this ROA couplet and the normal mode composition.

The remaining Raman bands, which can be assigned to the antisymmetric COO^- stretching mode and the symmetric and antisymmetric NH_3^+ bending modes, show no ROA intensity. The 6-31G* calculation reproduces these normal modes accurately with the exception of the symmetric NH_3^+ bending mode (*vide supra*).

The Raman and ROA spectra of alanine in 1N-HCl and 1N-NaOH (fig. 4.6) solutions can be identified as a combination of those in >6N-HCl and >6N-NaOH plus the spectrum measured in water, which indicates that the ROA in 1N-HCl and 1N-NaOH solutions is generated by the zwitterionic species.

4.4 Conclusions

This detailed study has demonstrated that the correlation between the experimental and theoretical spectra, both Raman and ROA, is satisfactory which is perhaps surprising if the size of the alanine molecule is considered. It is worth emphasizing that the absolute configuration of a chiral molecule follows automatically, with a high degree of confidence, from an *ab initio* calculation that correctly predicts most of the observed ROA features and thus provides a method for determining the absolute stereochemistry of chiral molecules without resorting to semi-empirical approximations. At the same time ROA can probe a wider range of frequencies without the associated solvent problems as compared with VCD, since water is an excellent solvent for Raman spectroscopy. The pH dependence study suggests that the behaviour or ROA and VCD is similar with respect to this experimental variable.

It has been suggested by Himmler and Eysel [109], based on changes in depolarization ratios, that at high concentrations (>1 mol l^{-1}) amino acids may form micelles with the carboxylate groups arranged with a fixed geometrical orientation to one another. The ROA spectrum of a 0.5 M solution of alanine (not shown) shows no significant differences from that shown here (fig. 4.2) for a 1.7 M solution which would seem to cast doubt on the micelle theory.

4.5 ROA and vibrational analysis of alaninol

Alaninol (2-amino-1-propanol) is, by analogy to alanine the simplest chiral amino alcohol. It differs from alanine in that a CH_2OH group has replaced the COO^- moiety of alanine, so that its physical properties are rather different from alanine. It is a viscous liquid which means that it has to be transferred directly into a cell rather than being distilled as usual. We recorded its Raman and ROA spectra in anticipation that they would assist the vibrational analysis of alanine.

Whereas alanine can exist in only one rotameric form I, alaninol can exist in three rotameric forms, II-IV. Intuitively, rotamer IV would seem

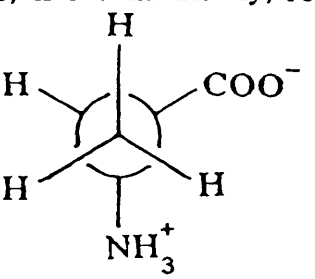

I

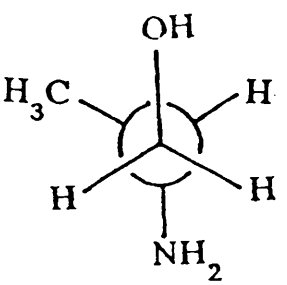

II

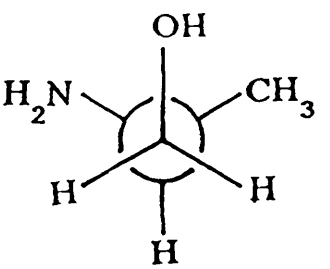

III

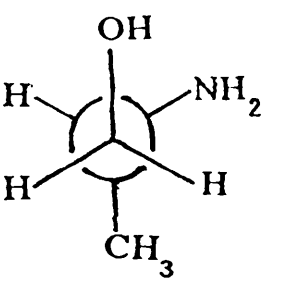

IV

to be lowest in energy since it allows hydrogen bonding between the amine and hydroxyl groups while minimizing steric interactions. However, in the discussion that follows the presence of contributions from rotamers II and III to the ROA cannot be ruled out completely.

The Raman (top) and ROA (bottom) spectra of L-alaninol are displayed in fig. 4.8. The corresponding vibrational frequencies, ROA Δ-values and suggested vibrational assignments are presented in table 4.4.

The ROA on the first two Raman bands at 815 and 851 cm^{-1} is unreliable due to polarization artefacts and will not be discussed further. The next band at 946 cm^{-1} shows negative ROA intensity and, by analogy with the assignment of the corresponding band at 922 cm^{-1} in alanine to the C^*-$C(O_2)$ stretch, we suggest this band be assigned to the C^*-$C(H_2OH)$ stretch, which, due to mass differences might be expected to occur at a slightly higher frequency in alaninol as compared to alanine. The change in sign of the ROA is less easy to explain, but assuming that the ROA is generated in a similar fashion in this molecule as in alanine (via interactions between the symmetric CCN stretch and the C-C stretch), it may be that in the dominant conformation these two groups are held in a different orientation with respect to one another.

The adjacent band at 1003 cm^{-1} exhibits negative ROA intensity. The corresponding Raman band at ~ 1000 cm^{-1} in alanine which also exhibits negative ROA intensity has been assigned by us to a mixture of NH_3^+ and methyl rocking modes with the ROA originating from the NH_3^+ rocking coordinates. In alaninol the ROA must presumably be associated with the methyl rocking modes as in alanine in >6N-NaOH solution. Although contributions to the normal mode from the symmetric CCO stretching vibration cannot be ruled out.

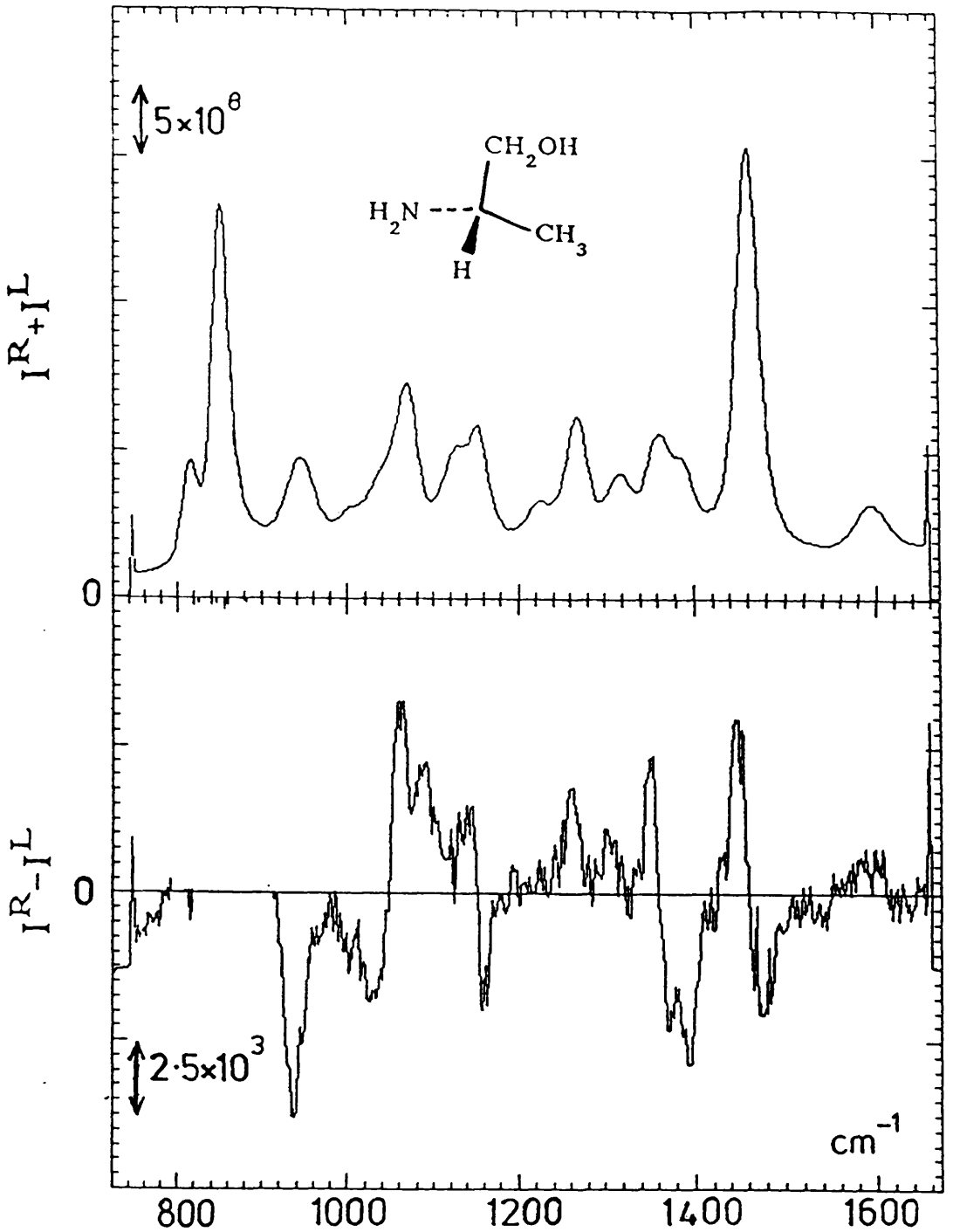

Fig. 4.8. Backscattered Raman (top) and ROA (bottom) spectra of neat L-alaninol. These spectra were recorded on the old Glasgow multichannel ROA instrument [67] equipped with an unthinned front illuminated CCD. Experimental conditions: exposure time 0.5 s, laser power 500 mW, acquisition time 2 hours.

Table 4.4 Vibrational frequencies, ROA Δ-values and assignmennts for L-alaninol

Frequencies (cm^{-1})		$\Delta(180^0)\times10^5$	Vibrational assignments
815			
851			
946		-17.3	C^*-$C(H_2OH)$ stretch
1003		-23.6	CH_3 rock + sym CCO stretch
	1028[a]	-5.01	
1045			complex normal mode composition see
	1062[a]	+9.58	text for details
1069			asym CCO stretch
1128			CH_3 rock
	1144[a]	+2.12	
1152			NH_2 twist + asym CCN stretch
	1162[a]	-2.63	
1226			CH_2 wag + O-H def
1268		+6.37	CH_2 twist
1318		+12.0	C^*H bend
	1350[a]	+8.98	
1361			C^*H bend
	1371[a]	-9.21	
1383		-19.4	sym CH_3 bend
	1445[a]	+2.11	
1460			asym CH_3 bend + CH_2 bend
	1475[a]	-1.49	

a position of ROA bands

The next two bands in the Raman spectrum give rise to an ROA couplet centered at ~ 1045 cm^{-1}, negative on the lower frequency side and positive on the higher, and a positive ROA band at 1086 cm^{-1}, for which no parent Raman band can be identified. The alanine spectrum at high pH shows a band at similar frequency with negative ROA intensity, which we assign to a vibration of the NH_2 group. A similar assignment appears to be also plausible for alaninol. The ROA couplet is probably generated by interactions between the C-C, C^*-N and C-O stretching modes plus the C-O-H and C-C-H deformations which generate large ROA in this region in carbohydrates [48]. In the Raman spectrum of serine (*vide* fig. 5.3 in the next chapter) we have assigned a band at 1052 cm^{-1} with virtually zero ROA intensity to the antisymmetric CCO stretching vibration. We therefore assign the alaninol Raman band at 1069 cm^{-1}, which also exhibits no ROA intensity, to this mode.

The next Raman band at 1128 cm^{-1} exhibits no ROA intensity and can probably be assigned to a methyl rocking mode which occurs in this spectral region in alanine. An ROA couplet, positive on the lower frequency side and negative on the higher, is observed in the next band at 1152 cm^{-1}. No similar ROA feature is identified in the alanine spectra which exhibits two bands in this region at 1110 and 1145 cm^{-1}. One possible assignment is to methyl rocking modes which in alanine are strongly mixed with the NH_3^+ rocking modes and the antisymmetric CCN stretch in this region. Another possible assignment is to a NH_2 twisting mode which occurs in this spectral region in proline and 4-hydroxyproline (*vide* chapter 6).

The Raman band at 1226 cm^{-1} which exhibits no ROA intensity can be assigned to a CH_2 wagging mode by analogy with serine (*vide* section 5.2.2 in the next chapter).

We then focus on the region of the Raman spectrum which is of most interest in alanine. The first two bands at 1268 and 1318 cm^{-1} exhibit positive ROA intensity. We assign two bands at 1301 and 1351 cm^{-1}, respectively, in the spectra of alanine to the orthogonal C^*-H deformation (bending) modes and since the ROA has the same sign we propose the latter of these bands in alaninol also be assigned to one of these C^*-H deformation (bending) modes. The former band can be assigned, by analogy with serine (*vide* section 5.2.2 in the next chapter) to a CH_2 twisting mode. The next Raman band at 1361 cm^{-1} shows an ROA couplet, positive on the lower frequency side and negative on the higher, while its high frequency neighbour at 1383 cm^{-1} exhibits negative ROA intensity. One of these bands must be associated with the methyl symmetric deformation (bending) which occurs at 1375 cm^{-1}, with negative ROA intensity, in the spectra of alanine. Since the band at 1383 cm^{-1} also exhibits negative ROA intensity we will assign it to the symmetric methyl deformation (bending) while the band at 1361 cm^{-1} can be assigned to the other C^*-H deformation (bending) mode.

The final band to show ROA occurs at 1460 cm^{-1} and is readily assignable to the degenerate antisymmetric methyl deformation (bending) mode and a CH_2 bending mode. It exhibits an ROA couplet, positive on the lower frequency side and negative on the higher, which is the opposite of that seen in the corresponding band in the spectrum of alanine. In arylethanes the generation of this mode via coupling of the degenerate antisymmetric methyl deformations with other modes is relatively easy to explain and a similar situation occurs here with the other mode being the adjacent CH_2 bending mode. In alanine the presence of another mode is less easy to explain (*vide supra*) but it may be that the methyl antisymmetric deformations (bends) are already sufficiently

split to generate ROA intensity.

4.6 Summary

The Raman and particularly the ROA spectra of alanine and alaninol are sufficiently different to emphasize the unique sensitivity of the ROA experiment. Comparison of the two sets of spectra discloses the origin of the ROA and the vibrational assignments of these two molecules, especially the alanine band at 1410 cm^{-1}. Due to lack of sensitivity, ROA on dilute solutions (<0.3M) is not practical at the moment. This means that a detailed concentration dependence study over the range 1.5-0.05 M could not be performed and thus hopefully resolve the question of the predominance of intermolecular versus intramolecular interactions in highly concentrated solutions of alanine. Even with all the data collected in this thesis the complete vibrational analysis of alanine remains elusive. However, the remaining problems in the vibrational analysis of alanine could well be resolved from ROA measurements of isotopically substituted alanine derivatives.

5.1 Introduction

In the preceeding chapter we discussed the ROA observed in the simplest naturally occuring chiral amino acid, alanine, and its amino alcohol analogue, alaninol. We now proceed to examine the Raman and ROA spectra of other simple naturally occuring amino acids which can be considered to be derived from alanine by formal substitutions. These can be divided into two classes: (i) serine and cysteine which differ from alanine by replacement of a hydrogen atom of the alanine methyl group with a hydroxyl or mercaptyl group, respectively (fig. 5.1), and (ii) valine,

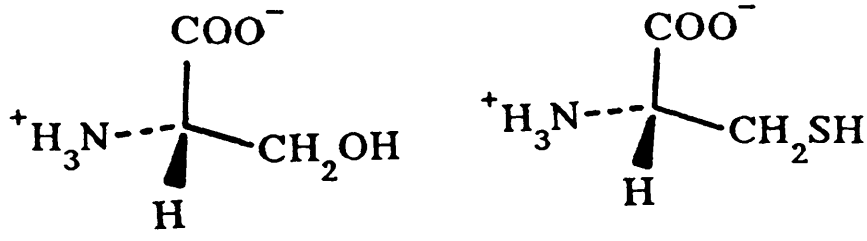

Fig. 5.1. Structures of L-serine (left) amd L-cysteine (right).

where two methyl groups replace two hydrogen atoms of the alanine methyl group; threonine, where a methyl and a hydroxyl group replace two hydrogen atoms of the alanine methyl group; and isoleucine, where two hydrogen atoms of the alanine methyl group have been replaced by a methyl and an ethyl group, respectively (fig. 5.2). Other possible schemes exist to classify the amino acids above but the one used here is the most convenient for comparative vibrational studies. Like alaninol the amino acids studied in this chapter can exist in three possible miniumun energy staggered rotameric forms, V-VII, which are shown on top of table 5.1. The fractional populations of these rotamers, p_V-p_{VII}, which have been calculated for selected pD values using coupling constants and

Table 5.1
Rotamer populations of selected amino acids

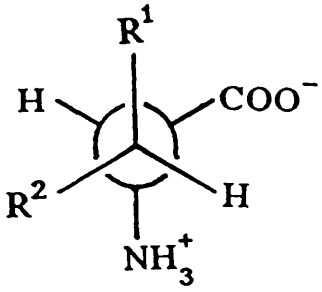

V

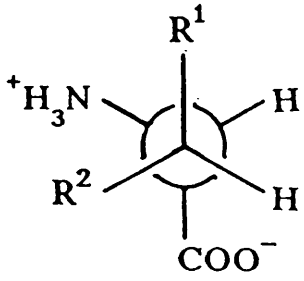

VI

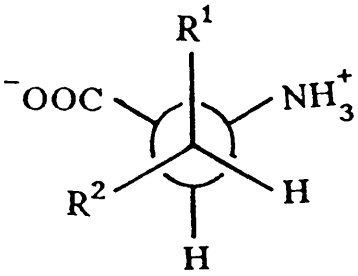

VII

Compound	R_1	R_2	pD	p_V	p_{VI}	p_{VII}
Serine[a,b]	OH	H	0.5	0.07	0.16	0.77
			7.5	0.10	0.28	0.62
			12.2	0.15	0.30	0.55
Cysteine[c,d]	SH	H	0.4	0.14	0.27	0.59
			13.2	0.07	0.56	0.37
Valine[b]	CH_3	CH_3	0.5	0.17	0.50	0.33
			5.7	0.17	0.59	0.24
			11.9	0.23	0.61	0.16
Threonine[b]	CH_3	OH	0.1	0.12	0.80	0.08
			5.1	0.21	0.72	0.07
			11.1	0.22	0.68	0.10
Isoleucine[e]	CH_3	CH_3CH_2	0.1	0	0.34	0.66
			7.3	0	0.50	0.50
			12.0	0.05	0.61	0.34

a from ref. 110, b from ref. 111, c from ref. 112, d from ref. 113, e from 114.

chemical shifts from ^{1}H and ^{13}C nuclear magnetic resonance (NMR) studies [110-114] are listed in table 5.1.

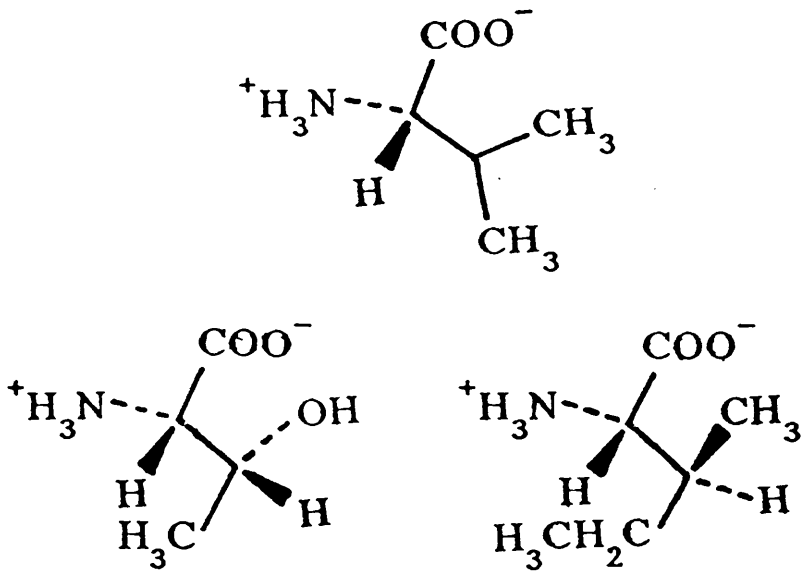

Fig. 5.2. Structures of L-valine (top), L-threonine (bottom left) and L-isoleucine (bottom right).

5.2 Serine

5.2.1 *Introduction*

From table 5.1 it can be seen that at pD = 7.5 the dominant rotamer of serine (2-amino-3-hydroxypropinoic acid) in solution is VII with a population of 62%. Our spectra are recorded at pH ~ 7, therefore we will assume that the population at this pH is similar to the figure quoted above. The major species in solution is relatively insensitive to pH changes and so the possibility of changing the major conformer by varying the pH and observing any differences in the ROA spectrum due to changes in conformation does not arise for this molecule (but needs to be considered for other molecules). A ROA study as a function of pH would still be a useful experiment in order to assist the assignments of bands due to the NH_3^+ and COO^- groups [50]. Unfortunately lack of time precluded such a study.

The vibrational analysis of serine has been reported by Susi *et al.* [115], based on polycrystalline Raman spectra of two isotopically substituted derivatives of serine (unfortunately they assumed the wrong conformation (V)) and a normal coordinate analysis similar to that for alanine [98]; Machida and co-workers [116], using a modified Urey-Bradley normal coordinate analysis and the Raman spectra of serine and oxygen and nitrogen deuterated DL-serine single crystals; and Inomata *et al.* [117] who measured the infrared spectra of serine and four metal-DL-serine chelates and their deuterated analogues and performed a normal coordinate analysis. Extensive use will be made of these assignments when considering the origin of the ROA observed in this molecule. No mid-infrared VCD spectrum of serine has been reported so unlike alanine no comparisons can be made in this region.

5.2.2 *Vibrational analysis and ROA of serine*

The Raman (top) and ROA (bottom) spectra of L-serine in H_2O solution, pH $\approx$ 7, are shown in fig. 5.3. The corresponding Raman frequencies, ROA Δ-values and suggested vibrational assignments are given in table 5.2.

Beginning at low frequency the ROA spectrum of serine shows a negative signal at $\sim$ 620 cm^{-1} for which the parent Raman band cannot be identified. A band at this frequency has been assigned in Raman studies of crystalline serine to either COO^- bending [115,116] or wagging [117] vibrations. Since a similar Raman band appears at approximately the same frequency and also with negative ROA intensity in the spectrum of alanine which has been assigned by us to a bending mode of the COO^- group, the assignments by Susi *et al.* [115] and Machida and co-workers [116] of this band to carboxylate bending modes seem correct for serine.

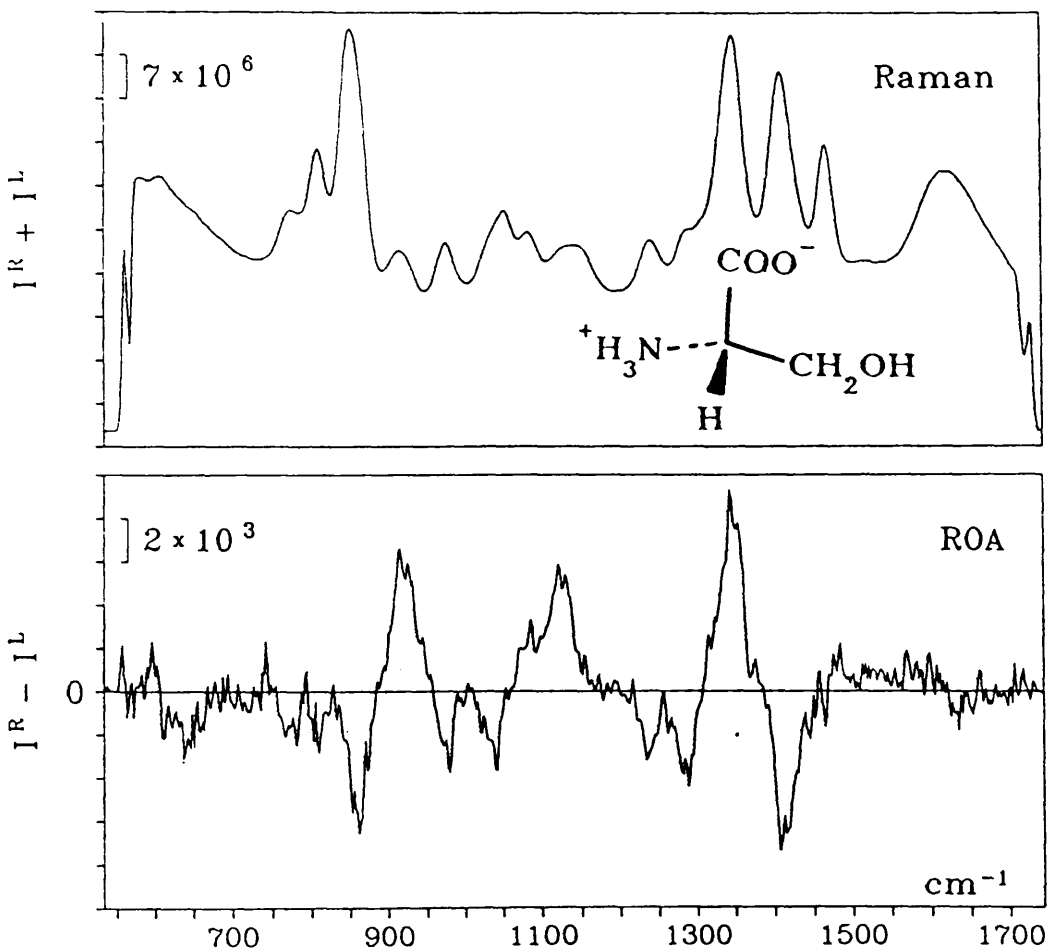

Fig. 5.3. Backscattered Raman (top) and ROA (bottom) spectra of L-serine in aqueous solution. Experimental conditions: exposure time 3 s, laser power 750 mW, acquisition 2 hours, slit width 0.12 mm.

Table 5.2 Raman frequencies, ROA Δ-values and vibrational assignments of L-serine in aqueous solution

Frequencies (cm^{-1})	$\Delta(180^0)\times10^4$	Vibrational assignments
620	negative	COO^- bend
773	-2.41	COO^- wag
809	-1.41	CH_2 rock
851	-2.07	sym CCN stretch
919	+11.7	C^*-$C(O_2)$ stretch
978	-5.03	sym CCO stretch
1040	-4.63	NH_3^+ rock
1052		asym CCO stretch
1083	+2.96	C^*–N stretch
1125	+9.57	NH_3^+ rock
1150		NH_3^+ rock
1242	-5.64	CH_2 wag+ in-plane O-H def
1294	-5.87	CH_2 twisting
1347	+2.86	C^*H bend
1412	-2.65	sym COO^- stretch
1460		CH_2 bend

The assignment of the next Raman band at 773 cm which exhibits negative ROA intensity is more complicated. Inomata *et al.* [117] assigned a very weak infrared band at 782 cm^{-1} to a CH_2 rocking mode, while Machida and co-workers [116] prefer the assignment of a solid state Raman band at 750 cm^{-1} to the COO^- wagging vibration and a solid state band at 815 cm^{-1} to the CH_2 rocking mode. At first glance, it would appear that this band would have to shift by ~ 40 cm^{-1} on going from the infrared spectrum to the Raman spectrum for these assignments to agree. However, it should be born in mind that this is based on the comparison of the spectra of L-serine with DL-serine and that these two samples need not have the same physical properties (for example the solubilities of L and DL amino acids are often dramatically different). Thus, the frequency shift does not need to be as large as it would first appear to be. The Raman spectrum recorded by Susi *et al.* [115] also has two bands in this region, at 728 cm^{-1}, arising from C-O-H torsion and CH_2 rocking modes and at 815 cm^{-1}, arising from C-O-H torsion, COO^- bending and COO^- wagging modes. However, the Raman spectrum of alanine has a band at 775 cm^{-1} which exhibits negative ROA intenstiy and which we have assigned to the carboxylate wagging mode (*vide supra*). The Raman spectrum of cysteine has a band at 779 cm^{-1} whose ROA is uncertain. The presence of a band at virtually the same frequency in all three spectra would suggest that it has the same origin namely a vibration of the COO^- group (probably the wagging mode).

The next band in the Raman spectrum of serine occurs at 809 cm^{-1} and exhibits negative ROA intensity. No similar band is observed in the Raman spectrum of alanine which suggests that it originates from either the CH_2 or the O-H group or a mixture of both. Inomata *et al.* [117] observe an infrared band at this frequency but do not assign it to a

particular vibration. The assignment of this band is therefore uncertain but would appear to be most probably a CH_2 rocking mode. The extra sensitivity of ROA is helpful here since the ROA spectrum of cysteine (fig. 5.4) also has a negative band at this frequency which indicates that it almost certainly arises from a CH_2 rocking mode.

The following two Raman bands will be discussed together; they occur at 851 and 919 cm^{-1} and exhibit negative and positive ROA intensity, respectively. Machida *et al.* [116] assign both bands to C-C stretching modes. This assignment is supported by Inomata and co-workers [117] for the lower frequency band (they do not assign the higher frequency band). The normal coordinate analysis by Susi *et al.* [115] suggests that both these bands have a complex normal mode composition, primarily involving the COO^- group but without a C-C stretching component. Similar Raman and ROA bands are observed in the spectra of alanine and we suggested that they arose from coupling of the symmetric CCN stretch with the C^*-$C(O_2)$ stretching mode. The presence of a similar feature in the serine spectra would indicate that it also has the same origin. Cysteine also exhibits a similar ROA signal pattern but at slightly different frequency.

The Raman and ROA spectrum of alanine are dominated by NH_3^+ rocking modes in the region 950-1250 cm^{-1}. It seems appropriate therefore to discuss together the bands that occur in this region in the spectrum of serine. The first of these bands occurs at 978 cm^{-1} and exhibits negative ROA intensity. It has been assigned by both Machida *et al.* [116] and Susi and co-workers [115] to a C-O(H) stretching vibration. However, they dispute the effect of deuterium substitution on this mode, Machida *et al.* [116] suggest that a new band at 985 cm^{-1} in the spectrum of the serine-N-d_3-O-d_1 species is still the C-O(D) stretching

vibration, while Susi and co-workers [115] suggest that this new band is assigned to a C-O-D bending vibration. The next band occurs at 1052 cm^{-1} and exhibits no discernible ROA intensity. It has a low frequency shoulder at ~ 1040 cm^{-1} with negative ROA intensity. Inomata *et al.* [117] assign the band at ~ 1040 cm^{-1} to the C-O(H) stretching vibration which is supported to some extent by Susi *et al.* [115] who predict that the principal component of the normal mode will be the C-O(H) stretch along with NH_3^+ rocking modes, while Machida and co-workers [116] prefer an assignment to the CCN stretching mode. The subsequent band at 1083 cm^{-1} exhibits positive ROA intensity. Machida *et al.* [116] assign this band to a mixture of NH_3^+ rocking and C^*-N stretching modes which agrees with the assignment of Inomata and co-workers [116] who also assigned this band to a C^*-N stretching vibration as did Susi *et al.* [115]. The next feature contains two Raman bands, the first of these, at 1125 cm^{-1}, exhibits positive ROA intensity, while the second, at ~ 1150 cm^{-1} exhibits no ROA intensity. Inomata *et al.* [117] assign the latter band to a NH_3^+ rocking mode, while Machida and co-workers [116] assign the former to a NH_3^+ rock and the latter to a mixture of NH_3^+ rock and CH_2 wagging vibrations. Susi *et al.* [115] assign the first band to a NH_3^+ rock and the second to a complex mixture which contains NH_3^+ rock as the primary component. The last band in this region occurs at 1242 cm^{-1} and gives rise to negative ROA intensity. Susi *et al.* [115] assign it to a C-O-H bending vibration, while Machida and co-workers [116] assign it to the in-plane O-H deformation as do Inomata *et al.* [117]. According to Dollish, Fately and Bentley [118] primary alcohols like serine are expected to have three bands in this region. Beginning at low frequency these are the symmetric CCO stretch at ~ 965 cm^{-1}, the antisymmetric CCO stretch at ~ 1060 cm^{-1} and a band due to a mixture of CH_2 twist and

C-O-H bending modes at ~ 1250 cm^{-1}. We will now attempt to rationalize these data to provide a plausible vibrational analysis for serine in this region. The first band at 978 cm^{-1} can be assigned to the symmetric CCO stretching vibration with its primary component being a C-O(H) stretch. The next band at ~ 1040 cm^{-1} probably arises from a NH_3^+ rocking mode since two bands at ~ 1000 cm^{-1} with overall negative ROA intensity in the spectrum of alanine were assigned by us to NH_3^+ rocking modes. The band at 1052 cm^{-1} may well arise from the antisymmetric CCO stretch. However, one might expect such a mode, which encompasses a highly chiral twisted structure, to generate large ROA intensity. The assignment of this band must therefore be considered as uncertain. The adjacent band with positive ROA intensity at 1083 cm^{-1} can be assigned to a C^*-N stretching vibration (*vide supra*) by analogy with a similar feature in alanine at slightly higher frequency, here however, it is probably mixed with NH_3^+ rocking coordinates. The C^*-N stretching vibration in glycine has also been assigned to a band at about this frequency [118]. The next band at 1125 cm^{-1} can be assigned to a NH_3^+ rocking mode. This mode which also exhibits positive ROA intensity occurs at 1110 cm^{-1} in the spectrum of alanine. The next band at 1150 cm^{-1} can be assigned to another NH_3^+ rocking mode, although it may have significant contributions from a CH_2 twisting mode which occurs in this region in the spectrum of glycine [118]. The final band in this region at 1242 cm^{-1} can be assigned to an in-plane O-H deformation coupled to a CH_2 wagging mode. Alanine has a NH_3^+ rocking mode in this region, also with negative ROA intensity. So the band at 1242 cm^{-1} in the serine spectrum may also have a NH_3^+ rock contribution to the normal mode. One possible way of examining the contributions to the normal modes and ROA of the NH_3^+ rocking modes is to study the Raman and

ROA spectra of serine at high pH, in a similar fashion to that reported in the last chapter for alanine, where the NH_3^+ group has been replaced by the NH_2 group, since this would enable one to observe changes in the ROA intensity pattern and to relate these changes to NH_3^+ rocking modes (unfortunately lack of time precluded such a study).

The assignments in the next region of the spectrum, ~ 1300-1460 cm^{-1}, are much easier, since all of the bands can be readily assigned via group frequencies and are therefore less ambiguous than in the preceeding region. The first of these bands occurs at 1294 cm^{-1} and exhibits negative ROA intensity. All three vibrational analyses [115-117] assign it to a vibration of the CH_2 group either twisting or wagging. The next band at 1347 cm^{-1} shows positive ROA intensity and can be assigned [115-117] to one of the orthogonal C^*-H deformation (bending) modes. This band occurs at the same frequency also with positive ROA intensity in the spectra of alanine which supports the assignment above. The other C^*-H deformation (bending) mode is also predicted [116] to occur in this region although some authors [115,117] favour the assignment of the other observed solid state Raman band to a CH_2 mode. The only way to clarify this situation is to perform a Raman and ROA study on serine-CD and serine-CD_2 and investigate changes in the Raman and ROA spectra. This should enable unambiguous assignments of modes due to the CH and CH_2 groups, respectively. As for the other amino acids studied so far the symmetric COO^- stretch is readily identified as a band at 1412 cm^{-1} with negative ROA intensity. Again as in alanine this band seems to be coupled to both the NH_3^+ group and the CH group, since deuteration of these groups results in significant frequency shifts of ~ 15 cm^{-1} for this band [115]. The final Raman band in this region at ~ 1450 cm^{-1} exhibits no ROA intensity, unlike the same band in the spectrum of cysteine (*vide*

infra) which shows positive ROA intensity. It can be assigned [115-117] to a bending vibration of the CH_2 group.

5.3 Cysteine

5.3.1 *Introduction*

Like serine, cysteine (2-amino-3-mercaptopropionic acid) can exist in three rotameric forms V-VII which are shown in table 5.1. Unlike serine, however, the conformation adopted by cysteine in solution is strongly dependent on pD (*vide* table 5.1), presumably due to electrostatic interactions between the S^- and COO^- groups, which are unfavourable at high pH. Unfortunately no NMR data is available for cysteine at neutral pH which is the pH at which we performed our ROA study. Our data (*vide infra*) suggest that the dominant conformer of cysteine in aqueous solution may be different from that observed for serine under similar conditions. The NMR data by extrapolation from the results for the other amino acids suggests that there are two dominant conformers of cysteine at neutral pH.

The vibrational analysis of cysteine is less well documented than that of serine but Susi *et al.* [115] have provided a normal coordinate analysis based on the solid state Raman spectra of cysteine and one isotopomer similar to that for serine. However, as for serine they assumed the wrong minimum energy conformation (V). Sze and co-workers [119] have presented a limited vibrational analysis of cysteine based on both solid state Raman and infrared spectra of cysteine and some related compounds. Ozaki *et al.* [120] have also studied the Raman spectrum of cysteine in the vicinity of the C-S stretching vibration. No VCD of this molecule has been reported in the region discussed in the present work.

5.3.2 *Vibrational analysis and ROA of cysteine*

The Raman (top) and ROA (bottom) spectra of L-cysteine in water, pH ≈ 7, are shown in fig. 5.4. The corresponding Raman frequencies, ROA Δ-values and suggested vibrational assignments are presented in table 5.3.

Beginning at low frequency the first Raman band at 615 cm^{-1} exhibits negative ROA intensity. As in alanine and serine (*vide supra*) we assign this band in cysteine to the carboxylate bending mode. Susi *et al.* [115] assign the corresponding solid state Raman band to the COO^- bending mode. Adjacent to this is a band at 685 cm^{-1} with positive ROA intensity which must originate from the C-S stretch [115,119,120]. The ROA in these two bands presumably originates in coupling between the C-S stretch and the COO^- bending mode. Inspection of structures V and VII shows that these two groups are held in a chiral arrangement to one another and any interaction between them would thus be expected to produce significant ROA intensity. This also gives information regarding the rotamer populations since to a first approximation (ignoring any interactions with other parts of the molecule) the ROA would be expected to cancel for a 50:50 mixture of these two rotamers. No ROA would be expected from structure VI since these two groups are held at 180^0 to one another (a position where the ROA is at a minimum). Interaction between the C-S stretch and adjacent bands is also observed in other molecules containing this moiety such as α-phenyl-ethylthiol [121]. Ozaki and co-workers [120] have suggested (in opposition to the NMR results where by analogy with the other amino acids (*vide* table 5.1) we would expect two confomers in solution) that only one rotamer of cysteine exisits in aqueous solution, VII (*vide* table 5.1) based on comparisons between Raman spectra of the two different crystal forms

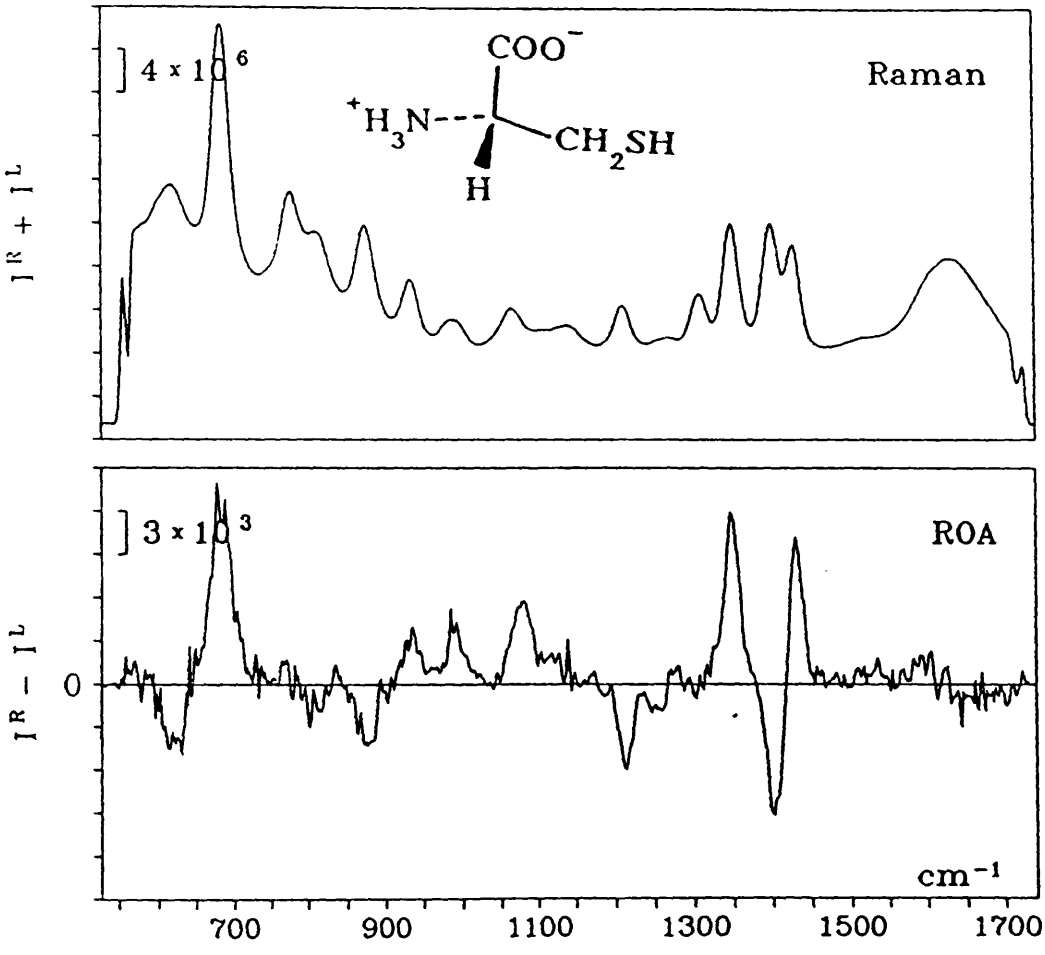

Fig 5.4. Backscattered Raman (top) and ROA (bottom) spectra of L-cysteine in aqueous solution. Experimental conditions: exposure time 4 s, laser power 650 mW, acquisition time 3 hours, slit width 0.12 mm.

Table 5.3 Raman frequencies, ROA Δ-values and vibratonal assignments for L-cysteine in aqueous solution

Frequencies (cm^{-1})	$\Delta(180^0)\times10^4$	Vibrational assignments
615	-6.56	COO^- bend
685	+3.27	C-S stretch
779	positive ?	COO^- wag + C-S-H def
813	-1.54	CH_2 rock
875	-3.34	sym CCN stretch
936	+4.47	C^*-$C(O_2)$ stretch
990	+13.2	NH_3^+ rock
1069	+9.74	C^*-N stretch
1118	+7.84	NH_3^+ rock
1145		CH_2 rock
1211	-8.50	CH_2 wag
1258[a]	-15.6	
1268		CH_2 twist
1278[a]	+8.98	
1312		
1351	+6.36	C^*H bend
1403	-4.59	sym COO^- stretch
1430	+6.15	CH_2 bend

a frequencies of ROA bands

of cysteine where the exact ratio of the rotamers is known as compared to the solution spectrum where the ratio is uncertain. The C-S stretching vibration exhibits very little frequency dependence as the pH is varied, which would suggest that the major conformer does not change significantly with pH, since the C-S stretching frequency is expected to be dramatically different for at least two of the possible confomers that cysteine can adopt in solution [120]. At high pH a band occurs in the Raman spectrum (not shown) at 756 cm^{-1} which may originate in a C-S stretching vibration of another conformer which according to Dollish, Fateley and Bentley [118] is expected to occur in this region, by analogy with haloalkanes. The Raman data therefore are consistent with only one major conformer (VII) over the entire pH range with the possibility of another conformer contributing at high pH. The ROA results (*vide supra*) appear to rule out rotamer VI, assuming that the ROA is indeed generated by interaction between the SH and COO^- groups, but can make no distinction between rotamers V and VII (without resort to semi-empirical models). Unfortunately the ROA data in other bands (*vide infra*) suggests that the major conformer in solution of cysteine is different from that for serine which is in conflict with the Raman results. Clearly this warrants a reinvestigation of the NMR data to determine if a mistake has been made in the assignments of the hydrogens in the NMR spectrum of cysteine.

The next Raman band at 779 cm^{-1} exhibits little or slightly positive ROA intensity. This is different from what is seen in similar bands in the ROA spectra of alanine and serine, where this band exhibits negative ROA intensity. We assigned these bands to a wagging mode of the COO^- group. This change in ROA behaviour may indicate conformational differences between these molecules. or that this band in the cysteine

spectrum has a different normal mode composition. Susi *et al.* [115] assign this mode to a mixture of C-S-H bending, CH_2 rocking and COO^- wagging (in that order) which could be taken as evidence in favour of the second hypothesis above. However, upon deuteration of the NH_3^+ and S-H groups a band occurs at exactly the same frequency as the band above. Susi *et al.* [115] have assigned this band to a ND_3^+ rocking mode. If this assignment is incorrect and the band does not actually shift on deuterium substitution then it must originate in a vibration of the COO^- group. The corresponding ND_3^+ rocking mode in serine occurs at 848 cm^{-1} and if it is an isolated normal mode there seems to be no reason for it to change by ~ 60 cm^{-1} in cysteine. Therefore, we suggest that the change in sign of this ROA band is best explained by differences in the normal mode composition between cysteine and serine probably via coupling of the C-S stretch with the C-S-H deformation (*vide infra*).

Susi *et al.* [115] have assigned the next Raman band at 826 cm^{-1}, in the solid state, to a COO^- wagging vibration. In solution a band occurs at 813 cm^{-1} and shows negative ROA intensity. Serine has a similar Raman band also with negative ROA intensity, at 809 cm^{-1}, while alanine does not. One plausible assignment of this band is therefore to a CH_2 rocking mode. However, the C-S-H deformation may also occur in this region and the Raman data for cysteine-ND_3^+-SD [115] indicate that this band is sensitive to this particular isotopic substitution. Ozaki and co-workers [120] postulate that the H_3C-CH_2-SH group of cysteine is closely related to the molecule 2-methyl-1-propanethiol where they have assigned the C-S-H deformation mode to a band at 774 cm^{-1}. Therefore, the band observed in cysteine at 813 cm^{-1} probably originates in a CH_2 rocking mode; indeed Ozaki *et al.* [120] assign a band at 802 cm^{-1} to the CH_2 rocking mode of rotamer VII in the spectrum of

1-chloro-2-methyl-propane. This assignment is supported by the fact that this band has the same ROA sign in both cysteine and serine.

The next two bands at 875 and 936 cm^{-1} exhibit negative and positive ROA intensity respectively. This ROA couplet is also observed in the the spectra of both alanine and serine and was explained by us as originating from coupling of the symmetric CCN stretch and the C^{*}-$C(O_2)$ stretch. A similar assignment appears to be likely here although the isotopic data suggests that both these bands are sensitive to both N and S deuteration; while, as in alanine, this would be expected for the 875 cm^{-1} band it is an unexpected result for the second band at 936 cm^{-1} and may indicate that the normal mode composition is less simple than described above. Indeed the Raman spectrum of cysteine at high pH (not shown), where it shifts by 26 cm^{-1}, would indicate that the the normal mode compostion of this band has some contribution from NH_3^+ rocking coordinates.

Following these two bands is an isolated broad Raman band at 990 cm^{-1} which exhibits positive ROA intensity. We assign this band to a NH_3^+ rocking mode, which is supported both by the normal coordinate analysis of Susi *et al.* [115], the isotopic data and the Raman spectrum of cysteine at high pH where this band disappears. The same mode in the spectra of alanine at ~ 1000 cm^{-1} exhibits negative ROA intensity as does the corresponding mode in the serine spectra. If these assignments are correct this mode changes sign on going from alanine and serine to cysteine. This may indicate that the NH_3^+ group is held in a different conformation in cysteine as compared to serine and alanine but more probably reflects different contributions to the normal modes. In alanine methyl rocking coordinates contribute to the normal mode composition and in serine the C-O(H) stretching mode can contribute to the normal mode composition. These additional contributions to the normal mode

may change the ROA sign. Therefore, in cysteine this mode may represent a relatively pure NH_3^+ rocking mode.

In the Raman spectrum of serine we assigned a band at 1083 cm^{-1} to the C^*-N stretching vibration (*vide supra*). The corresponding band in the spectrum of cysteine occurs at 1069 cm^{-1}. Both exhibit positive ROA intensity. This assignment is supported by the normal coordinate analysis of Susi *et al.* [115] but they also mixed in NH_3^+ rocking and CH_2 twisting modes.

The next Raman band at 1118 cm^{-1} can also be assigned to a NH_3^+ rocking mode in agreement with the assignment of Susi *et al.* [115] of a NH_3^+ rocking mode to a solid state Raman band at 1140 cm^{-1}. This band exhibits positive ROA intensity as does the corresponding NH_3^+ rocking mode in the ROA spectrum of serine at 1125 cm^{-1}. Following this feature is a Raman band at ~ 1145 cm^{-1} which shows no discernible ROA intensity and may originate from a mode of the CH_2 group but may also contain some contributions from a NH_3^+ rocking mode. This band is observed in the Raman spectra of cysteine at low, neutral and high pH which reinforces the assignment to a CH_2 mode.

In the Raman spectrum of serine the CH_2 wagging mode is coupled to the in-plane O-H deformation and occurs at 1242 cm^{-1} with negative ROA intensity. In cysteine, according to Susi *et al.* [115], the normal mode composition is almost pure CH_2 wagging and occurs at 1211 cm^{-1}. This band also exhibits negative ROA intensity which suggests that the ROA in both bands is generated primarily from the CH_2 moiety, perhaps via coupling with a NH_3^+ rocking mode which occurs in this region in the spectra of alanine (also with negative ROA intensity). This may indicate that the geometrical arrangement of the CH_2 and NH_3^+ groups is similar in both serine and cysteine.

We now consider the region of the spectrum which is dominated by CH and CH_2 modes. The first of these bands occurs at 1268 cm^{-1} and exhibits an ROA couplet, negative on the lower frequency side and positive on the higher. Susi *et al.* [115] have assigned a solid state Raman band at 1269 cm^{-1} to a CH_2 wagging mode. However, we prefer the assignment to a CH_2 twisting mode. No similar feature is identified in the ROA spectrum of serine. This may indicate that different conformations are adopted by these two molecules in solution. The next band at 1312 cm^{-1} shows no observable ROA intensity. Susi *et al.* [115] assign this band to a mixture of C^*-H deformation (bending), CH_2 twisting and the COO^- symmetric stretch. The only way to distinguish between these alternatives is to perform an isotopic substitution study on cysteine-CD and cysteine-CD_2. It would help to decide which Raman bands arose from which groups. The assignment of the next band at 1351 cm^{-1}, which has positive ROA intensity, to one of the orthogonal C^*-H deformation (bending) modes is much more straighforward. Susi *et al.* [115] have made a similar assignment and, the fact that the same ROA intensity pattern is identified in the spectra of alanine, serine and cysteine, also strongly supports this assignment to a C^*-H deformation (bending). The symmetric COO^- stretch occurs at 1403 cm^{-1} and, as in the spectra of the other amino acids studied, exhibits negative ROA intensity, probably generated via coupling with the adjacent C^*-H deformation (bending) mode.

The final band to exhibit ROA in the spectrum of cysteine occurs at 1430 cm^{-1} and has positive ROA intensity. In the ROA spectrum of serine no ROA intensity was observed for this band. This may once again indicate that the CH_2 group is held in a different conformation in these two molecules. However, this band does show some sensitivity to pH,

shifting by 5 cm^{-1} at pH ~ 0, which may indicate coupling of the CH_2 bend with the symmetric COO^- stretch in cysteine but not in serine giving rise to a different ROA pattern. It is the different behaviour of the CH_2 modes in cysteine as compared to serine which leads us to suspect that different conformations are adopted by these two molecules in solution.

5.4 Valine

5.4.1 *Introduction*

The three possible rotameric forms of valine (2-amino-3-methylbutyric acid) are shown in table 5.1. At pD = 5.7 the major rotamer in solution is VI. This differs from that observed for serine. One interesting point to note is that, unlike serine where the dominant conformer population reduces with increasing pD, for valine it actually increases. These data indicate that steric interactions are not the dominant force in deciding which conformer is favoured since one would expect V to have the lowest energy on this basis. No VCD has been reported for this molecule in the region discussed in the present work. As compared to the other molecules we have studied no detailed vibrational analysis of valine is available in the literature and so the assignments given below must be considered as tentative.

5.4.2 *Vibrational analysis and ROA of valine*

The Raman (top) and ROA (bottom) spectra of valine in water, pH ≈ 7, are shown in fig. 5.5. The corresponding Raman frequencies, ROA Δ-values and suggested vibrational assignments are given in table 5.4. The ROA is relatively weak compared to the other samples studied. We therefore achieved a lower SNR than that in previous spectra probably

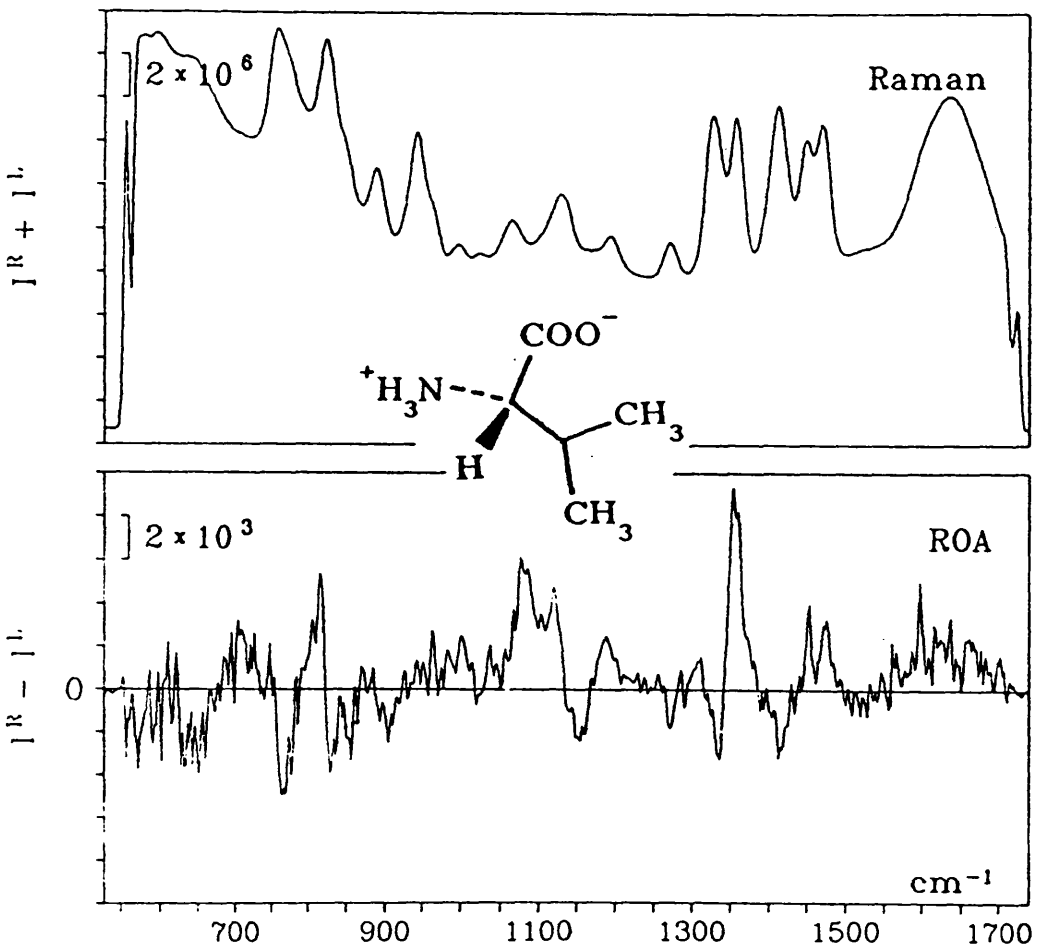

Fig. 5.5. Backscattered Raman (top) and ROA (bottom) spectra of L-valine in aqueous solution. Experimental conditions: exposure time 6 s, laser power 650 mW, acquisition time 4 hours, slit width 0.12 mm.

Table 5.4 Raman frequencies, ROA Δ-values and vibrational assignments for L-valine in aqueous solution

Frequencies (cm^{-1})	$\Delta(180^0)\times10^4$	Vibrational assignments
637	-4.85	COO^- bend
~710	positive	?
760	-3.29	COO^- wag
813[a]	+2.92	
826		sym C-C stretch
833[a]	-2.49	
845	negative	skel stretch
889		C^*-C stretch
905[a]	-4.34	
945		CH_3 rock
960		CH_3 rock
997	+16.8	NH_3^+ rock
1026	?	NH_3^+ rock/ CH_3 rock
1067		NH_3^+ rock
1079[a]	+1.42	
1110		asym CCN stretch
1121[a]	+7.15	
1140		CH_3 rock + C-C stretch
1155[a]	negative	
1188[a]	+1.03	
1193		CH_3 rock+ C–C stretch
1271	-5.38	CH bend
1329	-1.13	sym CH_3 bend
1357	+4.97	C^*H bend
1414	-1.75	sym COO^- stretch
1451	+1.20	asym CH_3 bend
1471	+2.34	asym CH_3 bend

a frequencies of ROA bands

because the solution is relatively dilute (~ 0.38M).

Beginning at low frequency, the first Raman band at 637 cm^{-1} exhibits negative ROA intensity and by analogy with the other amino acids (*vide supra*) we assign it to the bending vibration of the COO^- group.

An unidentified Raman band at ~ 710 cm^{-1} shows a broad positive ROA signal. The assignment of this band is not certain.

The next band at 760 cm^{-1} shows negative ROA intensity. The same feature is observed in the Raman and ROA spectra of all the amino acids investigated (except isoleucine and cysteine) and we therefore suggest that this band be assigned to a vibration of the COO^- group, probably the wagging mode. The bandshape is not symmetric which may indicate the presence of more than one conformer.

The adjacent band at 826 cm^{-1}exhibits a ROA couplet, positive on the lower frequency side and negative on the higher. It has a shoulder at ~ 845 cm^{-1} which exhibits negative ROA intensity. We assign the first of these bands to a symmetric C-C stretching vibration, which is known to occur in this region for isopropyl groups [118], and the second to a skeletal stretching mode of the carbon chain, which is basically n-butane in this molecule. In n-butane itself this skeletal mode occurs at 837 cm^{-1} which would support our assignment above. These two modes routinely generate large ROA in other molecules such as menthol and menthyl chloride [81] which also contain isopropyl groups.

The next Raman band occurs at 889 cm^{-1}. However, the negative ROA intensity is observed at 905 cm^{-1}. One plausible interpretation of the origin of this band is the symmetric CCN stretch which occurs at about 850 cm^{-1} in alanine and serine with negative ROA intensity. However, threonine (*vide infra*) exhibits a band at 899 cm^{-1} also with positive ROA intensity. This would indicate that a correct assignment might be to a

C^*-C stretching vibration, as in threonine. The question of the assignment of the symmetric CCN stretch in valine therefore, remains uncertain. However, it may occur between this band and the one at 845 cm^{-1}.

The next two bands at 945 cm^{-1} and a shoulder at ~ 960 cm^{-1} probably originate from methyl rocking modes. Since there are two non-equivalent methyl groups in this molecule, two bands from the separate methyl rocking modes might be expected to occur close to one another. They show little or no ROA intensity which is consistent with the behaviour of relatively pure methyl rocking modes as characterized by the behaviour of the methyl rocking modes of alanine in >6N-NaOH.

Following these two bands is a small Raman band at 997 cm^{-1} which shows positive ROA intensity. Our favoured assignment is to a NH_3^+ rocking mode by analogy to a similar feature in the spectrum of cysteine at 990 cm^{-1} (*vide supra*). The correlation between the ROA sign of these two bands suggests that the NH_3^+ group is held in a similar conformation in these two molecules.

The next Raman band at 1026 cm^{-1} exhibits uncertain ROA intensity and may originate from either a methyl or NH_3^+ rocking mode or a mixture of both of them. The measurement of valine in >6N-NaOH, where the complication of NH_3^+ rocking modes are removed, might permit a more definitive assignment.

The Raman spectrum is more complex in the region ~ 1050-1193 cm^{-1} adjacent to the 1026 cm^{-1} band. An illustration of this is that most of the ROA bands lie away from the apparent centre of the Raman bands. There are at least four Raman bands in this region at 1067, 1110, 1140 and 1193 cm^{-1}, respectively. The ROA bands occur at 1079 cm^{-1} with positive ROA intensity, 1121 cm^{-1} with positive ROA intensity, forming

part of a ROA couplet with the next ROA band at 1155 cm^{-1} which exhibits negative ROA intensity. The final ROA band in this region occurs at 1188 cm^{-1} and shows positive ROA intensity. Modes which would be expected to occur in this region include methyl and NH_3^+ rocking and C-C and C^*-N stretching. We suggest the following assignments; the band at 1067 cm^{-1} can probably be assigned to a NH_3^+ rocking mode and that at 1110 cm^{-1} probably originates from the antisymmetric CCN stretching mode which gives rise to a band with positive ROA intensity in the other amino acids at about the same frequency, while the band at 1140 cm^{-1} can be assigned to a methyl rocking mode plus C-C stretching modes of the ispropyl group [106]. The band at 1193 cm^{-1} can also be assigned to a mixture of methyl rocking and C-C stretching [106].

The next region of the Raman spectrum, ~ 1250-1480 cm^{-1}, at first inspection appears relatively simple in terms of the total number of bands. There are six clearly identifiable Raman bands at 1271, 1329, 1357, 1414, 1451 and 1471 cm^{-1}, respectively. They exhibit a negative, negative, positive, negative, positive, positive ROA intensity pattern. Of these bands that at 1414 cm^{-1} can be readily assigned to the symmetric stretching vibration of the COO^- group. This gives rise to negative ROA intensity in all the amino acids we have investigated (except isoleucine), which gives us confidence about this assignment. According to Colthup, Daly and Wiberley [106] the symmetric methyl deformation (bend) at 1370 cm^{-1} is split into two when the molecule contains an isopropyl group (such as valine) but the antisymmetric methyl deformation (bend) at 1465 cm^{-1} should give rise to only one Raman band. In valine we observe two Raman bands, at 1451 and 1471 cm^{-1}, in the region of the spectrum where the antisymmetric methyl deformation (bend) is expected to occur. This can only mean that the methyl groups in valine are non-equivalent. This

conclusion is supported by inspection of rotamer VI. Following Colthup *et al.* [106] this would indicate that we would expect to find four bands due to the antisymmetric methyl deformation (bend) at $\approx$ 1465 cm^{-1}, since in an isopropyl group the methyls are normally equivalent. This would be further complicated by the presence of the orthogonal C-H deformation (bending) modes in the same region of the Raman spectrum and since valine has two C-H groups we would expect four Raman bands. Although we should therefore have eight Raman bands below the frequency of the symmetric COO^- stretching vibration, we can identify only three. The first of these bands occurs at 1271 cm^{-1} and since its frequency is sufficiently low not to be a symmetric methyl deformation (bend), we favour its assignment to one of the orthogonal C-H deformation (bending) modes (probably from the C^{β}-H group). We assign the band at 1329 cm^{-1} to one of the symmetric methyl deformation (bending) modes, since none of the amino acids studied has a band with negative ROA intensity that can be assigned to a C-H group at this frequency. The remaining band at 1357 cm^{-1} is assigned to one of the orthogonal C^{α}-H (α here has the same meaning as *, both refer to the chiral carbon) deformation (bending) modes, since all the amino acids we have investigated (except isoleucine) have a band at about this frequency with positive ROA intensity which can only arise from the C-H group. It should be noted that the two C-H groups are held in a chiral arrangement to one another and that interaction between them might be responsible for the ROA intensity observed in the band at 1271 cm^{-1}. However, we still favour interaction between the symmetric COO^- stretch and the C-H deformation (bend) as the principal source of the ROA intensity observed in the band at 1357 cm^{-1}.

5.5 Threonine

5.5.1 *Introduction*

Threonine (2-amino-3-hydroxybutyric acid) like the other amino acids investigated in this chapter can adopt three minimum energy rotameric forms which are shown in table 5.1. Like valine the lowest energy rotamer is VI but unlike valine its stability is lowered with increasing pD to high pH. This is presumably the result of steric interactions since the rotamer population which increases is the sterically most favoured.

No VCD data have been reported for this molecule in the spectral region discussed in the present work. A vibrational analysis of threonine based on the infrared spectra of threonine and some bivalent metal complexes has been presented by Inomata *et al.* [122].

5.5.2 *Vibrational analysis and ROA of threonine*

The Raman (top) and ROA (bottom) spectra of L-threonine in water, pH $\approx$ 7, are shown in fig. 5.6. The corresponding Raman frequencies, ROA Δ-values and suggested vibrational assignments are given in table 5.5.

Beginning at low frequency the first Raman band at 659 cm^{-1} exhibits positive ROA intensity. Inomata *et al.* [122] observe no band in this region in the infrared spectrum of threonine. The other amino acids we have studied do have a Raman band in this region which exhibits negative ROA intensity and which we have assigned to the bending vibration of the COO^- group. We suggest that a similar assignment is valid for threonine. The sign change in the ROA spectrum may represent different contributions to the normal mode from the O-H out-of-plane deformation mode.

The next band at 760 cm^{-1} exhibits an ROA couplet, positive on the lower frequency side and negative on the higher. Inomata and co-workers

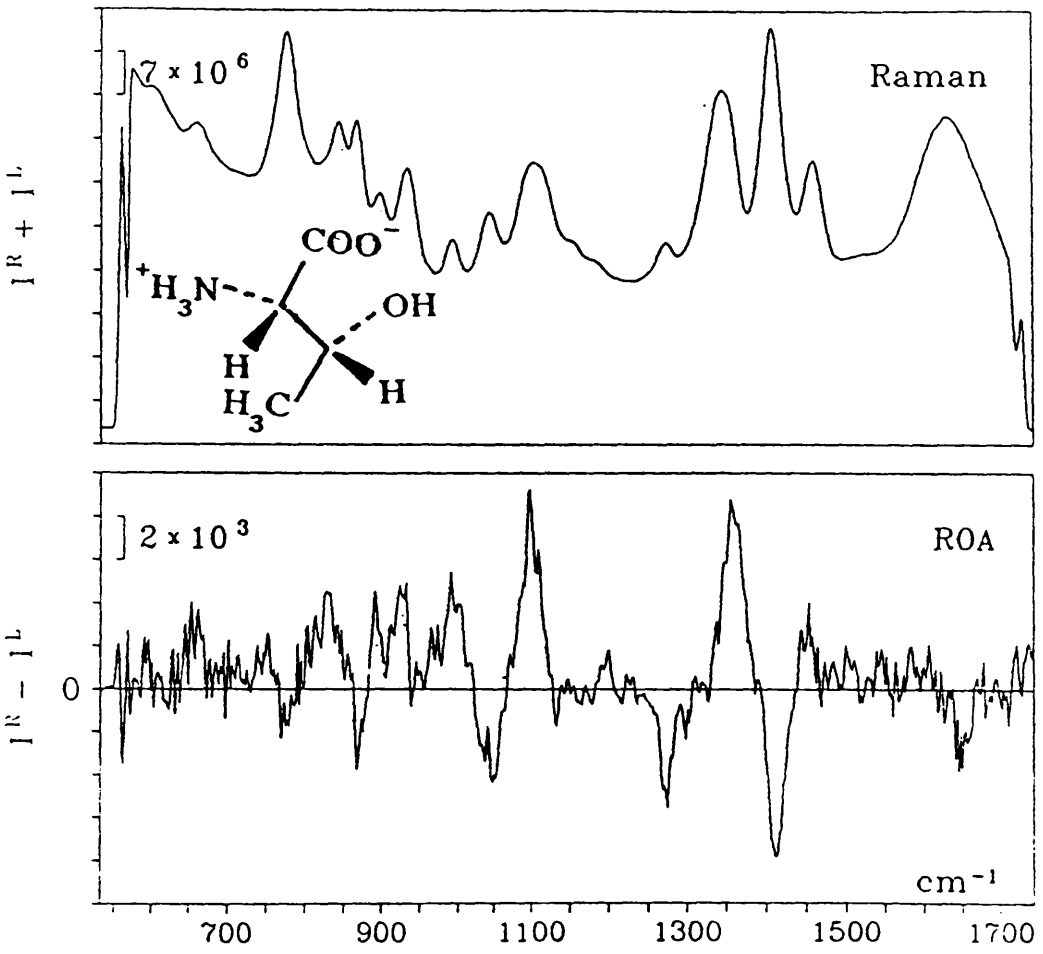

Fig. 5.6. Backscattered Raman (top) and ROA (bottom) spectra of L-threonine in aqueous solution. Experimental conditions: exposure time 4.5 s, laser power 750 mW, acquisition time 4 hours, slit width 0.12 mm.

Table 5.5 Raman frequencies, ROA Δ-values and assignments for L-threonine in aqueous solution

Frequencies (cm^{-1})	$\Delta(180^0)\times10^4$	Vibrational assignments
659	-6.00	COO^- bend+ out-of-plane O-H def
750[a]		
760	+0.59	COO^- wag+ out-of-plane O-H def
770[a]	-0.59	
831[a]	+2.75	
847		CH_3 rock+ out-of-plane O-H def
867	-1.87	sym CCN stretch
892[a]	+11.4	
899		C^*-$C(O_2)$ stretch
935	+2.73	CH_3+ NH_3^+ rock
995	+5.79	NH_3^+ rock
1045	-2.93	NH_3^+ rock
1108	+3.63	asym CCN stretch
1150		asyn CCO stretch
1175		CH_3 rock+ C-O(H) stretch+ C–O–H def
1275	-7.8	CH bend
1348	+3.04	C^*H bend
1409	-2.07	sym COO^- stretch
1460	+1.59	asym CH_3 bend
1654	-1.37	NH_3^+ def or asym COO^- stretch

a frequencies of ROA bands

assign an infrared band at 774 cm^{-1} to an out-of-plane O-H deformation mode. The Raman and ROA spectra of the other amino acids we have studied have a band at ~ 770 cm^{-1} with negative ROA intensity which we have assigned to a wagging mode of the COO^- group. The different ROA feature observed in threonine presumably arises from interactions between this mode and the out-of-plane O-H deformation in a similar fashion to that described above for the COO^- bending mode. This is possible since these two groups are geometrically arranged (*vide* rotamer VI) so that hydrogen bonding is possible.

The next region, 800-950 cm^{-1}, is more complex. Raman bands occur at 847, 867, 899 and 935 cm^{-1} respectively. These give rise to a positive (at 831 cm^{-1}), negative, positive (at 892 cm^{-1}), positive ROA intensity pattern. The ROA bandshape of the Raman band at 847 cm^{-1} is not symmetric and may indicate the presence of another Raman band at slightly lower frequency. This is also supported by the ROA data (*vide supra*). Inomata *et al.* [122] assign infrared bands at 877, 917 and 942 cm^{-1} to the following modes: methyl rocking plus C-O stretching, the CCN symmetric stretch and methyl rocking, respectively. In the spectra of the other amino acids we have investigated we have assigned the symmetric CCN stretch to a Raman band at ~ 850 cm^{-1} (which has negative ROA intensity) and the C^*-C stretch to a Raman band at ~ 920 cm^{-1} (which has positive ROA intensity). We favour the assignment of the Raman band at 867 cm^{-1} to the symmetric CCN stretch and the Raman band at 899 cm^{-1} to the C^*-C stretching vibration, primarily because they generate a negative-positive ROA pattern. The band at 935 cm^{-1} is probably a combination of methyl and NH_3^+ rocking while that at 847 cm^{-1} can be considered to arise from a combination of methyl rocking and the in-plane O-H deformation.

The next band occurs at 995 cm^{-1} and exhibits positive ROA intensity. Inomata and co-workers [122] observe no infrared bands in this region. We can assign this band, by analogy to cysteine (*vide supra*) to a NH_3^+ rocking mode since the frequencies and ROA signs are in agreement (it may also contain some methyl rocking coordinates).

Only one Raman band at 1045 cm^{-1} with negative ROA intensity is observed in the region 1000-1100 cm^{-1}. The most likely assignment is to a NH_3^+ rocking mode, since this is expected to occur in this region and by comparison with the ROA spectra of other amino acids might well be expected to give negative ROA intensity.

The next Raman band at 1108 cm^{-1} is broad and exhibits positive ROA intensity. The Raman bandshape probably indicates that there are at least two bands underneath the observed band. Since it has positive ROA intensity we favour its assignment to the antisymmetric CCN stretch by analogy with the spectra of the other amino acids. Following this band are two Raman bands at 1150 and 1175 cm^{-1}, respectively, both with little or no ROA intensity. The antisymmetric CCO stretch of a secondary alcohol (like threonine) is expected to occur in this region as is a vibration due to a combination of C-O(H) stretch, methyl rocking and C-O-H deformation [118]. We suggest that the band at 1150 cm^{-1} is assigned to the former and that at 1175 cm^{-1} to the latter.

The final region of the Raman spectrum of threonine is relatively easy to interpret based on the spectra we have already discussed. Four Raman bands at 1275, 1348, 1409 and 1460 cm^{-1} , respectively, give rise to a negative, positive, negative, positive ROA intensity pattern. The band at 1409 cm^{-1} can be immediately assigned to the symmetric stretching vibration of the COO^- group by analogy with the other amino acids investigated. The band at 1460 cm^{-1} is also easy to assign, since in this

molecule the only vibration which can occur in this region is the antisymmetric methyl deformation (bend). We assign the two remaining bands to C-H deformation (bending) modes. The first of these occurs at 1275 cm^{-1} and originates from the C^{β}-H deformation (bending) mode. Like valine the two C-H groups are held in a chiral arrangement to one another (which can be confirmed by visual inspection of rotamer VI in table 5.1) and so might be expected to generate significant ROA intensity. The other band at 1348 cm^{-1} arises from the C^{α}-H deformation (bend). This same feature at ~ 1345 cm^{-1} is observed in the spectra of the other amino acids we have investigated which gives us confidence in our assignment. No band which can be assigned to the symmetric methyl deformation (bend) is observable in the Raman or ROA spectra of threonine.

Finally, the ROA spectrum of threonine exhibits a negative band at 1654 cm^{-1} (since no similar feature is observed in the spectra of any of the other amino acids we have studied we are uncertain about the validity of this feature). It can be assigned to either the antisymmetric COO^{-} stretching vibration or the degenerate NH_3^{+} deformation as discussed by Inomata and co-workers [122] for an infrared band at 1631 cm^{-1}. The ROA may represent different interactions between the O-H, COO^{-} and NH_3^{+} groups in this molecule compared to the other amino acids investigated.

5.6 Isoleucine

As for the other α-amino acids studied in this chapter isoleucine (2-amino-3-methylpentanoic acid) can adopt three possible minimum energy conformations in solution which are shown in table 5.1. At neutral pD isoleucine is predicted from NMR data (*vide* table 5.1) to be a 50:50

mixture of rotamers VI and VII. It might be expected, therefore, that this molecule would exhibit little ROA intensity if the origin of the ROA intensity is similar in both rotamers.

The Raman (top) and ROA (bottom) spectra of isoleucine in water are presented in fig. 5.7. As can be seen from the ROA spectrum this molecule does indeed show little ROA intensity in solution. To illustrate why this is the case we will consider the generation of ROA in the C^{β}-H deformation (bending) mode at ~ 1280 cm^{-1} in valine and threonine. In rotamer VI the two C-H groups constitute a left-handed helix whereas in rotamer VII they form a right-handed helix. ROA generated by interaction between these two groups (ignoring any interactions with other groups) is expected to be opposite and equal in these two rotamers leading to an overall cancellation of ROA, which would appear to be what is being observed. By changing the pH the opportunity arises of determining the absolute stereochemistry of similar systems since, from the ROA sign pattern of this mode in valine and threonine (both negative corresponding to rotamer VI above), we can predict the sign of this mode at high and low pH for isoleucine (at low pH it should be positive corresponding to rotamer VII and at high pH it should be negative corresponding to rotamer VI). Therefore combining the ROA sign with the determination of rotamer populations from NMR spectroscopy should lead to the absolute stereochemistry of systems containing two adjacent C-H groups such as tartaric acid.

5.7 Conclusions

The main feature that can be identified in all the amino acid ROA spectra studied in this chapter (except isoleucine) is the couplet embracing the Raman bands originating in the C^{α}-H deformation (bend)

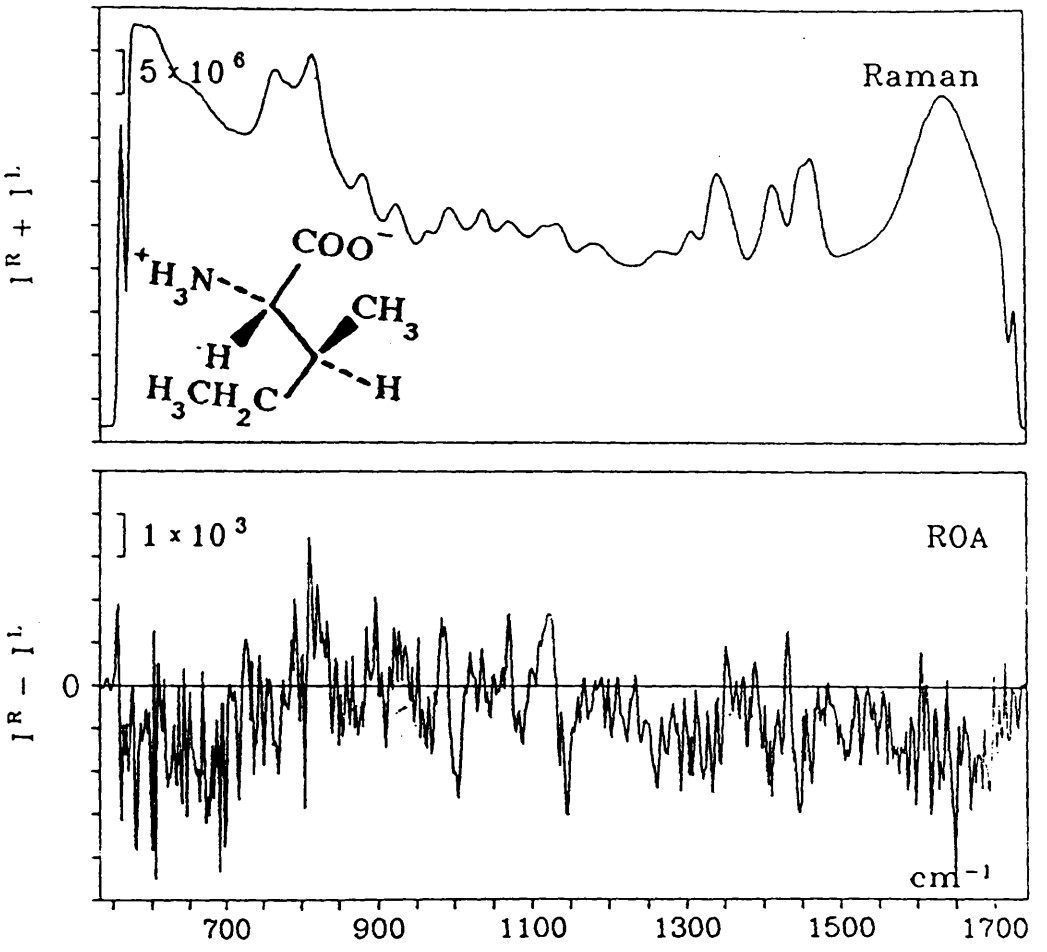

Fig. 5.7. Backscattered Raman (top) and ROA (bottom) spectra of L-isoleucine in aqueous solution. Experimental conditions: exposure time 6 s, laser power 750 mW, acquisition time 4 hours, slit width 0.12 mm.

and the symmetric COO^- stretch. Otherwise this study once again emphasizes the unique nature of the ROA experiment to act as a probe for the configuration and conformation of chiral molecules in solution, since very few features (except those noted above) recur throughout the ROA spectra of these molecules. In order to make more definitive vibrational assignments it would be useful to perform ROA studies on chiral isotopically substituted derivatives of the amino acids studied in this chapter. While realising that this may prove impossible for the larger amino acids such as valine, another strategy would be to perform a pH study since this would enable assignments of modes attributed to the COO^- and NH_3^+ groups to be made with more confidence while having very little effect on the rotameric populations in most cases (*vide* table 5.1).

6 ROA OF IMINO ACIDS

6.1 Introduction

In the preceeding chapters we considered the ROA of simple amino acids. We will now discuss the ROA exhibited by the imino acids proline (pyrrolidine-2-carboxylic acid) and 4-hydroxyproline (4-hydroxypyrrolidene -2-carboxylic acid) (fig. 6.1). These are unique among the amino acids on

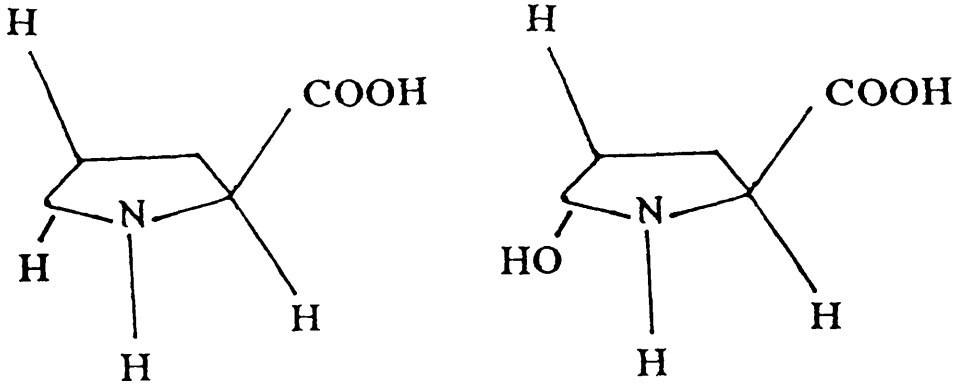

Fig. 6.1. Structures of proline (left) and 4-hydroxyproline (right).

account of their five-membered ring structure and of the possible cis-trans isomerism for a proline (4-hydroxyproline) residue preceeding a peptide bond (fig. 6.2).

Therefore, a preliminary study of the ROA of these molecules is important if further work on the nature of the peptide bond in proline and 4-hydroxyproline containing peptides and proteins is to be performed. A detailed vibrational analysis of proline based on infrared and Raman spectra of DL-proline and L-proline in the solid state and aqueous solutions at pH = 1.0, 6.0 and 11.0 and infrared and Raman spectra of N-deuterated DL-proline have been presented by Herlinger and Veach Long [123]. Inomata *et al.* [124] have given a vibrational analysis of 4-hydroxyproline based on infrared spectra of polycrystalline

4-hydroxy-L-proline and some metal complexes with 4-hydroxyproline as a ligand. VCD data in both H_2O and D_2O for three bands of proline in the region 1275-1331 cm^{-1} have been reported by Freedman *et al.* [95]. The comparison of Raman spectra of proline in the solid state and in solution has been reported by Deveney *et al.* [125] which indicated that the ring conformation in solution is the same as in the solid state. Higuchi *et al.* [126,127] have reported ROA for proline and 4-hydroxyproline in the spectral region 800-1500 cm^{-1} measured in a depolarized 90^0 scattering geometry on a poor scanning instrument: however, this data appears to be unreliable with no correlation to our results.

R^1=H or OH R^2=amino acid side chain

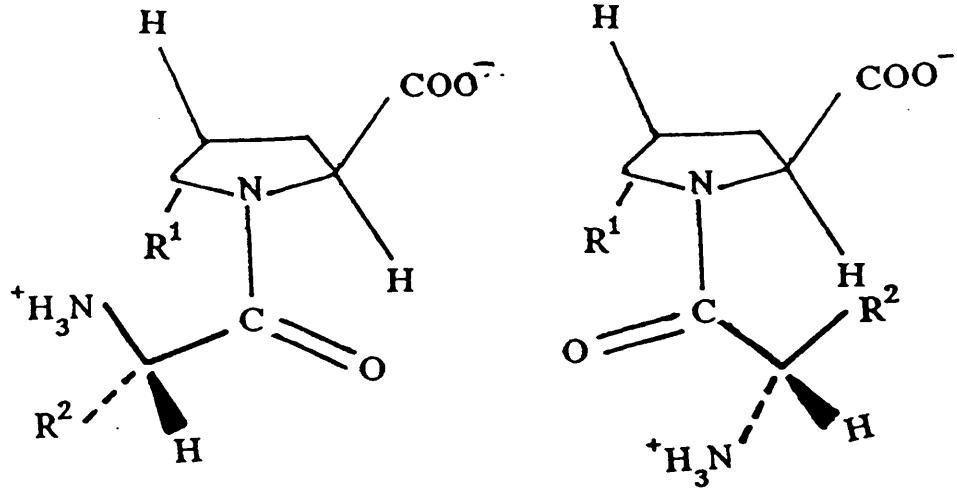

Fig. 6.2. Structures of trans-X-proline (left) and cis-X-proline (right).

6.2 Vibrational analysis and ROA of proline

The Raman (top) and ROA (bottom) of L-proline in aqueous solution, pH ≈ 7, are shown in fig. 6.3. The corresponding Raman frequencies, ROA Δ-values and suggested vibrational assignments are presented in table 6.1.

Beginning at low frequency the first two Raman bands at 627 and 683 cm^{-1}, respectively, show little or no ROA intensity. Herlinger and Veach

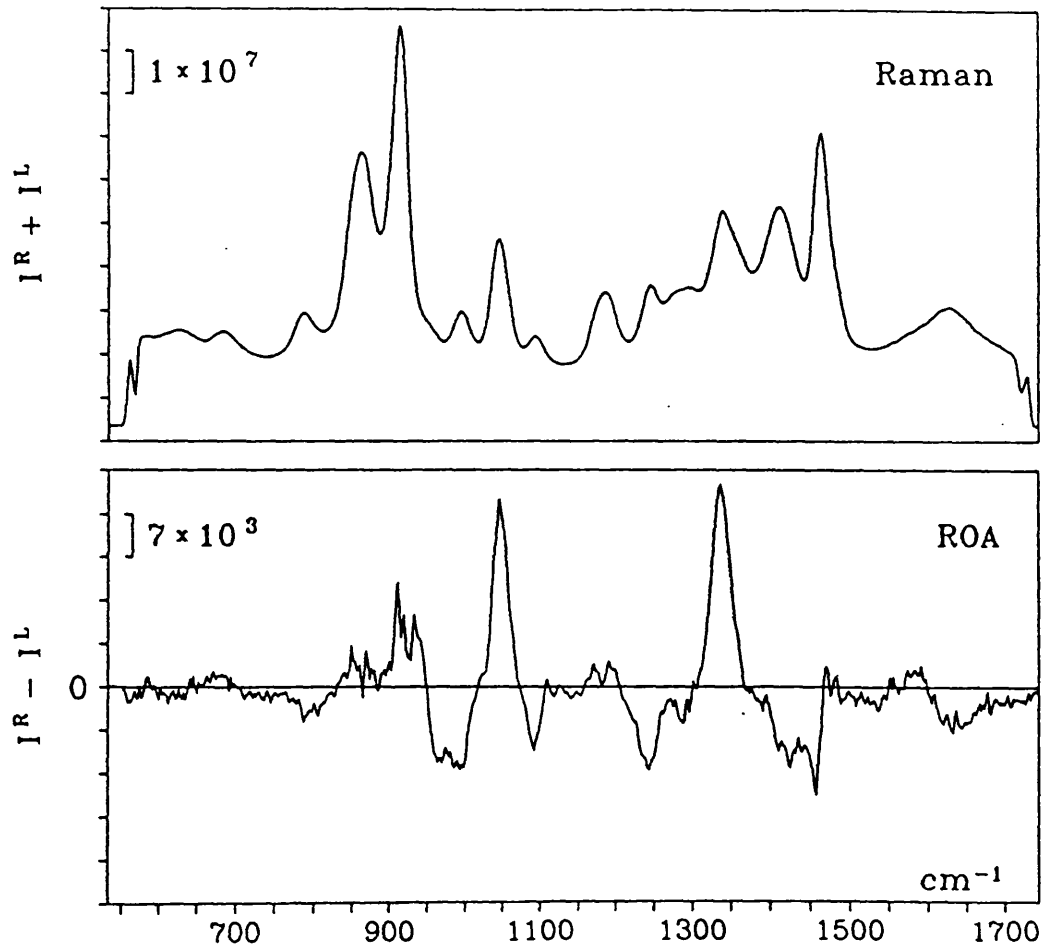

Fig. 6.3. Backscattered Raman (top) and ROA (bottom) spectra of L-proline in aqueous solution. Experimental conditions: exposure time 1.2 s, laser power 625 mW, acquisition time 2 hours, slit width 0.12 mm.

Table 6.1 Raman frequencies, ROA Δ-values and vibrational assignments for L-proline

Frequencies (cm^{-1})	$\Delta(180^0)\times10^4$	Vibrational assignment
627		COO^- bend
683		CH_2 rock
788	-2.61	COO^- wag
863	+0.47	skel. stretch
915	+1.14	ring breathing
936[a]	+7.01	
950		C^*–$C(O_2)$ stretch
966[a]	-7.97	
996	-7.48	ring mode
1045	+6.94	ring mode
1095	-12.2	CH_2 rock
1186	+1.22	NH_2^+ wag
1247	-4.68	CH_2 wag
1284	-2.14	CH_2 twist
1300		in-phase CH_2 twist
1340	+6.08	C^*H bend
1413	-1.70	sym COO^- stretch
1452[a]	-1.44	
1464		CH_2 bend
1473[a]	+0.26	
1580[a]	+1.47	
1606		asym COO^- stretch or NH_2^+ bend
1640[a]	-4.07	

a frequencies of ROA bands

Long [123] assign the former to a COO^- wagging vibration and the latter to a COO^- bending vibration but based upon our previous work we suggest that these assignments be revised. The band at 627 cm^{-1} can be assigned to a COO^- bending mode by analogy with our spectra of the other amino acids (*vide supra*) while the band at 683 cm^{-1} probably originates from a CH_2 rocking mode.

The next band at 788 cm^{-1} exhibits negative ROA intensity. Herlinger and Veach Long [123] observe an infrared band at 783 cm^{-1} and a Raman band at 785 cm^{-1} but assign neither of them to a particular vibration. The ROA spectra of other amino acids (*vide supra*) show a band at about this frequency, which has been assigned by us to a wagging mode of the COO^- group and we favour a similar assignment for proline.

Herlinger and Veach Long [123] identify three Raman bands between 800 and 900 cm^{-1}. These occur at 845 cm^{-1} (assigned to a CH_2 rock), 864 cm^{-1} (unassigned) and 889 cm^{-1} (assigned to a NH_2^+ rock). We on the other hand observe only one relatively broad Raman band at 863 cm^{-1} (fig. 6.3), which exhibits small positive ROA intensity. Garfinkel [128] suggests this band be assigned to a skeletal stretching vibration. This presumably corresponds to the pyrrolidine ring stretching mode at 872 cm^{-1} [118] which is observed in the Raman spectrum of pyrrolidine itself. Such a mode might be expected to generate little ROA intensity since it does not embrace a chiral structure.

The next Raman band at 915 cm^{-1} also exhibits small positive ROA intensity and is the most intense Raman band in the spectrum of proline. It can be assigned [118,125] to a ring breathing mode which, for the reasons discussed earlier, would not be expected to generate large ROA intensity. This ring breathing mode contains significant contributions from the CCN stretching vibration [125]. A shoulder on this band at ~ 950

cm^{-1} exhibits an ROA couplet, positive on the lower frequency side and negative on the higher. One possible assignment of this mode is to the C^*-$C(O_2)$ stretching vibration which occurs in this region in the spectra of the other amino acids we have studied so far (*vide supra*). The ROA on this band could then be generated by interaction of this mode with the CCN stretching vibration. We favour this explanation for the generation of ROA in these two modes in the spectra of the other amino acids. The difference in the two observed ROA signals presumably arises from the incorporation of a localised CCN stretching vibration into a rigid ring.

The next three Raman bands at 996, 1045 and 1095 cm^{-1}, respectively, give rise to a negative, positive, negative ROA intensity pattern. The vibrational assignment of these modes is complicated by the possibility of various normal modes contributing to this region of the spectrum. Herlinger and Veach Long [123] assign the latter two bands to CH_2 wagging and rocking vibrations, respectively. This is consistant with the observation that this region is completely different in the Raman and ROA spectra of 4-hydroxyproline, where the CH_2 chain of proline has been modified. However, another possible explanation for these differences is that these bands might arise from ring modes as has been suggested by Deveney *et al.* [125] who assign the bands at 996 and 1045 cm^{-1} to ring modes based on the comparison of the spectra of proline and pyrrolidine. We favour the latter explanation which only leaves the band at 1095 cm^{-1} unassigned in this region of the Raman spectrum. It occurs in the Raman spectrum at all three pH values [123,125] which strongly suggests that it does not arise from the NH_2^+ or the COO^- groups. One plausible assignment is to a CH_2 rocking mode and in the absence of any other data we suggest that it be assigned to this mode.

This is consistent with the assignment of Herlinger and Veach Long (*vide supra*) [123]. We cannot, however, rule out that this band in fact originates from the antisymmetric CCN stretching vibration which would be expected to occur in this region and does generate large positive ROA intensity in the spectra of the other amino acids we have studied (*vide supra*). Although its inclusion into a ring in this compound probably changes the normal mode composition sufficiently to ignore this possibility for the Raman band at 1095 cm^{-1}. It may be the primary component of the ring mode at 1045 cm^{-1} which does exhibit positive ROA intensity.

The next band at 1186 cm^{-1} with small positive ROA intensity is readily assigned to a NH_2^+ wagging vibration [123] on account of its frequency shift upon deuteration of the NH_2^+ group. No vibration of the COO^- group occurs in this spectral region which reinforces our assignment to a mode of the NH_2^+ group, since no other parts of this molecule should be sensitive to deuteration. In addition, a similar band occurs in the spectrum of 4-hydroxyproline, also with positive ROA intensity, which reinforces the assignment above.

Above 1200 cm^{-1} the Raman spectrum of proline is more complicated than those of the other amino acids we have studied. There are at least six Raman bands at 1247, 1284, 1300, 1340, 1413 and 1464 cm^{-1}, respectively. Of these the band at 1413 cm^{-1} which has negative ROA intensity can be assigned to the symmetric stretching vibration of the COO^- group while that at 1464 cm^{-1} must originate from a bending mode of the CH_2 group. This band probably exhibits a non-conservative ROA couplet, negative on the lower frequency side and positive on the higher. This leaves only the first four bands to be assigned. The band at 1340 cm^{-1} exhibits positive ROA intensity and by analogy with the other

amino acids we assign it to one of the orthogonal C^*-H deformation (bending) modes. According to Colthup *et al.* [106] the in-phase CH_2 twist vibration in CH_2 chains is a good group frequency which occurs in the Raman spectrum at 1300± 5 cm^{-1}. We therefore assign the band at 1300 cm^{-1} to this vibration: it exhibits no ROA intensity, as would be expected since this mode does not embrace a chiral structure. From the ROA spectra another Raman band can be identified at 1284 cm^{-1} with negative ROA intensity. The assignment of this band and that at 1247 cm^{-1} is aided by the assignment of Deveney *et al.* [125] of two Raman bands at 1283 and 1235 cm^{-1} to the CH_2 twisting and wagging vibrations, respectively, based on comparisons between the Raman spectra of proline and pyrrolidine. Freedman *et al.* [95] have assigned infrared bands at 1331 and 1275 cm^{-1} to the two orthogonal C^*-H deformation (bending) modes based on the comparison of the VCD sign pattern for proline, negative on the former band and positive on the latter, with other amino acids. They suggest that an infrared band at 1310 cm^{-1} with positive VCD intensity be assigned to a mode of the CH_2 group. This probably corresponds to the Raman band at 1300 cm^{-1}. The Raman band at 1235 cm^{-1} should therefore be assigned to a CH_2 wagging mode while that at 1284 cm^{-1} probably arises from a CH_2 twisting mode.

The final ROA signal observed in the spectrum of proline is a non-conservative ROA couplet centred at ~ 1606 cm^{-1}, positive on the lower frequency side and negative on the higher. A probable assignment of this band is to the antisymmetric COO^- stretching vibration although NH_2^+ bending cannot be ruled out since Herlinger and Veach Long [123] identify infrared bands at 1598 and 1611 cm^{-1}, respectively, with these modes (*vide* section on 4-hydroxyproline). A pH study would answer this question automatically as well as aid in the lower frequency assignments

of vibrations due to the COO^- and NH_2^+ groups but lack of time meant that this was not possible.

6.3 Vibrational analysis and ROA of 4-hydroxyproline

The Raman (top) and ROA (bottom) spectra of 4-hydroxyproline in water, pH ≈ 7, are shown in fig. 6.4. The corresponding vibrational frequencies, ROA Δ-values and suggested vibrational assignments are presented in table 6.2.

Beginning at low frequency a broad negative ROA band occurs at about 610 cm^{-1}. The only Raman band that can be observed in this region occurs at ~ 600 cm^{-1}. This suggests that there may be an unobserved very weak Raman band as a high frequency shoulder to the band at 600 cm^{-1}. Inomata *et al.* [124] assign an infrared band at 612 cm^{-1} to a COO^- wagging vibration and, based on the spectra of the other amino acids, we also favour an assignment to a vibration of the COO^- group, although we suggest that it is the COO^- bending mode.

The next Raman band at 700 cm^{-1} exhibits positive ROA intensity and, in agreement with the assignment of Inomata and co-workers [124], we assign this band to an out-of-plane O-H deformation. No similar feature is observed in the spectra of proline which reinforces the assignment given above.

Between 700 and 800 cm^{-1} two bands are observed in the Raman spectrum of 4-hydroxyproline as compared to only one in the Raman spectrum of proline. These occur at 761 and 786 cm^{-1} and exhibit positive and zero ROA intensity, respectively. Inomata *et al.* [124] assign an infrared band at 753 cm^{-1} to a COO^- bending mode and another infrared band at 765 cm^{-1} to an in-plane ring mode. In the spectrum of proline a band with negative ROA intensity at 788 cm^{-1} was assigned by us to the

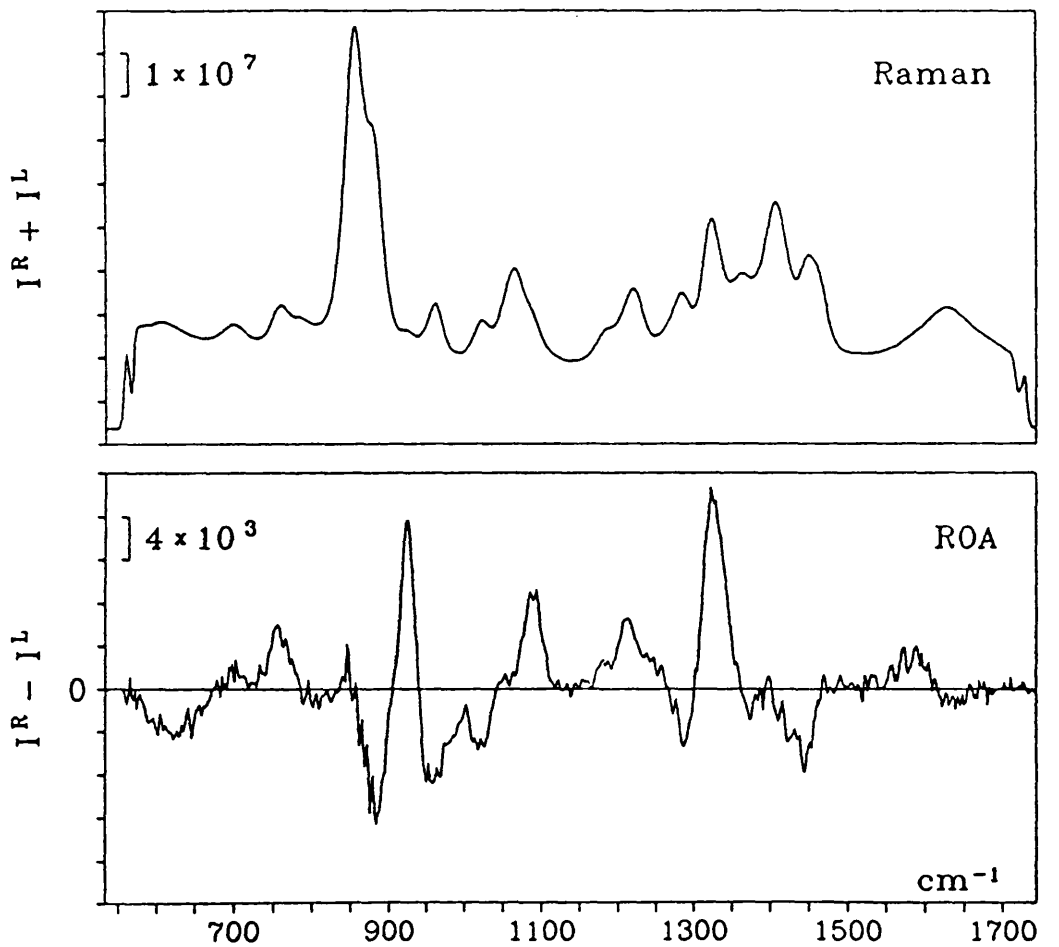

Fig. 6.4. Backscattered Raman (top) and ROA (bottom) spectra of 4-hydroxyproline in aqueous solution. Experimental conditions: exposure time 1.2 s, laser power 750 mW, acquisition time 2 hours, slit width 0.12 mm.

Table 6.2 Raman frequencies, ROA Δ-values and vibrational assignments for 4-hydroxy-L-proline

Frequencies (cm^{-1})	$\Delta(180^0)\times10^4$	Vibrational assignments
600		COO^- bend
610[a]	-7.63	
710	+4.03	out-of-plane O-H def
761	+5.12	O-H def or ring mode
786		COO^- wag
856		ring mode
881	-1.75	ring mode
923	+99.2	C^*-$C(O_2)$ stretch
961	-4.64	ring mode
1025	-4.04	ring mode
1066		C-O(H) stretch
1088	+5.66	CH_2 rock
1189	+2.39	NH_2^+ wag
1220	+2.91	CH_2 wag+ in-plane O-H def
1284	-2.34	CH_2 twist
1325	+4.23	C^*H bend
1366	-1.29	see text
1410	see text	sym COO^- stretch
1440[a]	-2.02	
1451		CH_2 bend
1469[a]	+0.46	
1584[a]	+3.02	
1608		NH_2^+
1639[a]	-1.59	

a frequencies of ROA bands

wagging mode of the COO^- group. We propose therefore that the second band in this region in the Raman spectrum of 4-hydroxyproline is assigned to this mode while the first band may originate from either an O-H deformation or a ring mode, with the latter being more likely.

The next two Raman bands at 856 and 881 cm^{-1} have been assigned by both Garfinkel [128] and Deveney *et al.* [125] to ring modes. Deveney and co-workers [125] suggest that this doublet corresponds to the Raman band in proline at 915 cm^{-1}, with the splitting caused by the presence of the hydroxyl group. The first of these bands shows zero ROA intensity while the second, which exhibits negative ROA intensity, seems to be involved in a ROA couplet with a Raman band at 923 cm^{-1} which exhibits positive ROA intensity. We suggest that this couplet originates in coupling between the C^*-$C(O_2)$ stretching vibration at 923 cm^{-1} and a ring vibration which originates predominately in the symmetric CCN stretching vibration since a similar feature is seen in the spectra of most of the amino acids studied so far. The ROA Δ-value for the band at 923 cm^{-1} (*vide* table 6.2) is an order of magnitude larger as compared to most observed Δ-values, which may indicate a large contribution to the ROA intensity from the $G'_{\alpha\beta}$ tensor but only a small contribution from $\alpha_{\alpha\beta}$. The ring mode at 856 cm^{-1} may well contain a contribution from the symmetric CCO stretching vibration which should occur in this region for secondary alcohols such as 4-hydroxyproline [118].

As discussed in the section on the vibrational analysis of proline the next region, 930-1100 cm^{-1}, of the two spectra shows the most differences. This is not unexpected since vibrations of the O-H group will contribute to the normal modes in this region in the spectrum of 4-hydroxyproline. The first band in this region occurs at 961 cm^{-1} and shows negative ROA intensity. Inomata *et al.* [124] assign an infrared

band at 960 cm^{-1} to an in-plane ring mode. Since we have assigned a band at 996 cm^{-1} in the Raman spectrum of proline with negative ROA intensity to a ring mode we favour a similar assignment here. We also assign the next Raman band at 1025 cm^{-1}, which shows negative ROA intensity, to another ring mode. This band has a different sign from the corresponding mode in the proline spectrum which presumably involves contributions from C-O(H) stretching coordinates. The next band at 1066 cm^{-1} exhibits no ROA intensity. Since no similar Raman band is observed in the spectrum of proline we assign it to a C-O(H) stretching mode. The final Raman band in this region occurs at 1090 cm^{-1} and exhibits positive ROA intensity and, by analogy with our assignment of a band at 1095 cm^{-1} in the proline spectrum to a CH_2 rocking mode, we suggest a similar assignment here. The ROA presumably changes sign because of the different environments of the CH_2 groups in 4-hydroxyproline.

The assignment of the next Raman band at 1189 cm^{-1} which exhibits positive ROA intensity is much easier. We assigned a band of the same frequency in the Raman spectrum of proline also with positive ROA intensity to the wagging mode of the NH_2^+ group and we favour a similar assignment in this case.

As for proline the next group of Raman bands will be discussed together. The first of these occurs at 1220 cm^{-1} and shows positive ROA intensity. Deveney *et al.* [125] assign this band to a CH_2 wagging mode, while Inomata and co-workers [124] assign an infrared band at 1211cm^{-1} to an in-plane O-H deformation mode and another band at 1232 cm^{-1} to a CH_2 wagging mode. We assigned a proline band at 1247 cm^{-1}, with negative ROA intensity, to a CH_2 wagging mode and since the ROA changes sign we propose that in 4-hydroxyproline this band is assigned to a mixture of CH_2 wagging and the in-plane O-H deformation modes.

The following band at 1284 cm^{-1} shows negative ROA intensity. Deveney and co-workers [125] postulate that the CH_2 twisting and CH_2 wagging modes of proline and pyrrolidine decrease in frequency in 4-hydroxyproline. While in our spectra this is true for the wagging mode (*vide supra*) it does not appear to be true for the twisting mode which occurs at exactly the same frequency and has the same ROA sign in the spectra of both proline and 4-hydroxyproline. We however, still prefer the assignment of the band at 1284 cm^{-1} in the spectrum of 4-hydroxyproline to a CH_2 twisting mode. The next band occurs at 1325 cm^{-1} and exhibits positive ROA intensity. From our previous studies on other amino acids we suggest that this band is assigned to one of the orthogonal C^{α}-H deformation (bending) modes. In the spectra of the other amino acids this band is involved in an ROA couplet with the symmetric COO^- stretching vibration which typically has negative ROA intensity. In this molecule this band occurs at 1410 cm^{-1} and probably exhibits negative ROA intensity (although the band shape is complicated). It therefore appears that in 4-hydroxyproline the interaction between these modes is not the same as in other amino acids. Inomata *et al.* [124] also assign this band to a C-H deformation (bending) mode. These two bands are separated by a band at 1366 cm^{-1} with negative ROA intensity. Inomata and co-workers [124] assign this band to a CH_2 twisting vibration. However, the presence of a deformation (bending) mode of the C^{γ}-H group cannot be ruled out. The final band in this spectral region occurs at 1451cm^{-1} and exhibits a non-conserative ROA couplet, large and negative on the lower frequency side and small and positive on the high. It can be assigned [124] to a CH_2 bending vibration. The parent Raman band is non-symmetric and this may indicate that the two CH_2 groups are in different environments in 4-hydroxyproline leading

to two separate CH_2 bending modes at about the same frequency.

The final Raman band at ~ 1613 cm^{-1} can be assigned to either the antisymmetric COO^- stretching vibration or the NH_2^+ bending vibration. It exhibits a non-conservative ROA couplet, positive on the higher frequency side and negative on the lower. The relative size of these two ROA bands are opposite to that measured in proline. This may indicate that this vibration originates from the NH_2^+ bending mode. In 4-hydroxyproline interactions between the NH_2^+ group and the solvent (water) are possible because the hydroxyl group destroys the hydrophobic character of the CH_2 chain and allows water molecules to approach the NH_2^+ group from the side of the molecule opposite to the COO^- group. The situation is different in proline because the CH_2 chain is hydrophobic and repels any water molecules that try to bond to the NH_2^+ group from the side of the ring opposite to the COO^- group.

6.4 Conclusions

The Raman and ROA spectra of proline and 4-hydroxyproline are completely different. The major correlations between the spectra are the vibration of the NH_2^+ group at ~ 1187 cm^{-1}, the CH_2 twisting mode at 1284 cm^{-1} and the C^{α}-H deformation mode at ~ 1330 cm^{-1} along with the mode at ~ 1610 cm^{-1} (which may arise from either the COO^- or NH_2^+ groups). Some of the Raman bands of proline and 4-hydroxyproline [123,125] shift in frequency upon pH changes, and in the future a pH dependent study of this molecule should be performed. This would (as for the other amino acids investigated) help to verify the assignments of bands due to the COO^- and NH_2^+ groups. Proline and 4-hydroxyproline differ from the other amino acids studied in this work. When proline and 4-hydroxyproline molecules are incorporated by condensation into a

peptide chain, the resultant peptide bond contains only one N-H group (fig. 6.2) as compared to two when other amino acids are linked together. The Raman band for this mode occurs in the amide III region of the spectrum (1230-1300 cm^{-1}) [44], and might therefore be used as a probe of the conformation around this particular peptide bond, especially since the possibility of cis-trans isomerism arises [129]. One possible way of probing the stereochemistry of this linkage is to measure the Raman and ROA spectra of simple peptides containing proline (4-hydroxyproline) residues and investigate the sign of the ROA on his mode. The results could then hopefully be applied to polypeptides and proteins.

Finally we once again emphasize that the vibrational analysis given for proline and 4-hydroxyproline is approximate, due mainly to the lack of isotopic substitution data and that care has to be taken in the interpretation of the spectra and especially its extrapolation to more complex systems containing proline (4-hydroxyproline) residues.

REFERENCES

[1] S. F. Mason, in 'Optical Activity and Chiral Discrimination,' ed. S. F. Mason, Reidel, Dordrecht, 1979, p.1.

[2] L. D. Barron and J. Vrbancich, in 'Advances in Infrared and Raman Spectroscopy,' eds. R. J. H. Clark and R. E. Hester, Wiley, Chichester, 1985, vol. 12, p.215.

[3] A. D. Buckingham and R. E. Raab, Proc. Roy. Soc. (London) A, 1975, **345**, 365.

[4] P. Salvadori and F. Ciardelli, in 'Fundamental Aspects and Recent Developments in Optical Rotatory Dispersion and Circular Dichroism,' eds. F. Ciardelli and P. Salvadori, Heyden, London, 1973, p.3.

[5] T. A. Keiderling, in 'Practical Fourier Transform Infrared Spectroscopy,' eds. J. R. Ferraro and K. Krishnan, Academic Press, San Diego, 1990, p.203.

[6] H. Wynberg and L. A. Hulshof, Tetrahedron, 1974, **30**, 1775.

[7] F. Khuong-Huu, J.-P. Le Forestier and R. Goutared, Tetrahedron, 1972, **28**, 5207.

[8] L. D. Barron, 'Molecular Light Scattering and Optical Activity,' Cambridge University Press, Cambridge, 1982.

[9] P. L. Polavarapu, in 'Vibrational Spectra and Structure,' eds. H. D. Bist, J. R. Durig and J. F. Sullivan, Elsevier, Amsterdam, 1989, vol. 17B, p.319.

[10] L. D. Barron, in 'Vibrational Spectra and Structure,' eds. H. D. Bist, J. R. Durig and J. F. Sullivan, Elsevier, Amsterdam, 1989, vol. 17B, p. 343.

[11] L. A. Nafie and C. G. Zimba, in 'Biological Applications of Raman Spectroscopy,' ed. T. G. Spiro, Wiley, New York, 1987, vol. 1, p.307.

[12] L. D. Barron, M. P. Bogaard and A. D. Buckingham, J. Am. Chem.

Soc., 1973, **95**, 603.

[13] W. Hug, S. Kint, G. F. Bailey and J. R. Scherer, J. Am. Chem. Soc., 1975, **97**, 5589.

[14] G. Holzwarth, E. D. Hsu, H. S. Mosher, T. R. Faulkner and A. Moscowitz, J. Am. Chem. Soc., 1974, **96**, 251.

[15] L. A. Nafie, J. C. Cheng and P. J. Stephens, J. Am. Chem. Soc., 1975, **97**, 3842.

[16] P. L. Polavarapu, Appl. Spectrosc., 1984, **38**, 26.

[17] F. Devlin and P. J. Stephens, Appl. Spectrosc., 1987, **41**, 1142.

[18] L. A. Nafie, M. Diem and D. W. Vidrine, J. Am. Chem. Soc., 1979, **101**, 496.

[19] C. Graham, Proc. Roy. Soc. (London) A, 1980, **369**, 517.

[20] L. D. Barron and J. R. Escribano, Chem. Phys., 1985, **98**, 437.

[21] K. M. Spencer, T. B. Freedman and L. A. Nafie, Chem. Phys. Lett., 1988, **149**, 367.

[22] D. Che, L. Hecht and L. A. Nafie, in 'Proceedings of the Twelfh International Conference on Raman Spectroscopy,' eds. J. R. Durig and J. F. Sullivan, Wiley, Chichester, 1990, p.846.

[23] L. Hecht, D. Che and L. A. Nafie, Appl. Spectrosc., 1991, **45**, 18.

[24] L. A. Nafie, D. Che, G.-S. Yu and T. B. Freedman, in 'Biomolecular Spectroscopy II,' eds. R. R. Birge and L. A. Nafie, SPIE, 1991, vol. 1432, p.37.

[25] L. A. Nafie and T. B. Freedman, Chem. Phys. Lett., 1989, **154**, 260.

[26] L. Hecht and L. D. Barron, Appl. Spectrosc., 1990, **44**, 483.

[27] D. Che, L. Hecht and L. A. Nafie, Chem. Phys. Lett., 1991, **180**, 182.

[28] L. Hecht and L. A. Nafie, Mol. Phys., 1991, **72**, 441.

[29] P. L. Polavarapu, Chem. Phys. Lett., 1988, **148**, 21.

[30] P. L. Polavarapu, Spectrochim. Acta., 1990, **45A**, 171.

[31] L. Hecht and L. A. Nafie, Chem. Phys. Lett., 1990, **174**, 575.

[32] M. R. Oboodi, M. A. Davis, U. Gunnia, M. B. Blackburn and M. Diem, J. Raman Spectrosc., 1985, **16**, 366.

[33] W. Hug and H. Surbeck, Chem. Phys. Lett., 1979, **60**, 186.

[34] L. Hecht and L. D. Barron, Spectrochim. Acta., 1989, **45A**, 671.

[35] W. Hug, in 'Raman Spectroscopy,' eds. J. Lascombe and P. V. Huong, Wiley-Heyden, Chichester, 1982, p.3.

[36] L. Hecht, L. D. Barron and W. Hug, Chem. Phys. Lett., 1989, **158**, 341.

[37] L. D. Barron, L. Hecht, A. R. Gargaro and W. Hug, J. Raman Spectrosc., 1990, **21**, 375.

[38] P. J. Stephens, J. Phys. Chem., 1985, **89**, 748.

[39] A. D. Buckingham, P. W. Fowler and P. A. Galwas, Chem. Phys., 1987, **112**, 1.

[40] P. L. Polavarapu, J. Phys. Chem., 1990, **94**, 8106.

[41] W. R. Salzman, J. Chem. Phys., 1977, **67**, 291.

[42] P. L. Polavarapu, J. Chem. Phys., 1987, **86**, 1136.

[43] L. D. Barron and C. J. Johnston, J. Raman Spectrosc., 1985, **16**, 208.

[44] L. D. Barron, A. R. Gargaro and Z. Q. Wen, J. Chem. Soc. Chem. Commun., 1990, 1034.

[45] L. D. Barron, A. R. Gargaro and L. Hecht, in 'Proceedings of the Twelfh International Conference on Raman Spectroscopy,' eds. J. R. Durig and J. F. Sullivan, Wiley, Chichester, 1990, p.834.

[46] L. D. Barron, A. R. Gargaro, Z. Q. Wen, D. D. MacNicol and C. Butters, Tetrahedron Asymmetry, 1990, **1**, 513.

[47] L. D. Barron, A. R. Gargaro, L. Hecht, Z. Q. Wen and W. Hug, in 'Laser Applications in Life Sciences Part One: Laser Diagnostics of Biological Molecules and Living Cells-Linear and Nonlinear Methods,' eds.

S. A. Akhmanov and M. Y. Poroshina, SPIE, vol. 1403, p.66.

[48] L. D. Barron, A. R. Gargaro and Z. Q. Wen, Carbohydr. Res., 1991, **210**, 39.

[49] L. D. Barron, A. R. Gargaro, L. Hecht and P. L. Polavarapu, Spectrochim. Acta., 1991, **47A**, 1001.

[50] L. D. Barron, A. R. Gargaro, L. Hecht and P. L. Polavarapu, Spectrochim. Acta., *in press.*

[51] L. D. Barron, A. R. Gargaro, L. Hecht, H. Sugata, P. K. Bose and P. L. Polavarapu, Spectrochim Acta., *submitted for publication.*

[52] L. D. Barron, L. Hecht, A. R. Gargaro, Z. Q. Wen and W. Hug, J. Raman Spectrosc., *submitted for publication.*

[53] L. B. Barron and A. D. Buckingham, Mol. Phys., 1971, **20**, 1111.

[54] L. D. Barron and A. D. Buckingham, Ann. Rev. Phys. Chem., 1975, **26**, 381.

[55] W. Hug, Appl. Spectrosc., 1981, **35**, 115.

[56] J. R. Escribano, Chem. Phys. Lett., 1985, **121**, 191.

[57] L. Hecht, B. Jordanov and B. Schrader, Appl. Spectrosc., 1987, **41**, 295.

[58] L. Hecht and B. Jordanov, Optik, 1987, **75**, 167.

[59] D. L. Andrews, J. Chem. Phys., 1980, **72**, 4141.

[60] M. J. Frish, Y. Yamaguchi, J. F. Gaw, H. F. Schafer III and J. S. Binkley, J. Chem. Phys., 1986, **84**, 531.

[61] R. D. Amos, Chem. Phys. Lett., 1986, **124**, 376.

[62] R. D. Amos, Chem. Phys. Lett., 1982, **87**, 23.

[63] R. D. Amos and J. E. Rice, CADPAC: The Cambridge Analytical Derivative Package, Issue 4.0, Cambridge, 1987.

[64] P. K. Bose, L. D. Barron and P. L. Polavarapu, Chem. Phys. Lett., 1989, **155**, 423.

[65] P. K. Bose, P. L. Polavarapu, L. D. Barron and L. Hecht, J. Phys. Chem., 1990, **94**, 1734.

[66] T. M. Black, P. K. Bose, P. L. Polavarapu, L. D. Barron and L. Hecht, J. Am. Chem. Soc., 1990, **112**, 1479.

[67] L. D. Barron, J. F. Torrance and D. J. Cutler, J. Raman Spectrosc., 1987, **18**, 281.

[68] M. R. Vavra and T. A. Keiderling, in 'Proceedings of the Eleventh International Conference on Raman Spectroscopy,' eds. R. J. H. Clark and D. A. Long, Wiley, Chichester, 1988, p.973.

[69] D. N. Batchelder, European Spectroscopy News, 1988, **80**, 28.

[70] J. E. Pemberton, R. L. Sobocinski, M. A Bryant and D. A. Carter, Spectroscopy, 1990, **5**, 26.

[71] L. D. Barron, L. Hecht, W. Hug and M. J. MacIntosh, J. Am. Chem. Soc., 1989, **111**, 8731.

[72] M. M. Carrabba, K. M. Spencer, C. Rich and D. Rauh, Appl. Spectrosc., 1990, **44**, 1558.

[73] M. J. Pelletier and R. C. Reeder, Appl. Spectrosc., 1991, **45**, 765.

[74] C. G. Zimba, T. B. Freedman, K. M. Spencer, X.-M. Hu and L. A. Nafie, Chem. Phys. Lett., 1987, **134**, 233.

[75] P. M. Epperson and M. B. Denton, Anal. Chem., 1989, **61**, 1513.

[76] H.-O. Hamaguchi, Appl. Spectrosc. Rev., 1988, **24**, 137.

[77] L. D. Barron, in 'Optical Activity and Chiral Discrimination,' ed. S. F. Mason, Reidel, Dordrecht, 1979, p.219.

[78] L. D. Barron, J. R. Escribano and J. F. Torrance, Mol. Phys., 1986, **57**, 653.

[79] L. D. Barron, L. Hecht and P. L. Polavarapu, Chem. Phys. Lett., 1989, **154**, 251.

[80] L. D. Barron and P. L. Polavarapu, Mol. Phys., 1988, **65**, 659.

[81] L. D. Barron, L. Hecht and S. M. Blyth, Spectrochim. Acta., 1989, **45A**, 375.

[82] L. D. Barron and J. R. Escribano, Chem. Phys. Lett., 1986, **126**, 461.

[83] D. J. Carter, 4th year project, University of Glasgow, 1986.

[84] J. O. Bjarnason, H. C. Anderson and B. S. Hudson, J. Chem. Phys., 1980, **72**, 4132.

[85] J. L. Oudar, C. Minst and B. A. Garetz, J. Chem. Phys., 1982, **76**, 2227.

[86] G. Wagnière, J. Chem. Phys., 1982, **77**, 2786.

[87] F. W. Schneider and R. Brakel, in 'Proceedings of the Tenth International Conference on Raman Spectroscopy,' eds. W. L. Peticolas and B. S. Hudson, University Printing Department, University of Oregon, Oregon, 1986, 20-4.

[88] S. A. Akhmanov. V. F. Kamalov and N. I. Koroteev, in 'Laser Scattering Spectroscopy of Biological Molecules,' eds. J. Štěpánek, P. Anzenbacher and B. Sedláček, Elsevier, Amsterdam, 1987, p.67.

[89] R. Brakel and F. W. Schneider, in 'Advances in Non-Linear Spectroscopy,' eds. R. J. H. Clark and R. E. Hester, Wiley, Chichester, 1988, p.149.

[90] F. W. Schneider, R. Brakel and H. Spiegal, Ber. Bunsenges. Phys. Chem., 1989, **93**, 304.

[91] P. C. Lyu, P. C. Wang, M. I. Liff and N. R. Kallenbach, J. Am. Chem. Soc., 1991, **113**, 3568.

[92] M. Diem, P. L. Polavarapu, M. Oboodi and L. A. Nafie, J. Am. Chem. Soc., 1982, **104**, 3329.

[93] S. F. A. Kettle, E. Lugwisha, P. Vorderwisch and J. Eckert, Spectrochim. Acta., 1990, **46A**, 921.

[94] M. Diem, J. Am. Chem. Soc., 1988, **110**, 6967.

[95] T. B. Freedman, A. C. Chernovitz, W. M. Zuk, M. G. Paterlini and L. A. Nafie., J. Am. Chem Soc., 1988, **110**, 6970.

[96] W. M. Zuk, T. B. Freedman and L. A. Nafie, J. Phys. Chem., 1989, **93**, 1171.

[97] D. M. Byler and H. Susi, Spectrochim. Acta., 1979, **35A**, 1365.

[98] H. Susi and D. M. Byler, J. Mol. Struct., 1980, **63**, 1.

[99] G. C. Percy and H. S. Stenton, J. Chem. Soc. Dalton Trans., 1976, 2429.

[100] R. Hohmann, Doctoral Thesis, University of Toledo, 1982.

[101] W. J. Hehre, L. Radom, P. v. R. Schleyer and J. A. Pople, '*Ab Initio* Molecular Orbital Theory,' Wiley, New York, p.226.

[102] J. S. Alper, H. Dothe and M. A. Lowe, Chem. Phys. Lett., 1989, **163**, 571.

[103] P. L. Polavarapu, Chem. Phys. Lett., 1989, **163**, 576.

[104] C. Destrade, C. Garrigou-Lagrange and M.-T. Forel, J. Mol. Struct., 1971, **30**, 203.

[105] F. D. Verderame, J. A. Lannon, L. E. Harris, W. G. Thomas and E. A. Lucia, J. Chem. Phys., 1972, **56**, 2638.

[106] N. B. Colthup, L. H. Daly and S. E. Wiberly, 'Introduction to Infrared and Raman Spectroscopy,' Academic Press, New York, 1975, 2nd ed.

[107] R. Bursi, F. J. Devlin and P. J. Stephens, J. Am. Chem. Soc., 1990, **112**, 9430.

[108] R. Bursi and P. J. Stephens, J. Phys. Chem., 1991, **95**, 6447.

[109] H. J. Himmler and H. H. Eysel, Spectrochim. Acta., 1989, **45A**, 1077.

[110] M. Kainosho and K. Ajisaka, J. Am. Chem. Soc., 1975, **97**, 5630.

[111] P. E. Hansen, J. Feeney and G. C. K. Roberts, J. Magn. Reson., 1975, **17**, 249.

[112] B. J. Dale and D. W. Jones, Spectrochim Acta., 1975, **31A**, 83.

[113] K. D. Bartle, D. W. Jones and R. L'Amie, J. Chem. Soc. Perkin Trans. II, 1972, 646.

[114] P. E. Hansen, J. G. Batchelor and J. Feeney, J. Chem. Soc. Perkin Trans. II, 1977, 50.

[115] H. Susi, D. M. Byler and W. V. Gerasimowicz, J. Mol. Struct., 1983, **102**, 63.

[116] K. Machida, M. Izumi and A. Kagayama, Spectrochim Acta., 1979, **35A**, 1330.

[117] Y. Inomata, T. Inomata and T. Moriwaki, Bull. Chem. Soc. Jpn., 1971, **44**, 365.

[118] F. R. Dollish, W. G. Fateley and F. F. Bentley, 'Characteristic Raman Frequencies of Organic Compounds,' Wiley, New York, 1974.

[119] Y. K. Sze, A. R. Davis and G. A. Neville, Inorg. Chem., 1975, **14**, 1969.

[120] Y. Ozaki, H. Sugeta and T. Miyazawa, Chem. Lett., 1975, 713.

[121] L. Hecht, unpublished results.

[122] Y. Inomata, T. Takeuchi and T. Moriwaki, Spectrochim. Acta., 1984, **40A**, 179.

[123] A. W. Herlinger and T. Veach Long II, J. Am. Chem. Soc., 1970, **92**, 6481.

[124] Y. Inomata, T. Takeuchi and T. Moriwaki, Inorg. Chim. Acta., 1983, **68**, 187.

[125] M. J. Deveney, A. G. Walton and J. L. Koenig, Biopolymers, 1971, **10**, 615.

[126] S. Higuchi, K. Tanaka and T. Hattori, Asahi Garash Kogyo Gijutsu Shoreikai, 1985, **47**, 99.

[127] S. Higuchi, K. Tanaka and S. Tanaka, Nippon Kagaku Kaishi, 1986,

11, 1632.

[128] D. Garfinkel, J. Am. Chem. Soc., 1958, **80**, 3827.

[129] G. P. Harhay and B. S. Hudson, J. Phys. Chem., 1991, **95**, 3511.

PUBLICATIONS

A Refereed Journals

Vibrational Raman optical activity in forward scattering: trans-pinane and β-pinene.

L. D. Barron, L. Hecht, A. R. Gargaro and W. Hug, J. Raman Spectrosc., 1990, **23**, 375-379.

Vibrational Raman optical activity in peptides and proteins.

L. D. Barron, A. R. Gargaro and Z. Q. Wen, J. Chem. Soc. Chem. Commun., 1990, 1034-1036.

Vibrational Raman optical activity of cyclodextrins.

L. D. Barron, A. R. Gargaro, Z. Q. Wen, D. D. MacNicol and C. Butters, Tetrahedron Asymmetry, 1990, **1**, 513-516.

Vibrational Raman optical activity of carbohydrates.

L. D. Barron, A. R. Gargaro and Z. Q. Wen, Carbohydr. Res., 1991, **210**, 39-49.

Experimental and *ab initio* theoretical vibrational Raman optical activity of alanine.

L. D. Barron, A. R. Gargaro, L. Hecht and P. L. Polavarapu, Spectrochim. Acta., 1991, **47A**, 1001-1016.

Vibrational Raman optical activity of alanine as a function of pH.

L. D. Barron, A. R. Gargaro, L. Hecht and P. L. Polavarapu, Spectrochim. Acta., in press.

A Raman optical activity instrument for biomedical studies.

L. D. Barron, L. Hecht, A. R. Gargaro, Z. Q. Wen and W. Hug, J. Raman Spectrosc., submitted for publication.

Experimental and *ab initio* theoretical vibrational Raman optical activity of tartaric acid.

L. D. Barron, A. R. Gargaro, L. Hecht, H. Sugeta, P. L. Polavarapu and P. K. Bose, Spectrochim. Acta., submitted for publication.

B Conference Proceedings

Raman optical activity of amino acids.

L. D. Barron, A. R. Gargaro and L. Hecht, in 'Proceedings of the Twelfh International Conference on Raman Spectroscopy,' eds. J. R. Durig and J. F. Sullivan, Wiley, Chichester, 1990, p.834.

Vibrational Raman optical activity of biological molecules.

L. D. Barron, A. R. Gargaro, L. Hecht, Z. Q. Wen and W. Hug, in 'Laser Applications in Life Sciences Part One: Laser Diagnostics of Biological Molecules and Living Cells-Linear and Nonlinear Methods,' eds. S. A. Akhmanov and M. Y. Poroshina, SPIE, 1990, vol. 1403, p.66.

Vibrational Raman optical activity of carbohydrates.

Z. Q. Wen, L. D. Barron, A. R. Gargaro and L. Hecht, in 'Sixth European Symposium on Carbohydrate Chemistry,' The Royal Society of Chemistry, Cambridge, 1991, A.7.

Vibrational Raman optical activity of biological molecules.

L. D. Barron, A. R. Gargaro, L. Hecht and Z. Q. Wen, in 'Spectroscopy of

Biological Molecules,' eds. R. E. Hester and R. B. Girling, The Royal Society of Chemistry, Cambridge, 1991, p.117.

ate Research, 210 (1991) 39–49
ience Publishers B.V., Amsterdam

tional Raman optical activity of carbohydrates

e D. Barron, Angelo R. Gargaro, and Zai Q. Wen
Department, The University, Glasgow G12 8QQ (Great Britain)

June 1st, 1990; accepted for publication, July 19th, 1990)

T

brational Raman optical activity (R.o.a.) spectra of a range of carbohydrates in aqueous solution, n back-scattering between 700 and 1500 cm^{-1}, are presented. Features were revealed that appear cteristic of details of the stereochemistry. Effects associated with the glycosidic linkage in di- and harides are prominent.

CTION

leasurements of vibrational optical activity on chiral molecules can provide new tion on stereochemistry because a vibrational spectrum contains bands associ- h every part of the molecule[1]. Vibrational optical activity in typical chiral s in the disordered phase was first observed using the Raman optical activity technique, which measures small differences in the Raman scattered intensities and left-circularly polarised incident light[2,3]. Until recently, lack of sensitivity icted R.o.a. studies to favourable samples such as neat liquids[4,5], with the nentary technique of vibrational circular dichroism (v.c.d.) finding more appli- n studies of stereochemistry[6]. However, a recent major advance in R.o.a. ntation, based on the use of a back-scattering geometry[7,8] (in place of the usual tering arrangement) together with a cooled charge-coupled device as detector[9], rendered a much wider range of samples accessible to study. We now report pectra of a range of carbohydrates in aqueous solution, which indicate that this ue has potential for studies of the structure and stereochemistry of carbo- s.

lost carbohydrates are not amenable to conventional electronic circular di- (e.c.d.) studies because they absorb below the short-wavelength limit of ~ 190 nost commercial instruments. Therefore, studies have been restricted to the velength tails of the first e.c.d. bands[10], or elaborate procedures, such as the ate exciton chirality method[11], have been employed. Several v.c.d. studies of drates have been reported that covered both the C–H stretching region[6,12,13] and i.r[14,15], and, although they demonstrated the potential value of vibrational activity, they also exposed problems associated with the complexity of the ar vibrations, together with low sensitivity. Moreover, water is not a useful for i.r. spectroscopy. Although water is an excellent solvent for Raman spectros-

91/$ 03.50

copy, prior to the present studies, the auspices for R.o.a. studies of carbohydrates in aqueous solution did not appear to be favourable because conventional Raman spectroscopy has not been used widely on account of difficulties in the interpretation of spectra because of the delocalisation of many of the normal modes over the many C–O and C–O linkages[16]. Also, the superiority of conventional F.t.-i.r spectroscopy over conventional Raman spectroscopy for following structural changes in the structures of carbohydrates in solutions in D_2O has been demonstrated[17] (but the new technique of F.t.-Raman spectroscopy gives excellent spectra of crystalline mono- and poly-saccharides[18]). However, the delocalisation of normal modes over chiral arrangements of nuclei is a prerequisite for large vibrational optical activity. In the event, because of this greater spectral range accessible to R.o.a. compared with v.c.d., the characteristic optical activity "fingerprints" associated with these delocalised vibrations are discernible immediately. Also, since the mechanisms of R.o.a. and v.c.d are quite different[1,19], weak v.c.d. intensities in carbohydrates do not necessarily mean that the R.o.a. intensities will also be weak. Indeed, the presence of C–O–C linkages has been found to be particularly favourable for large R.o.a. effects[20–22].

EXPERIMENTAL

The R.o.a. spectra were recorded using the Glasgow multi-channel instrument. The original intensified diode array detector on this instrument has now been replaced by a cooled (unintensified) charge-coupled device as detector (Wright Instruments Ltd. Model AT1), which has significant advantages[9] that include increased quantum efficiency and low read-out noise. The optical system employed for the back-scattered R.o.a. measurements was similar to that described by Hug[8].

The carbohydrate samples were studied as near-saturated aqueous solutions contained in quartz microfluorescence cells that were allowed to equilibrate for several days. The R.o.a. measurements were made using a focused 600-mW argon-ion laser beam at 488.0 nm and a spectral resolution of ~ 8 cm^{-1}. All the R.o.a. spectra were acquired for 2 h.

Although R.o.a. spectra have been measured previously down to 80 cm^{-1} in 90°-scattering configuration, back-scattering places severe demands on the capability of the spectrometer to reject stray light because laser light reflected back from the surfaces enters the spectrometer. For this reason, reliable R.o.a. measurements could not be made on aqueous solutions of carbohydrates below ~ 700 cm^{-1} using the existing instrument. Sharp changes in some of the R.o.a. spectra at the join between the two segments at 1060 cm^{-1} should be treated with circumspection.

'dra AND DISCUSSION
ıan
tati *Glucose and* D-*xylose.* — The back-scattered R.o.a. spectrum of D-glucose is
any Fig. 1. This molecule exists preponderantly in the $^4C_1$ pyranose conformation
opy us solution[24] with an α:β ratio of ~1:2. For comparison, the R.o.a. spectrum of
ıctu is shown in Fig. 2, since this molecule has the same conformation in solution as
ınique with a similar α:β ratio[24] but lacks the CH_2OH group. One difference is the
/-sac of a broad couplet centred at 1325 cm^{-1}, negative at low and positive at high
men, only in the former spectrum. Bands in the conventional Raman spectrum of
ıse on this region have been assigned[25,26] to CH_2, C–O–H, and C–H deformations,
acte *et al.*[27] have described a complex calculated mode of α-D-glucose at 1335 cm^{-1}
are of CH_2 twisting, several C–O–H bends, and a high degree of C–C–H bending.
te di there are small differences in the puckering of the pyranoid rings in α- and
ıe R ose with associated differences in the conformation of the pendant side
four β-D-glucose would be expected to have a similar mode of vibration, perhaps
ightly in frequency. Therefore, it seems likely that this couplet in the solution of
e originates in deformations of the CH_2OH group together with deformations
ent parts of the pyranoid structure, and is broadened a little due to contributions

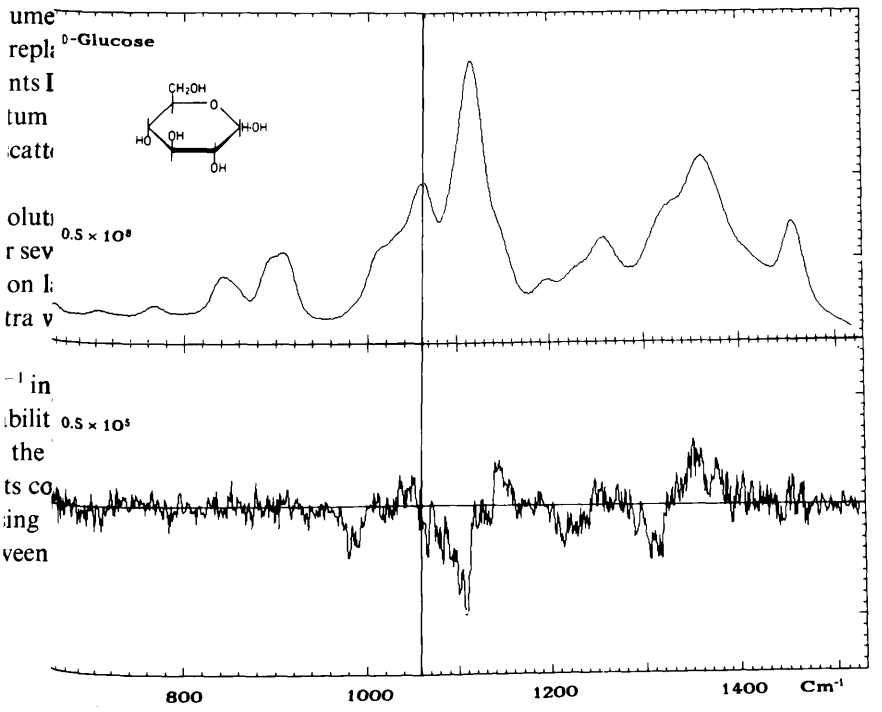

The back-scattered Raman ($I^R + I^L$) and R.o.a. ($I^R - I^L$) spectra of D-glucose in aqueous solution. sity scales (in electron counts) are arbitrary.

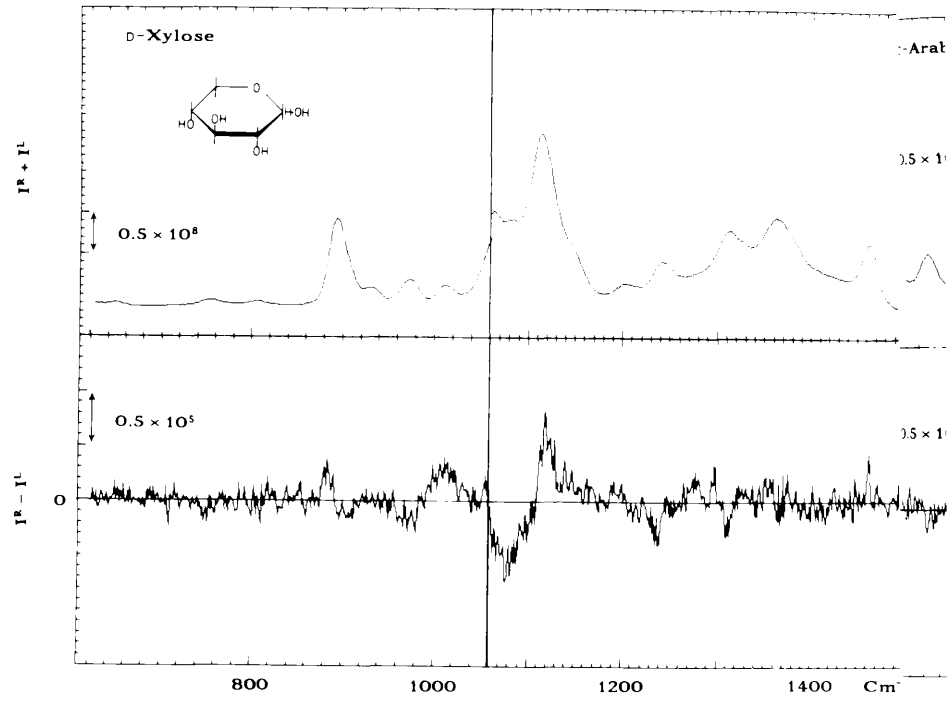

Fig. 2. The back-scattered Raman and R.o.a. spectra of D-xylose in aqueous solution.

from both anomers, a conclusion that is reinforced by the appearance of a sin couplet in the R.o.a. spectra of maltose, maltotriose, and α-cyclodextrin (see belo

A second broad, but weaker, couplet appears in the R.o.a. spectrum of D-glu centred at ~1235 cm^{-1}, and is negative on the low- and positive on the high-freque side. A similar couplet appears in the spectrum of D-xylose centred at ~1260 cr Again, bands in this region for D-glucose have been assigned[26,27] to deformations of CH_2OH group together with contributions from all the C–O–H deformations as we several C–C–H deformations, so that the shift to higher frequency of the D-xy couplet can be attributed, amongst other things, to the lack of participation of CH_2OH deformations in the normal modes.

The v.c.d. spectra of D-glucose and D-xylose were recorded also in the regio the above R.o.a. spectra and, in contrast to the R.o.a. spectrum, the v.c.d. spectrun D-xylose was richer than that of D-glucose[15].

Both D-glucose and D-xylose show similar R.o.a. "fingerprints" between ~ and 1170 cm^{-1}, with that of D-xylose shifted by ~20 cm^{-1} to lower frequency. positive R.o.a. feature at ~1150 cm^{-1} for D-glucose can be assigned to a mode descril by Cael *et al.*[27] as a complex coupling of ring C–O and C–C stretching together w C–O–H and C–C–H bending. The curious sharp drop to a small negative "step" mi be due to contributions of opposite sign from the α and β anomers, for which this mod

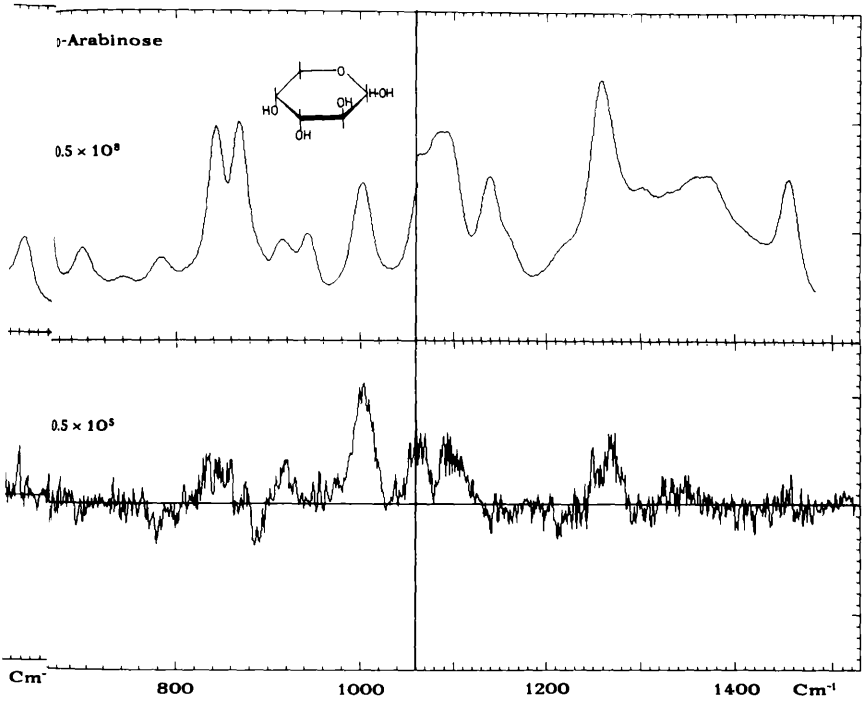

The back-scattered Raman and R.o.a. spectra of D-arabinose in aqueous solution.

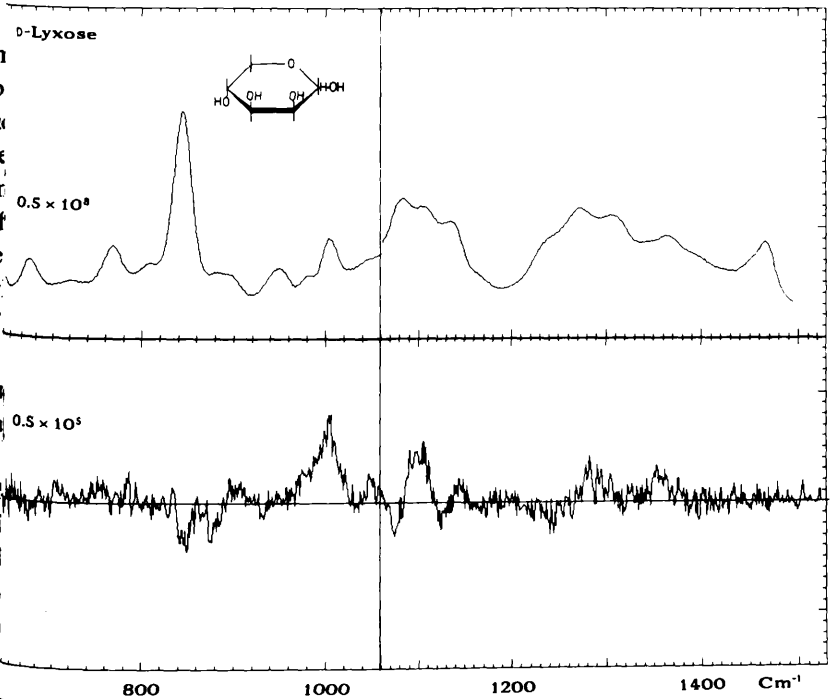

The back-scattered Raman and R.o.a. spectra of D-lyxose in aqueous solution.

predicted[27] to occur at 1155 and 1150 cm^{-1}, respectively. The positive feature at sl lower frequency for D-xylose presumably arises from a similar mode. A v.c.d. fe was observed also in this vibration and was correlated with the absolute stereocher and conformation of several simple pyranoses, including D-glucose and D-xylos fact, all of the Raman bands in the region covered by this particular R.o.a. finge for D-glucose have been assigned to modes that contain significant contributions the same internal vibrational co-ordinates as those listed above for the ~1150 mode[25-27], and since these co-ordinates are mainly from the pyranoid ring stru rather than from the CH_2OH group, it is gratifying that the R.o.a. fingerprii D-glucose and D-xylose are so similar in this region.

D-Arabinose and D-lyxose. — The back-scattered R.o.a. spectra of D-arab and D-lyxose are shown in Figs. 3 and 4. Each sugar exists mainly in the pyra conformation in aqueous solution[24]. Although a detailed analysis is not given her pointed out that, whereas some similarities can be discerned (especially the positive R.o.a. at ~1000 cm^{-1} in each spectrum), overall the fingerprints are di from each other and from those of D-xylose and D-glucose, and clearly reflec different stereochemistry.

Comparison of the R.o.a. spectrum of D-altrose (not shown), which has the pyranoid structure at C-2,3,4 as D-arabinose, was complicated by the presence significant amount of the furanose structure in aqueous solution[24]. However, alth the R.o.a. features are broader generally than those of D-arabinose, there are se similar features and it may prove possible to separate the superimposed spectra pyranose and furanose forms.

Maltose and cellobiose. — Comparison of the back-scattered R.o.a. spect maltose and cellobiose (Figs. 5 and 6, respectively) reveals marked differences.

The spectrum of maltose is similar to that of D-glucose. The couplet centr ~1325 cm^{-1} for D-glucose and associated with deformations of the CH_2OH gro also given by maltose, except that it is spread over a larger region and is more in with the appearance of distinct structure. This difference could reflect less confo tional possibilities for the two CH_2OH groups in maltose with similar but not ider chiral environments. The smaller couplet centred at 1235 cm^{-1} for D-glucose is also by maltose, and the fingerprint for D-glucose between ~960 and 1170 cm reproduced closely with maltose. On the other hand, most of the equivalent featur cellobiose are generally weaker and less structured, which could be associated w different hydrogen-bonding network and, perhaps, greater conformational flexit around the glycosidic linkage (see below).

The most important feature in this pair of R.o.a. spectra is the couplet for ma centred at ~910 cm^{-1}, positive on the low- and negative on the high-frequency side significant feature appears in the spectrum of D-glucose in this region, so that couplet for maltose may be associated with the glycosidic linkage. Raman band α-D-glucose at 845 and 914 cm^{-1} have been assigned[26,27] to modes that invol significant contribution from C-1′–H deformations. The C–O–C stretch that inv the α-(1→4) linkage in maltose appears[28,29] in the region 920–960 cm^{-1}, and this co

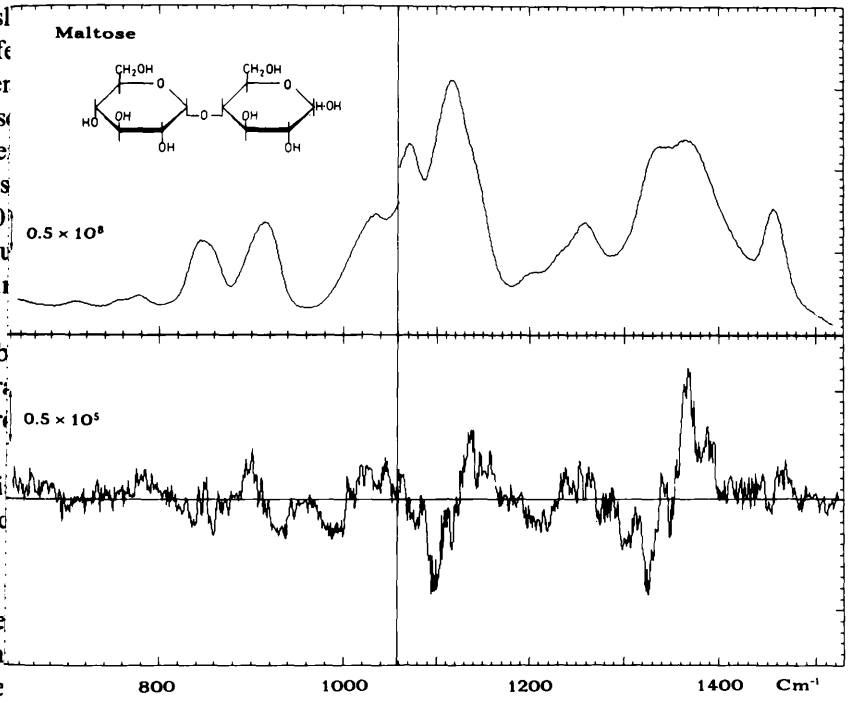

The back-scattered Raman and R.o.a. spectra of maltose in aqueous solution.

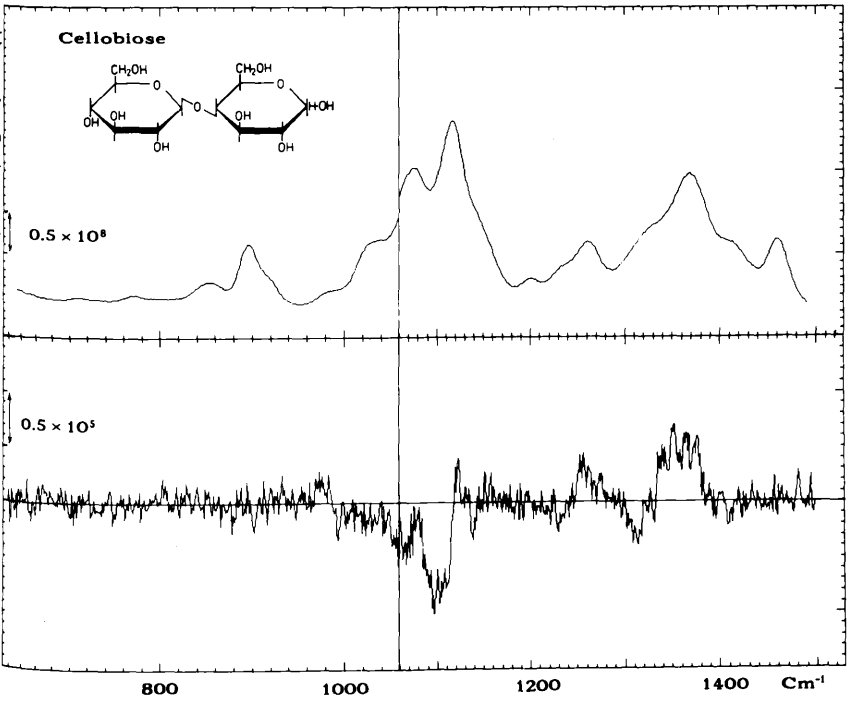

The back-scattered Raman and R.o.a. spectra of cellobiose in aqueous solution.

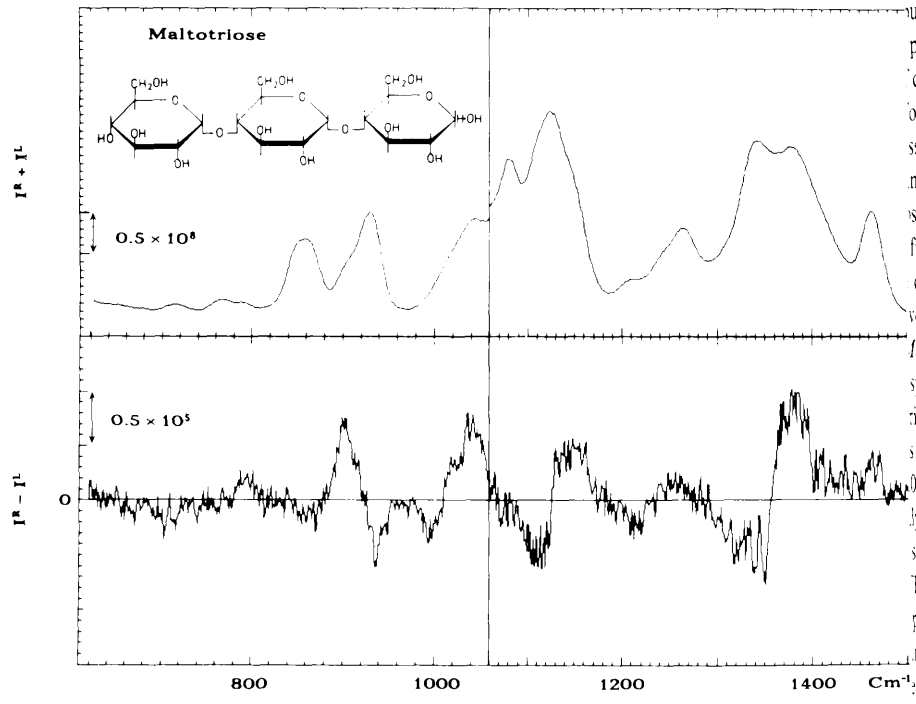

Fig. 7. The back-scattered Raman and R.o.a. spectra of maltotriose in aqueous solution.

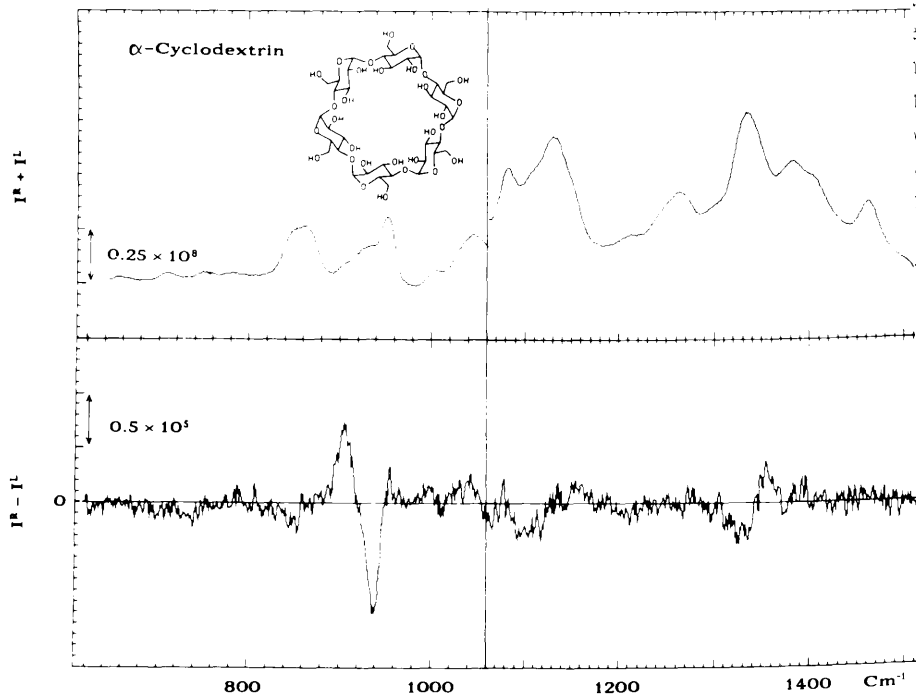

Fig. 8. The back-scattered Raman and R.o.a. spectra of α-cyclodextrin in aqueous solution.

uted to interactions of the C-1′–H deformations and the glycosidic C–O–C perhaps with some involvement of the C-4–H deformations. The R.o.a. spec- cellobiose contains no significant features in the region in which this couplet or maltose, even though there are conventional Raman bands in the same place. ssible explanation is that the C-1′–H and C-4–H bonds are more nearly co- in cellobiose than in maltose, which is supported by the X-ray crystal data for se[30] and maltose[31]. Also, molecular dynamics calculations indicated there to be freedom of motion of the *eq,eq* linkage of cellobiose compared with the *ax,eq* of maltose[32], so that cellobiose can adopt more conformations in solution, would tend to remove the R.o.a.

Maltotriose and α-cyclodextrin (αCD, cyclomaltohexaose). — The back-scattered spectra of maltotriose and αCD are shown in Figs. 7 and 8, respectively. riose shows basically the same features as maltose, but most are broadened, s consistent with the increased conformational possibilities. The couplet centred 0 cm^{-1} has grown relative to the other features, which reinforces its assignment lycosidic linkage and indicates that the conformation around the two glycosidic s in this molecule are similar to each other and to that in maltose.

The glycosidic feature for αCD is enormous with a Δ-value $[(I^R - I^L)/(I^R + I^L)]$ of parts in 10^2, which is an order of magnitude larger than the largest dimensionless intensities usually encountered (it is not possible to provide a better estimate e the associated Raman bands are weak and overlap). A new, weak, positive has appeared also on the high-frequency side, which is connected with the fact e associated Raman bands now constitute a triplet rather than the doublet for e and maltotriose. It has been suggested that this multiplicity indicates that not he glycosidic linkages in αCD are equivalent[29]. Most of the other features shown ose and maltotriose are discernible.

Maltose, maltotriose, and αCD each has a small but significant negative feature at cm^{-1} that, presumably, involves the second mode mentioned above, which s a significant contribution from C-1′–H deformations.

1,6-Anhydro-β-D-glucopyranose. — The back-scattered R.o.a. spectrum of 1,6- o-β-D-glucopyranose is shown in Fig. 9. Generally, the R.o.a. bands are more and sharper than for the other carbohydrates, and reflect the more rigid re. The large bands in the region 820–950 cm^{-1} probably originate in modes to those involved in the glycosidic linkage; the fingerprint in the region 980–1160 reminiscent of those for D-glucose and D-xylose, and the two large positive at ~1190 and 1225 cm^{-1} together with the broad negative feature at 1250–1450 ight involve deformations of the CH_2 bridge.

Thus, the R.o.a. results re-affirm the considerable delocalisation of the vibration- es of pyranosides, which renders experimental assignment of the majority of ncies problematic, even in the most recent work[33], but gives readily discernible rints characteristic of structural units, which obviates the need to assign the ted Raman bands in detail. The presence of detailed structure in some spectra contrasting broadening in others has implications for studies of conformational

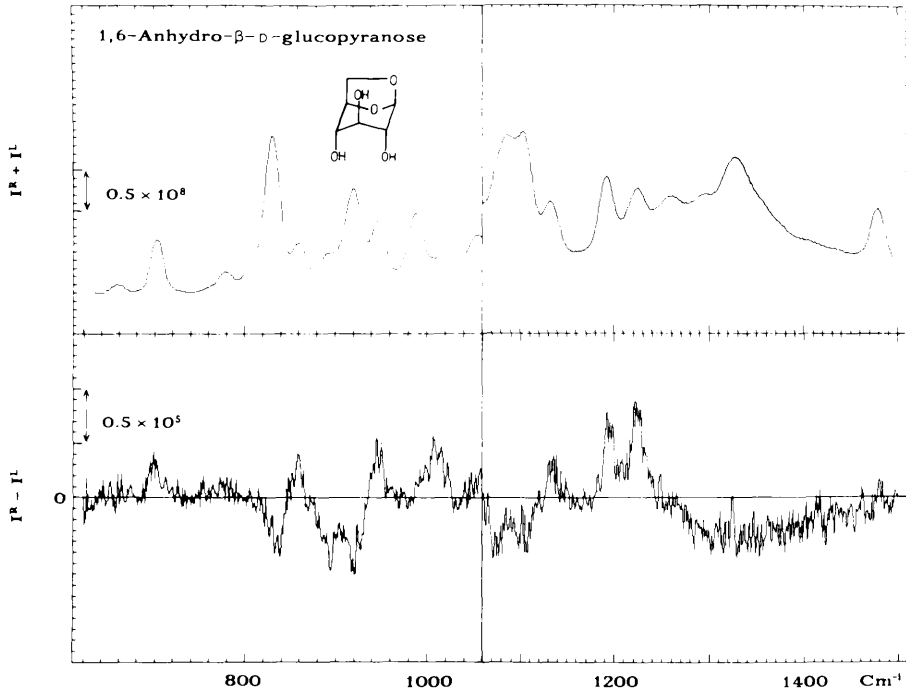

Fig. 9. The back-scattered Raman and R.o.a. spectra of 1,6-anhydro-β-D-glucopyranose in aqu solution.

equilibria and hydrogen bonding. The potentially most valuable result is the identifi tion of clear R.o.a. features associated with the glycosidic linkage, which appear to sensitive to the conformation.

The use of near-saturated solutions with a rather long acquisition time (2 h) temporary limitations which will be removed soon by current developments in strumentation.

ACKNOWLEDGMENTS

We thank the S.E.R.C. and the Wolfson Foundation for research grants, S.E.R.C. for a research studentship (to A.R.G.), Mr. R. Sood for assistance, and Dr. F. Drake and Professor P. L. Polavarapu for discussion.

REFERENCES

1 L. D. Barron, *Molecular Light Scattering and Optical Activity*, Cambridge University Press, Cambrid 1982.
2 L. D. Barron, M. P. Bogaard, and A. D. Buckingham, *J. Am. Chem. Soc.*, 95 (1972) 603–605.

ug, S. Kint, G. F. Bailey, and J. R. Scherer, *J. Am. Chem. Soc.*, 97 (1975) 5589–5590.
Barron, in H. D. Bist, J. R. Durig, and J. F. Sullivan (Eds.), *Vibrational Spectra and Structure*, Vol. Elsevier, Amsterdam, 1989, pp. 343–368.
Nafie and C. G. Zimba, in T. G. Spiro (Ed.), *Biological Applications of Raman Spectroscopy*, Vol. 1, New York, 1987, pp. 307–343.
Freedman and L. A. Nafie, *Top. Stereochem.*, 17 (1987) 113–206.
cht, L. D. Barron, and W. Hug, *Chem. Phys. Lett.*, 158 (1989) 341–344.
g, in J. Lascombe and P. V. Huong (Eds.), *Raman Spectroscopy*, Wiley–Heyden, Chichester, 1982, -12.
Barron, L. Hecht, W. Hug, and M. J. MacIntosh, *J. Am. Chem. Soc.*, 111 (1989) 8731–8732.
Johnson, Jr., *Adv. Carbohydr. Chem. Biochem.*, 45 (1987) 73–124.
Wiesler and K. Nakanishi, *Croat. Chem. Acta*, 62 (1989) 211–226.
rcott, H. A. Havel, J. Overend, and A. Moscowitz, *J. Am. Chem. Soc.*, 100 (1978) 7088–7089.
Paterlini, T. B. Freedman, and L. A. Nafie, *J. Am. Chem. Soc.*, 108 (1986) 1389–1397.
Back and P. L. Polavarapu, *Carbohydr. Res.*, 133 (1984) 163–167.
Tummalapalli, D. M. Back, and P. L. Polavarapu, *J. Chem. Soc., Faraday Trans. 1*, 84 (1988) 2594.
Carey, *Biochemical Applications of Raman and Resonance Raman Spectroscopies*, Academic Press, York, 1982.
Back, D. F. Michalska, and P. L. Polavarapu, *Appl. Spectrosc.*, 38 (1984) 173–180.
al and V. Zichy, *Spectrochim. Acta*, 46A (1990) 253–275.
Escribano and L. D. Barron, *Mol. Phys.*, 65 (1988) 327–344.
Barron and P. L. Polavarapu, *Mol. Phys.*, 65 (1988) 659–667.
Black, P. K. Bose, P. L. Polavarapu, L. D. Barron, and L. Hecht, *J. Am. Chem. Soc.*, 112 (1990) 1489.
Bose, P. L. Polavarapu, L. D. Barron, and L. Hecht, *J. Phys. Chem.*, 94 (1990) 1734–1740.
Barron, D. J. Cutler, and J. F. Torrance, *J. Raman Spectrosc.*, 18 (1987) 281–287.
Angyal, *Angew. Chem. Int. Ed. Engl.*, 8 (1969) 157–166.
Koenig, *Macromol. Rev.*, 6 (1972) 59–177.
Vasko, J. Blackwell, and J. L. Koenig, *Carbohydr. Res.*, 23 (1972) 407–416.
Gael, J. L. Koenig, and J. Blackwell, *Carbohydr. Res.*, 32 (1974) 79–91.
Gael, J. L. Koenig, and J. Blackwell, *Carbohydr. Res.*, 29 (1973) 123–134.
Tu, J. Lee, and F. P. Milanovich, *Carbohydr. Res.*, 76 (1979) 239–244.
C. Chu and G. A. Jeffrey, *Acta Crystallogr., Sect. B*, 24 (1968) 830–838.
Kusagawa and R. A. Jacobson, *Acta Crystallogr., Sect. B*, 34 (1978) 213–218.
French, *Carbohydr. Res.*, 188 (1989) 206–211.
Korolevich, R. G. Zhbankov, and V. V. Sivchik, *J. Mol. Struct.*, 220 (1990) 301–313.

ymmetry Vol. 1, No. 8, pp. 513-516, 1990
Britain

0957-4166/90 $3.00+.00
Pergamon Press plc

Vibrational Raman Optical Activity of Cyclodextrins

**Laurence D. Barron*, Angelo R. Gargaro, Zai Q. Wen
David D. MacNicol and Colin Butters**

Chemistry Department, The University, Glasgow, G12 8QQ, U.K.

(*Received* 5 *June* 1990)

Abstract: Vibrational Raman optical activity spectra of aqueous solutions of α-, β- and γ-D-cyclodextrin in the range 700-1500 cm^{-1} are reported. As well as showing features characteristic of D-glucose, the ROA spectra all show remarkably intense features between 890 and 960 cm^{-1} originating in coupled C(1)-H deformations and glycosidic C-O stretches delocalized around the cyclodextrin ring and which reflect the stereochemistry of the glycosidic links.

ibrational optical activity measurements on chiral molecules can provide much new hemical information because a vibrational spectrum contains bands associated with art of the molecule.[1] Vibrational optical activity in typical chiral molecules in the ed phase was first observed using the Raman optical activity (ROA) technique, which es a small difference in the Raman-scattered intensity in right and left circularly ed incident light.[2,3] Until recently, lack of sensitivity has restricted ROA studies to uble samples such as neat liquids;[4,5] but a major breakthrough in ROA instrumentation on the use of a backscattering geometry[6,7] together with a cooled CCD detector[8] has ndered a much wider range of samples accessible to such studies. This communication ROA spectra of cyclodextrins in aqueous solution which indicate that this technique at potential for stereochemical studies of these and other polysaccharides.

Most carbohydrates are not well suited to conventional electronic circular dichroism measurements, which are restricted to the long-wavelength tails of the first ECD Nonetheless, some useful information about conformations of cyclodextrins has been ed in this way.[10] Vibrational optical activity spectra of simple carbohydrates obtained ROA's sibling technique of vibrational circular dichroism (VCD) have been reported,[11] but D spectra of cyclodextrins have so far been published.

The ROA spectra were recorded using the Glasgow multichannel instrument[12] modified ckscattering[6,7] and CCD detection.[8] The cyclodextrin samples were purchased from and Fluka and studied as near-saturated solutions, in water for α- and clodextrin, and in 1N NaOH for β-D-cyclodextrin in order to boost the solubility. The easurements were made using a focused 500 mW argon-ion laser beam with a spectral ion (FWHH) of ~ 8 cm^{-1}. All the ROA spectra were acquired for 2 hours.

The ROA spectra of α-, β- and γ-D-cyclodextrin are shown in Figs. 1-3 respectively. The pectra of D-glucose, D-maltose and D-maltotriose, to be published elsewhere as part of

a preliminary survey of ROA spectra of a range of carbohydrates,[13] are of central importa tha in discussing the cyclodextrin results. Thus all three cyclodextrin ROA spectra sho cosic negative-positive couplet centred at ~ 1340 cm^{-1} that also appears in D-glucose (at slig have lower frequency) where it has been associated with deformations of the CH_2OH group; and[5,16] three show an ROA 'fingerprint' between ~ 980 and 1170 cm^{-1} similar to that in glucose an associated with ring C-O and C-C stretching together with C-O-H and C-C-H bending w is characteristic of the pattern of OH ring substituents. The most striking cyclodextrin R features are the enormous positive-negative couplets between ~ 890 and 960 cm^{-1}: no sim features appear in D-glucose, but they appear with much less intensity in D-maltose D-maltotriose where they have been associated with modes involving contributions from anomeric C(1)-H deformations and the glycosidic C-O-C stretch.

The general appearance of the three cyclodextrin ROA spectra is itself quite reveal Thus the ROA features of β-D-cyclodextrin (as predominantly monoanion in base[14]) sh sharp structure, especially in the couplet centred at ~ 1340 cm^{-1}: the same characteristics seen in the ROA spectrum of D-maltose,[13] and may reflect a similar restriction conformational possibilities in β-cyclodextrin and maltose. The ROA features γ-D-cyclodextrin are generally broader and much less structured than those β-D-cyclodextrin (anion), and are remarkably similar to those of D-maltotriose,[13] indicat that γ-cyclodextrin might have a similar increase in conformational possibilities to maltotri on account of the larger ring.

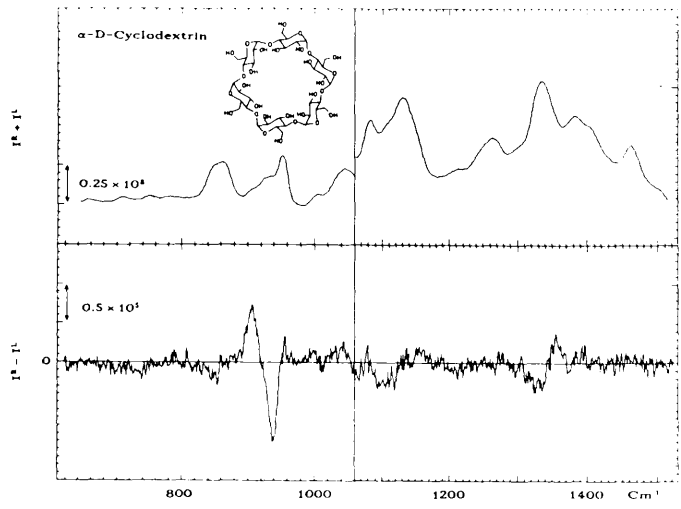

Figu

Figure 1. The backscattered Raman ($I^R + I^L$) and ROA ($I^R - I^L$) spectra of α-D-cyclodextrin in water.

The enormous glycosidic couplets seen in all three cyclodextrin ROA spectra between 890 and 960 cm^{-1} have dimensionless ROA intensities $\Delta = (I^R - I^L)/(I^R + I^L)$ of several par Figu in 10^2, which is an order of magnitude larger than the largest Δ-values usually encountere The fact that the Δ-values of the similar glycosidic ROA feature in maltose and maltotrio lized have more typical magnitudes, with those of maltotriose roughly double those of maltose, of th

porte
shov
slig
; and
ose
ıg wl
rin I
) sim
ose
rom

eveal
) sl
stics
tion
res
ose
idicat
totri

veen
l par
nter
otrid

e that these large cyclodextrin ROA couplets originate in coupled vibrational modes of ycosidic links delocalized around the cyclodextrin ring. In fact Raman bands in this have been assigned previously to skeletal ring modes involving the glycosidic [15,16] but only the bands at 949 cm^{-1} in α-cyclodextrin and 945 cm^{-1} in β-cyclodextrin analogy that at 945 cm^{-1} in γ-cyclodextrin) were explicitly associated with a

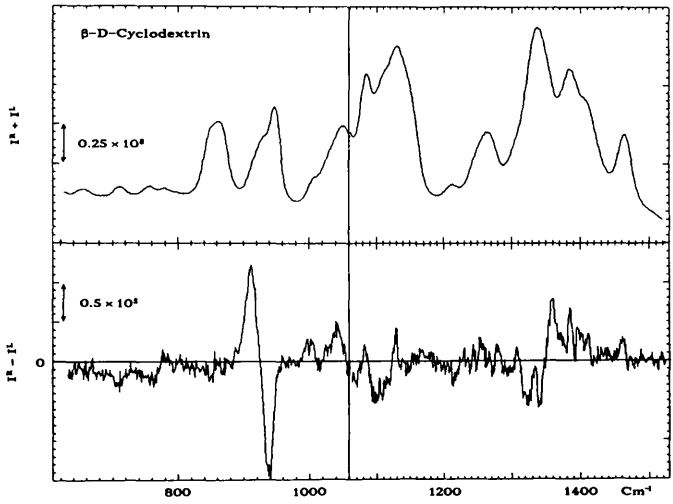

Figure 2. The backscattered Raman and ROA spectra of β-D-cyclodextrin in 1N NaOH.

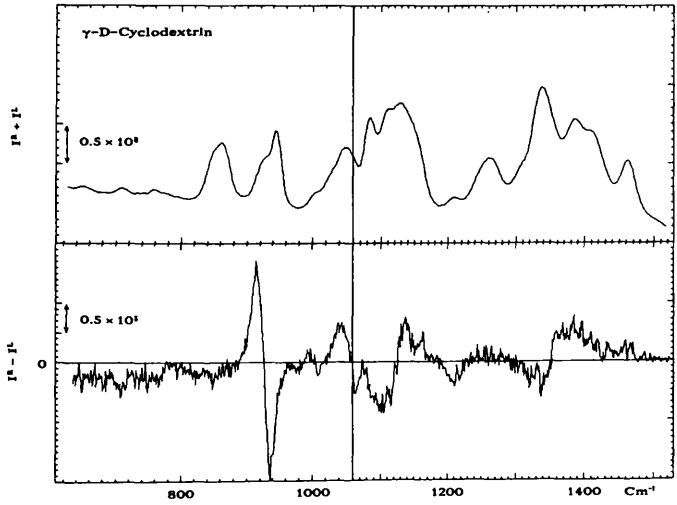

Figure 3. The backscattered Raman and ROA spectra of γ-D-cyclodextrin in water.

ized ring mode;[15] yet close inspection of our ROA spectra reveals that the negative ose, of the glycosidic ROA couplets are not in fact associated with these particular bands

but are at slightly lower frequency. We therefore conclude that, in all three cyclodextrin there are at least two overlapping bands on the low-frequency side of the previously-assign delocalized ring mode that are also delocalized around the cyclodextrin ring.

We have also measured ROA spectra of aqueous solutions of α-D-cyclodextrin containi the guest molecules sodium benzoate and the two enantiomers of phenylalanine. While th are generally very similar to the spectra shown here, there are some small but significa local differences which may reflect a transformation from a 'tense' to a more symmetric 'relaxed' conformation corresponding to the model of Saenger et al.[17]

Instrumental improvements are now in hand which should provide an order of magnitu increase in speed of the measurements. This will enable quantitative differences in RC features to be measured when different guests are incorporated, thereby providing completely new source of information on the details of conformational changes associat with the accommodation of different guests in cyclodextrins in aqueous solution.

Acknowledgments: We thank the S.E.R.C and the Wolfson Foundation for research grants, tl S.E.R.C. for a research studentship for A.R.G., and Prof. P. L. Polavarapu and Drs. A. F. Drak and G. E. Tranter for discussions.

References

1. L. D. Barron, 'Molecular Light Scattering and Optical Activity', Cambridge University Pres Cambridge, 1982.
2. L. D. Barron, M. P. Bogaard and A. D. Buckingham, *J. Am. Chem. Soc.*, 1972, **95**, 603.
3. W. Hug, S. Kint, G. F. Bailey and J. R. Scherer, *J. Am. Chem. Soc.*, 1975, **97**, 5589.
4. L. D. Barron, in 'Vibrational Spectra and Structure', H. D. Bist, J. R. Durig and J. Sullivan, Eds., Elsevier, Amsterdam, 1989, Vol. 17B, p. 343.
5. L. A. Nafie and C. G. Zimba, in 'Biological Applications of Raman Spectroscopy', T. G. Spir Ed., Wiley, New York, 1987, Vol. 1, p. 307.
6. L. Hecht, L. D. Barron and W. Hug, *Chem. Phys. Lett.*, 1989, **158**, 341.
7. W. Hug, in 'Raman Spectroscopy', J. Lascombe and P. V. Huong, Eds., Wiley-Heyden Chichester, 1982, p. 3.
8. L. D. Barron, L. Hecht, W. Hug and M. J. MacIntosh, *J. Am. Chem. Soc.*, 1989, **111**, 8731.
9. C. W. Johnson, Jr., *Advances in Carbohydrate Chemistry and Biochemistry*, 1987. **45**, 73.
10. D. G. Lewis and W. C. Johnson, Jr., *Biopolymers*, 1978, **17**, 1439.
11. C. M. Tummalapalli, D. M. Back and P. L. Polavarapu, *J. Chem. Soc., Faraday Trans.* 1988, **84**, 2585, and references therein.
12. L. D. Barron, D. J. Cutler and J. F. Torrance, *J. Raman Spectrosc.*, 1987, **18**, 281.
13. L. D. Barron, A. R. Gargaro and Z. Q. Wen, *Carbohydr. Res.*, submitted for publication.
14. R. I. Gelb, L. M. Schwartz, J. J. Bradshaw and D. A. Laufer, *Bioorg. Chem.*, 1980, **9**, 299.
15. J. J. Cael, J. L. Koenig and J. Blackwell, *Carbohydr. Res.*, 1973, **29**, 123.
16. A. T. Tu, J. Lee and F. P. Milanovich, *Carbohydr. Res.*, 1979, **76**, 239.
17. W. Saenger, M. Noltemeyer, P. C. Manor, B. Hingerty and B. Klar, *Bioorg. Chem.*, 1976, 187.

mica Acta, Vol. 47A, No. 8, pp. 1001–1016, 1991
Great Britain

0584-8539/91 $3.00+0.00

erimental and *ab initio* theoretical vibrational Raman optical activity of alanine

L. D. BARRON,† A. R. GARGARO and L. HECHT
Chemistry Department, University of Glasgow, Glasgow G12 8QQ, U.K.

and

P. L. POLAVARAPU
Department of Chemistry, Vanderbilt University, Nashville, TN 37235, U.S.A.

(*Received* 12 *February* 1991; *accepted* 26 *February* 1991)

ct—The vibrational Raman optical activity (ROA) spectra of L-alanine in water, 1 N NaOH and 1 N etween 720 and 1500 cm^{-1} measured in backscattering are reported. Unlike the associated vibrational ir dichroism (VCD), the main ROA features are relatively insensitive to pH changes. *Ab initio* Raman OA intensities were evaluated using 6-31G and 6-31G* basis sets and found to agree remarkably well he experimental parameters in the lower-frequency region.

INTRODUCTION

ITE its early observation [1, 2], vibrational Raman optical activity (ROA) has so far little impact on stereochemical studies of biologically significant molecules such as o acids in aqueous solution on account of insufficient sensitivity. The substantial of ROA work carried out to date has tended to concentrate on fundamental studies r than the solving of particular stereochemical problems [3,4]. ROA's younger g, vibrational circular dichroism (VCD), has so far set the pace in this area [5–9]. ever, a recent major advance in ROA instrumentation based on the use of a scattering geometry [10, 11] (in place of the usual 90° scattering arrangement) ther with a cooled CCD detector [12] has provided a "quantum leap" in sensitivity h has rendered biologically significant molecules in aqueous solution accessible to A studies, with good results on peptides and proteins [13] and carbohydrates [14, 15] rted at the time of writing. This advance in ROA instrumentation has been mpanied by a recent theoretical advance whereby ROA intensities can be computed essfully using modern *ab initio* methods [16–19]. This paper reports experimental theoretical results on alanine which demonstrate that ROA and VCD measurements ide very different perspectives on molecular stereochemistry.

lanine is an ideal subject for initial ROA studies of biologically significant molecules queous solution since it is the simplest chiral amino acid and has been the subject of nsive vibrational studies, including VCD, over many years. The most important ier articles for the present work are one by DIEM *et al.* [20] on vibrational analysis and gnments of alanine based primarily on solution-phase Raman spectra with results of and Raman solid-phase spectra and a Urey–Bradley normal coordinate analysis taken consideration; one on intermolecular vibrational coupling in crystals of DL-alanine KETTLE *et al.* [21]; and two on mid-IR VCD studies of alanine in H_2O and D_2O ution by DIEM [22] and by FREEDMAN *et al.* [23]. It should also be mentioned that A data (acquired in depolarized 90° scattering) for several Raman bands of alanine in ter are presented in a doctoral thesis by HOHMANN [24], but the instrumental sitivity was marginal.

The methine C*–H deformations are of particular interest in this study since they have n found to dominate the mid-IR VCD spectrum and are implicated in the large VCD

†Author to whom correspondence should be addressed.

The calculations were performed on the L(S) configuration of alanine in the zwitterionic form $(CH_3)CH(NH_3^+)(CO_2^-)$ it adopts at neutral pH and also on the hypothetical neutral form $(CH_3)CH(NH_2)CO_2H$. Only the results on the zwitterionic form are presented and discussed in detail, with reference being made to the results on the neutral form in cases where they assist the interpretation of changes in observed ROA features of alanine on going from neutral solution to acid and base solution where CO_2H and NH_2 groups, respectively, are present.

The crystal structure of zwitterionic L-alanine was determined several years ago using neutron diffraction data [35]. This experimental geometry was used as the starting point to optimize the theoretical geometry using the 6-31G and 6-31G* basis sets. The optimized coordinates are summarized in Table 1 and the atomic numbering shown in Fig. 2. The theoretical vibrational frequencies and intensities obtained at these optimized geometries and the mode descriptions, using the internal coordinates defined in Table 2, are given in Table 3. (The infrared intensities that are listed in Table 3 for completeness were obtained by evaluating electric dipole component derivatives in a similar fashion to the polarizability tensor component derivatives.) Table 4 lists the theoretical ROA tensor product invariants, with the resulting theoretical backscattered dimensionless ROA intensities listed in Table 5 together with the experimental values. The theoretical backscattered Raman and ROA spectra for comparison with the experimental spectra in the range 750 to 1500 cm^{-1} are shown in Figs 3 and 4.

Discussion

Vibrational analysis

We are not aware of any previous *ab initio* vibrational analysis for alanine. However, several papers on the vibrational analysis of zwitterionic alanine employing force constants that were either assumed or transferred from related molecules have been reported: the most recent is that by DIEM *et al.* [20], who utilized the experimental vibrational frequency data on several isotopic species in arriving at plausible vibrational assignments which we have found very useful for comparison with our *ab initio* assignments. Also the paper by KETTLE *et al.* [21] provides useful assignments derived purely from experimental data on several crystalline isotopic species of DL-alanine: although Ref. [21] reported that no evidence was found for intermolecular vibrational coupling in undeuterated crystalline DL-alanine, this data must nevertheless be used with caution here since we are discussing solution spectra.

Table 1. Optimized Cartesian coordinates (Å) for zwitterionic (S)-alanine in the principal axes of inertia†

		6-31G basis set			6-31G* basis set		
		X	*Y*	*Z*	*X*	*Y*	*Z*
1	O	−0.3182	−1.2178	1.0491	−0.3057	−1.1755	1.0858
2	O	0.1547	0.9571	1.5691	0.1485	0.9800	1.5270
3	N	0.1095	−1.1197	−1.3386	0.0989	−1.1433	−1.3048
4	C	0.0465	−0.0176	0.8278	0.0412	−0.0043	0.8384
5	C	0.4153	0.2181	−0.6735	0.4103	0.1959	−0.6758
6	C	−0.3618	1.3626	−1.3011	−0.3483	1.3307	−1.3387
7	H	1.4799	0.3828	−0.7490	1.4777	0.3458	−0.7585
8	H	−0.1793	−1.6606	−0.4605	−0.1648	−1.6592	−0.4104
9	H	−0.6521	−1.0690	−1.9897	−0.6826	−1.1162	−1.9369
10	H	0.9018	−1.5421	−1.7840	0.8764	−1.5767	−1.7701
11	H	−1.4292	1.1731	−1.2702	−1.4202	1.1587	−1.2983
12	H	−0.1743	2.2521	−0.7183	−0.1419	2.2360	−0.7864
13	H	−0.0634	1.5466	−2.3271	−0.0534	1.4738	−2.3743

† Energy (in atomic units) at the 6-31G* geometry is −321.825889682 and at the 6-31G geometry is −321.681677901.

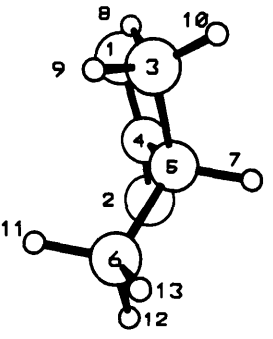

Fig. 2. Atomic numbering for zwitterionic L(S)-alanine.

though, as mentioned above, the *ab initio* theoretical vibrational frequencies are % higher than the corresponding experimental frequencies, they can be brought closer correspondance with the experimental frequencies without affecting the cted intensities by using a constant scale factor. We therefore base our correlations alculated modes with experimental bands on the comparison of the calculated and ved relative intensity patterns. Since the calculations of frequencies and associated an and ROA intensities using the 6-31G* basis set are generally in slightly better ement with the experimental quantities than those calculated with the 6-31G basis or simplicity we refer mostly to the former in the discussion below, which is limited e region for which we have ROA data, namely $\sim$700–1500 cm^{-1}. Our suggested lations between the experimental band frequencies and the frequencies of the G* theoretical modes are listed in Table 5.

the $\sim$750–1250 cm^{-1} region of the experimental Raman spectrum at neutral pH e 1), the band at $\sim$850 cm^{-1} is intense and those at 775, 992, 995, 1001, 1110, 1145 nt 1220 cm^{-1} are relatively weak, with similar intensities. This is also the pattern found th the 6-31G and 6-31G* theoretical Raman spectra (Figs 3 and 4): concentrating on *init*tter spectrum, we see that the predicted 881 cm^{-1} mode exhibits much the largest rivesity with those predicted at 838, 942, 1060, 1080, 1164, 1205 and 1314 cm^{-1} evely weak and of roughly similar intensity. We therefore have confidence in the ionlation of the experimental band at $\sim$850 cm^{-1} with the 6-31G* mode at 881 cm^{-1}. with remaining experimental bands can be correlated with the remaining 6-31G* modes eir corresponding order of frequency, but some uncertainty can be present here use the theoretical ordering of modes need not always match that of the experimen- pectra, and the relative intensities are too similar to use as a criterion for lations. However, the ROA spectrum plays an important role at this point because ROA signs provide an extra criterion for these correlations: we shall see that a parison of the experimental and predicted ROA signs suggests that our predicted ring of this set of modes is indeed correct.

orrelation of the experimental Raman bands in the $\sim$1250–1500 cm^{-1} region at ral pH with the *ab initio* results is not as satisfactory as in the lower region, and it is ful to invoke the assignments of DIEM *et al.* [20] and KETTLE *et al.* [21] in this region use they both make use of valuable isotopic data.

he experimental bands at 1301 and 1351 cm^{-1} were assigned by DIEM *et al.* [20] to -H bending modes. However, there must also be significant contributions from NH_3^+ ding motions because these bands shift to 1291 and 1337 cm^{-1}, respectively, upon terating the NH_3^+ group. A similar shift to lower frequency upon NH_3^+ deuteration also been observed for the corresponding bands in the DL-alanine crystals [21]. relation of the 6-31G* theoretical modes at 1395 and 1447 cm^{-1} with these two erimental bands therefore seems reasonable because they both have significant ing of C*–H and NH_3^+ bending motions.

he experimental Raman bands at 1375 and 1459 cm^{-1} were assigned by DIEM *et al.* to methyl deformations, again using isotopic data: this is supported by the

Table 2. Internal symmetry coordinates for zwitterionic alanine†

Coordinate		Definition	Abbreviation	Coordinate	Definition	Abbreviation
R_1	$r_{1,4}$		C–O	R_{18}	$\frac{1}{\sqrt{6}}(2\alpha_{3,5,6}-\alpha_{3,5,4}-\alpha_{6,5,4})$	Asym C* bend
R_2	$r_{2,4}$		C–O	R_{19}	$\frac{1}{\sqrt{2}}(\alpha_{3,5,4}-\alpha_{6,5,4})$	Asym C* bend
R_3	$r_{3,5}$		C*–N	R_{20}	$\frac{1}{\sqrt{6}}(\alpha_{5,6,11}+\alpha_{5,6,12}+\alpha_{5,6,13}-\alpha_{11,6,12}-\alpha_{11,6,13}-\alpha_{12,6,13})$	Sym CH_3 bend
R_4	$r_{4,5}$		C*–C(O)			
R_5	$r_{5,6}$		C*–C(H_3)	R_{21}	$\frac{1}{\sqrt{6}}(2\alpha_{5,6,11}-\alpha_{5,6,12}-\alpha_{5,6,13})$	CH_3 rock
R_6	$r_{7,5}$		C*–H	R_{22}	$\frac{1}{\sqrt{2}}(\alpha_{5,6,12}-\alpha_{5,6,13})$	CH_3 rock
R_7	$r_{8,3}$		N–H	R_{23}	$\frac{1}{\sqrt{6}}(2\alpha_{11,6,12}-\alpha_{11,6,13}-\alpha_{12,6,13})$	Asym CH_3 bend
R_8	$r_{9,3}$		N–H	R_{24}	$\frac{1}{\sqrt{2}}(\alpha_{11,6,13}-\alpha_{12,6,13})$	Asym CH_3 bend
R_9	$r_{10,3}$		N–H	R_{25}	$\frac{1}{\sqrt{6}}(\alpha_{5,3,8}+\alpha_{5,3,9}+\alpha_{5,3,10}-\alpha_{8,3,9}-\alpha_{8,3,10}-\alpha_{9,3,10})$	Sym NH_3 bend
R_{10}	$r_{11,6}$		C(H_3)–H			
R_{11}	$r_{12,6}$		C(H_3)–H	R_{26}	$\frac{1}{\sqrt{6}}(2\alpha_{5,3,8}-\alpha_{5,3,9}-\alpha_{5,3,10})$	NH_3 rock

R_{12}	$r_{13,6}$	$C(H_3)$–H	R_{27}	$\frac{1}{\sqrt{2}}(\alpha_{5,3,9}-\alpha_{5,3,10})$	NH_3 rock
R_{13}	$\alpha_{2,4,1}$	Sym COO bend	R_{28}	$\frac{1}{\sqrt{6}}(2\alpha_{8,3,9}-\alpha_{8,3,10}-\alpha_{9,3,10})$	Asym NH_3 bend
R_{14}	$\frac{1}{\sqrt{2}}(\alpha_{2,4,5}-\alpha_{1,4,5})$	Asym COO bend	R_{29}	$\frac{1}{\sqrt{2}}(\alpha_{8,3,10}-\alpha_{9,3,10})$	Asym NH_3 bend
R_{15}	$\frac{1}{\sqrt{6}}(\alpha_{7,5,4}+\alpha_{7,5,3}+\alpha_{7,5,6}-\alpha_{3,5,6}-\alpha_{3,5,4}-\alpha_{6,5,4})$	Sym C* bend	R_{30}	$\delta_{5,4,1,2}$	COO wag
R_{16}	$\frac{1}{\sqrt{6}}(2\alpha_{7,5,4}-\alpha_{7,5,3}-\alpha_{7,5,6})$	C*H bend	R_{31}	$\tau_{8,3,5,7}+\tau_{9,3,5,7}+\tau_{10,3,5,7}$	NH_3 torsion
			R_{32}	$\tau_{11,6,5,7}+\tau_{12,6,5,7}+\tau_{13,6,5,7}$	CH_3 torsion
R_{17}	$\frac{1}{\sqrt{2}}(\alpha_{7,5,3}-\alpha_{7,5,6})$	C*H bend	R_{33}	$\tau_{1,4,5,7}+\tau_{2,4,5,7}$	COO torsion

† $r_{i,j}$ represents the change in bond length between atoms i and j.
$\alpha_{i,j,k}$ represents the change in angle between i–j and j–k bonds.
$\delta_{i,j,k,l}$ represents the change in angle between bond i–j and the plane of atoms j, k, l.
$\tau_{i,j,k,l}$ represents the torsional angle between the planes of i–j–k and j–k–l.

Table 3. Vibrational frequencies and intensities for zwitterionic alanine†

6-31G basis set					6-31G* basis set					
Frequency (cm^{-1})	IR (km/mol)	Raman (A^4/amu)	Dep. ratio	Mode description‡	Frequency (cm^{-1})	IR (km/mol)	Raman (A^4/amu)	Dep. ratio	Mode description	Potential energy distribution
3809	72.8	44.8	0.72	Asym NH	3809	65.3	45.8	0.71	Asym NH	$R_9(59)$, $R_8(41)$
3723	53.7	66.9	0.11	Sym NH	3727	53.9	64.8	0.11	Sym NH	$R_8(59)$, $R_9(41)$
3320	2.3	49.8	0.58	Asym CH_3	3333	3.7	52.2	0.55	Asym CH_3	$R_{11}(92)$
3289	14.2	48.8	0.21	C*–H	3295	20.7	51.2	0.23	C*–H	$R_6(93)$
3257	25.3	87.3	0.72	Asym CH_3	3258	32.2	84.0	0.73	Asym CH_3	$R_{10}(50)$, $R_{12}(45)$
3194	26.7	112	0.04	Sym CH_3	3204	31.9	105	0.05	Sym CH_3	$R_{12}(48)$, $R_{10}(43)$
2707	520	22.2	0.10	N–H	2813	581	24.3	0.10	N–H	$R_7(81)$
1894	251	3.0	0.44	Asym COO stretch	1996	442	1.5	0.55	Asym COO stretch	$R_2(75)$, $R_1(32)$
1845	74.5	5.8	0.74	Asym NH_3 bend	1822	42.1	4.9	0.74	Asym NH_3 bend	$R_{28}(87)$
1821	51.7	8.7	0.69	Asym NH_3 bend	1790	24.6	7.8	0.67	Asym NH_3 bend	$R_{29}(68)$, $R_{23}(60)$
1654	20.2	14.7	0.75	Asym CH_3 bend	1641	11.9	11.9	0.74	Asym CH_3 bend	$R_{23}(90)$
1649	3.9	16.2	0.75	Asym CH_3 bend	1639	3.9	14.2	0.75	Asym CH_3 bend	$R_{24}(88)$
1586	69.5	3.9	0.74	Sym CH_3 bend	1568	47.0	2.7	0.73	Sym CH_3 bend	$R_{20}(84)$
1552	699	5.9	0.62	Sym NH_3 bend	1523	388	5.0	0.64	Sym NH_3 bend + C*H bend + sym COO stretch	$R_{25}(25)$, $R_{17}(20)$, $R_1(18)$, $R_2(17)$
1505	6.6	6.3	0.68	C*H bend + COO torsion	1501	69.9	4.5	0.74	C*H bend + COO torsion	$R_{17}(71)$, $R_{33}(16)$
1446	10.3	1.7	0.75	C*H bend + NH_3 torsion	1447	143	2.4	0.39	C*H bend + sym NH_3 bend + NH_3 torsion	$R_{16}(53)$, $R_{25}(15)$, $R_4(14)$, $R_{31}(12)$
1387	283	9.3	0.22	C–O + sym COO bend	1395	238	8.2	0.24	sym NH_3 bend + C – O + C*H bend	$R_{25}(44)$, $R_1(23)$, $R_{16}(21)$
1339	57.6	3.7	0.71	NH_3 rock + CH_3 rock	1314	18.0	2.6	0.69	NH_3 rock + CH_3 rock + C*–C(H_3)	$R_{27}(23)$, $R_{21}(19)$, $R_5(13)$
1234	105	3.0	0.73	C*H bend + NH_3 rock	1205	41.8	2.0	0.69	C–H bend + CH_3 rock + NH_3 rock	$R_{16}(30)$, $R_{22}(26)$, $R_{26}(14)$
1185	25.3	5.1	0.64	CH_3 rock + NH_3 rock + asym C* bend	1164	38.7	3.9	0.66	NH_3 rock + CH_3 rock + C*–N + C*–C(H_3)	$R_{26}(30)$, $R_{22}(18)$, $R_3(16)$, $R_5(16)$

				C* bend				$C-N+C-C(H_3)$	$R_3(16)$, $R_5(16)$
1108	49.3	2.6	0.72	CH_3 rock + C*–C(H$_3$) + C*–H bend + NH_3 rock	1080	72.9	4.1	0.72	NH_3 rock + CH_3 rock + C*–C(H$_3$)	$R_{26}(32)$, $R_{21}(20)$, $R_5(18)$
1083	32.6	5.7	0.75	NH_3 rock + C*–C(H$_3$)	1060	22.6	2.6	0.75	NH_3 rock + CH_3 rock	$R_{27}(49)$, $R_{21}(18)$
916	73.3	3.9	0.57	C*–C(O) + C*–N + sym COO bend	942	99.2	3.5	0.47	C*–C(O) + sym COO bend + C*–N	$R_4(44)$, $R_{13}(39)$, $R_3(23)$
860	48.6	10.1	0.21	C*–N + sym COO bend + sym C* bend + COO wag	881	34.1	8.5	0.24	C*–N + sym COO bend	$R_3(43)$, $R_{13}(17)$
809	21.5	3.5	0.60	COO wag + sym COO bend	838	16.2	2.6	0.63	COO wag + sym COO bend	$R_{30}(46)$, $R_{13}(20)$
675	13.5	5.5	0.37	Asym COO bend + COO wag + C*–C(O) + sym COO bend	681	7.9	4.8	0.32	Asym COO bend + C*–C(O) + COO wag + C*–C(H$_3$)	$R_4(21)$, $R_{14}(21)$, $R_{30}(13)$, $R_5(11)$
566	41.0	4.0	0.18	Asym COO bend + C*–C(O) + N–C*	562	34.9	3.1	0.18	Asym COO bend + C*–(O) + N – C*	$R_{14}(33)$, $R_4(25)$, $R_3(14)$
419	12.4	0.57	0.63	Asym C* bend + sym C* bend	413	3.0	0.60	0.60	Sym C* bend + asym C* bend	$R_{15}(56)$, $R_{18}(46)$
375	102	1.41	0.70	Asym COO bend + N–H + sym C* bend	352	111	0.72	0.66	N–H + asym C* bend + asym COO bend	$R_7(44)$, $R_{18}(38)$, $R_{14}(33)$, $R_{26}(20)$
336	18.2	0.88	0.75	NH_3 torsion + asym NH_3 bend	303	30.4	0.57	0.74	NH_3 torsion + NH_3 bend	$R_{31}(148)$, $R_{28,31}(-114)$, $R_{28}(60)$
276	15.4	1.33	0.63	C* bends	275	17.2	0.88	0.64	C* bends	R_{19} (71), $R_{14}(25)$
257	1.9	0.32	0.75	CH_3 torsion	255	3.3	0.28	0.68	CH_3 torsion	$R_{32}(76) + R_{19}(26)$
65	3.7	0.69	0.75	NH_3 torsion + COO torsion	54	3.5	0.39	0.75	NH_3 torsion + COO torsion	Several contributions from R_{28} to R_{33}

† Raman intensities listed are $45\alpha_j + 7\beta_j^2$; depolarization ratio is given as $3\beta_j^2/(45\alpha_j^2 + 4\beta_j^2)$.

‡ Based on potential energy distribution.

assignments of KETTLE *et al.* [21] for corresponding bands in crystalline DL-alanine. T 1375 cm^{-1} band is due to the symmetric methyl bending mode and correlates with 6-31G* mode at 1568 cm^{-1}. The 1459 cm^{-1} band is due to the nearly degenerate pai antisymmetric methyl bending modes and correlates with the 6-31G* modes at 1639 a 1641 cm^{-1}.

DIEM *et al.* [20] assigned the experimental Raman band at 1410 cm^{-1} to the symme CO_2^- stretch, as did KETTLE *et al.* [21] for the corresponding band in crystall DL-alanine. Although the 6-31G* theoretical modes at 1523 and 1501 cm^{-1} have so contribution from the CO_2^- group, in neither of them does the CO_2^- symmetric stre dominate. The combined Raman intensity of these two theoretical modes wo correlate with the large intensity observed in the experimental 1410 cm^{-1} band, but i not large enough to surpass the intensity of the antisymmetric methyl bending mod which conflicts with the significantly larger intensity of the experimental Raman band 1410 cm^{-1} relative to that at 1459 cm^{-1}. It should also be noted that, while t experimental bands due to the methyl symmetric and antisymmetric deformations separated by the 1410 cm^{-1} band, the 6-31G* theoretical methyl bending modes a adjacent. Hence the predicted ordering of these modes is not correct and they must re-arranged to achieve a satisfactory correlation with the experimental Raman bands

Table 4. *Ab initio* Raman optical activity parameters for zwitterionic (S)-alanine†

6-31G basis set				6-31G* basis set			
Frequency (cm^{-1})	$\frac{\alpha G'}{\omega} \times 10^2$	$\frac{\gamma^2}{\omega}$	$\frac{\delta^2}{\omega}$	Frequency (cm^{-1})	$\frac{\alpha G'}{\omega} \times 10^2$	$\frac{\gamma^2}{\omega}$	$\frac{\delta^2}{\omega}$
3809	−0.39	−0.10	−0.13	3809	−0.35	−0.08	−0.14
3723	−0.26	0.05	0.11	3727	−0.42	0.04	0.10
3320	−0.37	−0.24	−0.22	3334	−0.63	−0.23	−0.19
3289	0.52	0.53	0.50	3295	0.26	0.46	0.44
3257	−0.25	−0.40	−0.08	3258	−0.19	−0.30	−0.05
3194	−0.68	0.02	−0.10	3204	−0.11	0.03	−0.11
2707	0.54	−0.04	0.02	2813	0.76	−0.04	0.01
1894	0.08	0.03	0.01	1996	0.04	0.01	−0.00
1845	0.14	0.09	0.02	1822	0.13	0.13	0.02
1821	−0.09	−0.10	−0.05	1790	−0.12	−0.11	−0.05
1654	−0.08	0.05	−0.01	1641	−0.09	0.14	0.05
1649	0.02	−0.11	0.08	1639	0.01	−0.14	0.04
1586	−0.01	0.04	−0.02	1568	0.02	−0.01	−0.07
1552	0.04	−0.15	−0.01	1523	−0.07	0.02	0.07
1504	−0.26	0.13	−0.04	1501	0.06	−0.13	−0.15
1446	0.01	−0.03	−0.05	1447	0.09	−0.15	−0.06
1387	−0.11	0.09	0.07	1395	−0.34	0.26	0.11
1339	−0.01	−0.16	−0.10	1314	0.03	−0.13	−0.07
1233	0.02	0.17	0.03	1205	0.04	0.02	−0.01
1185	0.06	0.02	0.03	1164	0.02	0.16	0.06
1108	0.0	−0.11	−0.05	1080	0.03	−0.11	−0.04
1083	0.01	0.01	−0.0	1060	0.0	−0.0	−0.00
916	−0.08	0.08	0.03	942	−0.08	0.07	0.02
860	0.02	−0.06	−0.05	881	0.09	−0.06	−0.03
809	0.07	−0.02	−0.01	838	0.03	0.0	−0.02
675	0.11	−0.07	0.02	681	0.07	−0.04	0.01
566	−0.0	0.02	0.02	562	−0.02	0.01	0.01
419	0.03	0.00	−0.00	413	0.02	−0.00	−0.00
375	−0.03	−0.05	−0.01	352	−0.03	−0.07	−0.01
336	−0.0	0.02	0.01	303	0.02	0.02	0.01
276	0.01	0.03	0.01	275	0.01	0.03	0.00
257	−0.0	0.01	0.00	255	−0.0	0.01	0.01
65	−0.0	0.01	0.00	54	0.0	0.01	0.00

† ROA parameters are given in A^5/amu units.

Table 5. Comparison of the experimetnal and *ab initio* theoretical ROA parameters for L-alanine

Experimental		*Ab initio* 6-31G*		*Ab initio* 6-31G		Assignments	
Frequency (cm^{-1})	$\Delta(180)\times10^4$	Frequency (cm^{-1})	$\Delta(180)\times10^4$	Frequency (cm^{-1})	$\Delta(180)\times10^4$	631G*	Ref. [20]
875	−11.7	838	−0.7	809	−2.2	COO wag + sym COO bend	COO wag
850	−2.4	881	−2.6	860	−2.5	C*–N + sym COO bend	Sym CCN stretch
922	+17.7	942	+6.5	915	+7.4	C*–C(O) + sym COO bend + C*–N	CH_3 rock
995	−7.0	1060	−0.4	1083	+0.3	NH_3 rock + CH_3 rock	CH_3 rock
1001		1080	−9.8	1108	−15.0	NH_3 rock + CH_3 rock + C*–C(H_3)	C–C(O) stretch
1110	+4.1	1164	+14.3	1185	+1.6	NH_3 rock + CH_3 rock + C*–N + C*–C(H_3)	Asym CCN stretch
1145	+14.8	1205	+2.7	1234	+18.3	C*H bend + CH_3 rock + NH_3 rock	NH_3 rock
1220	−3.4	1314	−18.0	1339	−16.4	NH_3 rock + CH_3 rock + C*–C(H_3)	NH_3 rock
1301	+4.0	1395	+11.2	1387	+4.0	Sym NH_3 bend + C–O + C*H bend	C*H bend
1351	+2.6	1447	−21.7	1446	−9.4	C*H bend + NH_3 bend	C*H bend
1375	−0.6	1568	−3.5	1586	2.9	Sym CH_3 bend	Sym CH_3 bend
1410	−2.4	1523	2.5	1552	−7.8	Sym NH_3 bend + C*H bend + sym COO stretch	Sym COO stretch
		1501	−12.5	1505	5.9	C*H bend + COO torsion	
1459	−0.7	1639	−2.7	1649	−1.6	Asym CH_3 bend	Asym CH_3 bend
1459	+3.0	1641	+4.1	1654	+0.9	Asym CH_3 bend	Asym CH_3 bend

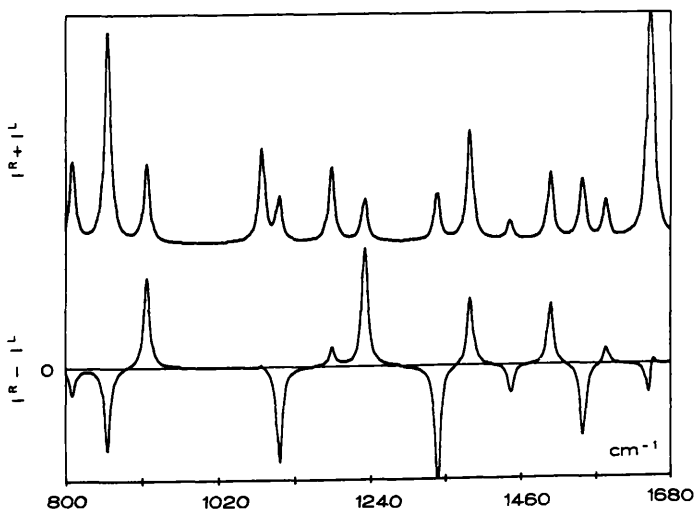

3. *Ab initio* backscattered Raman $I^R + I^L$ and ROA $I^R - I^L$ spectra of zwitterionic L(S)-alanine obtained with the 6-31G basis set. The intensity scales are arbitrary.

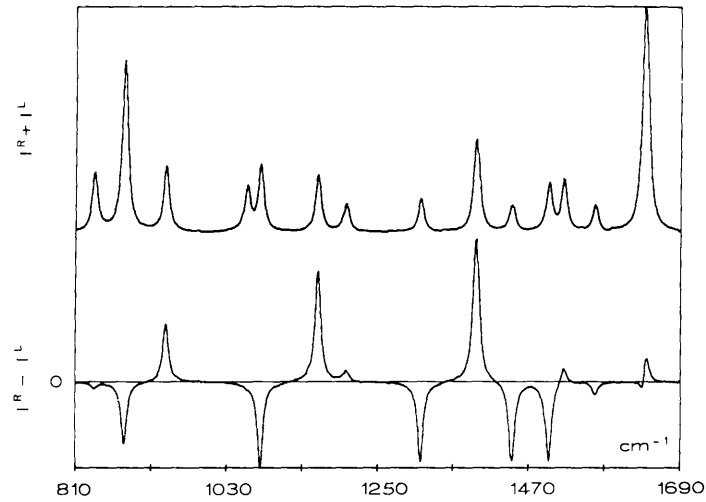

Fig. 4. *Ab initio* backscattered Raman and ROA spectra of zwitterionic L(S)-alanine obtained with the 6-31G* basis set.

Raman optical activity

Starting at the low-frequency end of the experimental ROA spectra of L-alanine (Fi 1), we observe a small negative ROA in the band at $\sim 775\,cm^{-1}$ in the H_2O solutio assigned by DIEM *et al.* [20] to the CO_2^- wag. The corresponding band of crystallir DL-alanine was identified as a CO_2^- bending mode rather than as the wag [21]. Th 6-31G* calculations support both these assignments since both modes contribute, an correctly predict the negative ROA. The same Raman and ROA features appear in th NaOH solution, which is consistent with the CO_2^- group remaining unprotonated an maintaining approximately the same conformation as at neutral pH. However, in th HCl solution a second band appears at $\sim 745\,cm^{-1}$, both bands showing a small negativ ROA: this could be interpreted as arising from two dominant conformations of the intac CO_2H group, from dimer formation, or from deformations of the carbonyl group whic of course is not present at high and neutral pH. In fact our calculations on *neutral* alanin support the third interpretation because they predict a band with negative ROA in thi region arising from the out-of-plane C=O deformation plus the O–H torsion.

The next band, appearing at $\sim 850\,cm^{-1}$ in the H_2O solution and assigned both b DIEM *et al.* [20] and by KETTLE *et al.* [21] to the CCN symmetric stretch, shows a larg negative ROA. The 6-31G* calculations support the CN stretch assignment, with th addition of a contribution from the symmetric CO_2^- bend, and predict the negativ ROA. A similar negative ROA band is seen in the NaOH solution. In the HCl solutio the band shifts to slightly lower frequency with reduced intensity and a second ban appears at $\sim 820\,cm^{-1}$, both bands having a small negative ROA. These changes at lov pH are presumably associated with the loss of the symmetric CO_2^- bend contributior and the presence of new contributions from the CO_2H group: the calculations on *neutra* alanine support this presumption because they predict a band with a small negative ROA in this region associated with the out-of-plane C=O deformation plus the C–C(O stretch.

DIEM *et al.* [20] assign the band at $\sim 922\,cm^{-1}$ to a methyl rocking mode, and that at $\sim 1000\,cm^{-1}$ to a methyl rock at $995\,cm^{-1}$ plus the C–C(O_2) stretch at $1001\,cm^{-1}$. A well-characterized ROA couplet, positive in the lower-frequency band and negative in the higher, appears in all three solutions. It is tempting to think of this couplet as arising from symmetric and antisymmetric combinations of the two orthogonal methyl rock coordinates; however, the 6-31G* assignments indicate that this idea is incorrect since it contains large C–C(O_2) stretch but little methyl rock contributions at $922\,cm^{-1}$, and NH_3^+ rock plus methyl rock at $\sim 1000\,cm^{-1}$. The 6-31G* assignments are reinforced by the assignment of the corresponding two bands in crystalline DL-ananine to C–C stretch

methyl rocking modes, respectively [21], and by the correct prediction of the 6-31G* ulations of the observed ROA signs. Also, alanine in NaOH solution lacks the NH_3^+ p yet still shows ROA at $\sim 1000\,cm^{-1}$ similar to that in the H_2O and HCl solutions so an deduce that the ROA at this frequency is associated mostly with the methyl rock er than with the NH_3^+ rock.

ll the ROA features discussed so far are at frequencies below the reported mid-IR) studies of alanine [22, 23] so no ROA–VCD comparisons can be made. However next feature, comprising two bands at ~ 1110 and $1145\,cm^{-1}$ in water, comes within range of these VCD studies: these bands were assigned by DIEM *et al.* [20] to the symmetric CCN stretch and to NH_3^+ rocking, respectively; whereas KETTLE *et al.* assigned the corresponding bands in crystalline DL-alanine to the antisymmetric N stretch and to methyl rocking. The broad $1145\,cm^{-1}$ band shows a broad positive A with a dip where it overlaps the $1110\,cm^{-1}$ band, indicating that the latter has a ll negative ROA. The same Raman and ROA features are repeated in the HCl and)H solutions, but in the latter a new band with a small negative ROA appears at 075 cm^{-1} that must originate in the NH_2 group. The fact that essentially the same man and ROA intensity is seen in these two bands in all three solutions indicates that contribution from one of the NH_3^+ rock coordinates to the $1145\,cm^{-1}$ band is less n suggested in Ref. [20] and reinforces the methyl rock assignment in Ref. [21]. The 3G* calculation predicts the correct ROA sign for the band at $1145\,cm^{-1}$ but not for t at $1110\,cm^{-1}$ (assuming that the latter is indeed negative), and suggests that there Fi significant contributions from methyl rocking and the methine C*–H deformations as tio as from NH_3^+ rocking at $1145\,cm^{-1}$, which accords with the statement in the llin vious sentence. The next band at $\sim 1220\,cm^{-1}$ should be discussed in conjunction Th the previous two since it has also been assigned to NH_3^+ rocking: however, this an gnment is not fully consistent with our observations because the Raman band still th ears in the NaOH solution (where the NH_3^+ group is not present) and all three an tions show a negative ROA (very small in H_2O and NaOH). On the other hand the th 3G* calculation supports this assignment since it contains a significant NH_3^+ rock tiv tribution in this band and predicts a negative ROA. The VCD spectrum of L-alanine ta this region shows negative, negative and positive features, respectively, in IR bands at nic 7, 1139 and $1221\,cm^{-1}$. The second and third vibration generate opposite signs in both lin)A and VCD: DIEM [22] has suggested that coupling between orthogonal NH_3^+ rock thi rdinates is a plausible mechanism for the generation of this VCD couplet, and a ilar mechanism could be responsible for the corresponding ROA couplet (but bear in b nd the reservations expressed above concerning the contributions of NH_3^+ rocking to rg 1145 and $1220\,cm^{-1}$ Raman bands). The new very weak band with a small positive th)A at $\sim 1260\,cm^{-1}$ in the HCl solution is probably associated with O–H deformations tiv m the CO_2H group (the *neutral* alanine calculations do predict O–H deformation ion tributions in this region).

an The last group of five bands is the most interesting. As mentioned above, the first two ow nds at 1301 and $1351\,cm^{-1}$ have been assigned by DIEM *et al.* [20] to the methine C*–H ion formations. These two bands show very large VCD with opposite signs in water tra 23] which completely disappears at high and low pH [23]. It has been suggested that)A s VCD feature and its dramatic dependence on pH are associated with a ring current O chanism involving electron flow, induced by the C*–H deformation, in the ring closed hydrogen bonding between the carboxylate and amino groups [23]; but DIEM [22] has a pressed reservations about whether a ring current mechanism can be invoked in this A nation, and the whole concept of the ring current mechanism has recently been in estioned on the basis of *ab initio* VCD computation results [36]. The ROA is quite ing ferent from the VCD in these two bands, showing a positive feature of approximately ck same magnitude in each that is independent of pH since it is virtually the same in all it ree solutions (which rules out a significant contribution from NH_3^+). Another differ- nd ce is that the positive ROA in the second C*–H deformation band at $\sim 1351\,cm^{-1}$ by ms part of a couplet with a band at $\sim 1375\,cm^{-1}$ assigned by DIEM *et al.* [20] to the ch mmetric methyl deformation exhibiting a negative ROA: the VCD in this symmetric

methyl deformation band is very small and has the same sign as the VCD in the seco for t C*–H deformation band [22, 23]. As well as emphasizing that ROA and VCD mech a wi nisms are quite different, these ROA observations are perplexing because one possit obt interpretation of the ROA couplet is that there is significant interaction between t res C*–H deformations and the symmetric methyl deformations; yet it has been previou date concluded [22] that this interaction is minimal because the Raman spectra of t anis deuterated species L-Ala-C-d_3 show little change in the methine vibrational frequenc ole [20]. Unfortunately the 6-31G* calculations are not helpful here: although significance C*–H deformation contributions appear in the normal modes at 1301 and 1351 cm^{-1}, t site first band is predicted to have the observed positive ROA but the second is wrong ncec predicted to have a negative ROA. And although the symmetric methyl deformation ctly predicted to have the observed negative ROA, its calculated frequency is rather high. cule is worth mentioning that the *neutral* alanine calculations do predict strong mixi ests between the C*–H deformations and the symmetric methyl deformation. Unfortunate rat the crystalline DL-alanine results add to the confusion because the band at 1366 cm^{-1} is als unlike the corresponding solution band at 1351 cm^{-1}, shifts very little on deuteration mati the methine proton, which supports its assignment (along with the crystalline DL-alani icts band at 1386 cm^{-1}) to the symmetric methyl deformation in Ref. [21]. nally

The next band, at ~1410 cm^{-1}, assigned to the symmetric CO_2^- stretch [20, 21], shows in a significant negative ROA in all three solutions. The VCD spectra show a small positi lle f feature in this vibration of opposite sign to the feature in the symmetric meth in c deformation band [22, 23] suggestive of some coupling between the symmetric meth ssing deformation and the symmetric CO_2^- stretch. The discussion is complicated by the fa gr that there is still significant Raman and ROA intensity in this band in the HCl solutio our where symmetric CO_2^- contributions cannot exist, which suggests that the symmetr spec CO_2^- stretch must be less dominant than previously supposed (but there is no questio of that the CO_2H group, either protonated or unprotonated, is largely responsible for thove 1410 cm^{-1} band because we observed no sign of it in the Raman spectrum of alanino which has the same structure as alanine except that CO_2H is replaced by CH_2OH). Thi owle suggestion is supported somewhat by the 6-31G* calculations because, corresponding t eutsc the experimental 1410 cm^{-1} band, there are two modes with frequencies 1523 an vation 1501 cm^{-1} with large negative and small positive ROA, respectively, and neither of thes have the CO_2^- stretch as the major contribution (they contain a mixture of C*–H deformations, CO_2^- stretch and CO_2^- torsion motions). Also the *neutral* alanin calculations suggest that methyl symmetric deformations mixed with C*–H deformation contribute in this region.

L. D
W. F
L. D.
J. F.
L. A
T. G
T. B
Wile
P. J.
P. P
P. L.
and
G. M
L. H
L. H
L. D
L. D
L. D
(199
L. D
P. K
P. K
T. M
(199
P. L
M. I

The final band, at ~1460 cm^{-1}, assigned to the degenerate pair of antisymmetri methyl deformations [20, 21], shows an ROA couplet in all three solutions, whic suggests that ROA of opposite sign is generated in the two split antisymmetric methy deformations through coupling with other modes. No significant VCD is observed ir these antisymmetric methyl deformations [22]. It is gratifying that the 6-31G* calcula tions do predict the observed negative–positive ROA couplet in the split antisymmetric methyl deformations even though the calculated frequencies are rather high. This situation is similar to another much-studied case in arylethanes where ROA couplets are generated in the antisymmetric methyl deformations through coupling with an aromatic mode that coincides in frequency [37–39].

We have not shown the bands between ~1600 and 1650 cm^{-1}, assigned to the antisymmetric CO_2^- deformation and to the antisymmetric NH_3^+ deformations [20, 21], because no significant ROA was observed; but VCD data is available in this region [22, 23]. We did not attempt to obtain ROA spectra in the C–H stretch region; but extensive VCD studies as a function of pH have been carried out in this region [40].

CONCLUSIONS

This study has demonstrated that ROA has great potential for stereochemical investigations of biologically significant molecules in aqueous media. The instrument

for the measurements was not the currently attainable optimum, yet useful spectra a wider range at lower frequency than that accessible to VCD at the present time obtained without the associated solvent problems. The fact that the main ROA res of alanine are similar at neutral, high and low pH indicates firstly that the ated conformations are very similar; and secondly that, unlike VCD, the dominant anisms generating ROA are more directly linked to the basic structural features of olecule and so might provide more reliable stereochemical information. Also the nce of ROA structure (arising from closely spaced bands with ROA intensities of site sign) where none is seen in the parent Raman band emphasizes the greatly nced resolution capability of ROA. The success of the *ab initio* calculations in ctly predicting the signs of many of the observed ROA features of such a "large" cule (at least when the corresponding normal modes have been reliably computed) ests that it should eventually be possible to interpret ROA spectra at a fundamental , rather than simply relying on empirical correlations to extract information.

is also worth emphasizing that the absolute configuration of a chiral molecule follows matically with a high degree of certainty from an *ab initio* calculation that correctly icts most of the observed ROA band signs.

nally, we should mention that a recent study of depolarization ratios of Raman s in alanine and other amino acids as a function of concentration have indicated that lle formation takes place at high concentration [41]. Since saturated solutions were in our ROA studies, the possible presence of micelles should be born in mind when ssing our results: in particular, the possibility of a fixed geometrical orientation of groups against each other on the surface of a micelle, which was suggested to be ource of the enhanced isotropic scattering with increasing concentration [41], would pected to significantly affect the corresponding ROA. We intend to investigate the t of micelle formation on the ROA of alanine when further planned instrumental rovements will make ROA measurements on dilute solutions possible.

owledgements—Grants from the Science and Engineering Research Council, the Wolfson Foundation, eutsche Forschungsgemeinschaft (III 02-He 1588/1–1), the National Institutes of Health (GM 29375) and ational Science Foundation (CHE 8808018) are gratefully acknowledged.

References

L. D. Barron, M. P. Bogaard and A. D. Buckingham, *J. Am. Chem. Soc.* **95**, 603 (1973).
W. Hug, S. Kint, G. F. Bailey and J. R. Scherer, *J. Am. Chem. Soc.* **97**, 5589 (1975).
L. D. Barron, in *Vibrational Spectra and Structure*, Vol. 17B, p. 343 (edited by H. D. Bist, J. R. Durig and J. F. Sullivan). Elsevier, Amsterdam (1989).
L. A. Nafie and C. G. Zimba, in *Biological Applications of Raman Spectroscopy*, Vol. 1, p. 307 (edited by T. G. Spiro). Wiley, New York (1987).
T. B. Freedman and L. A. Nafie, in *Topics in Stereochemistry*, Vol 17, p. 113 (edited by E. Eliel and S. Wilen). Wiley, New York (1987).
P. J. Stephens and M. A. Lowe, *Ann. Rev. Phys. Chem.* **36**, 213 (1985).
P. Pancoska, S. C. Yasui and T. A. Keiderling, *Biochemistry* **28**, 5917 (1989).
P. L. Polavarapu, in *Vibrational Spectra and Structure*, Vol. 17B, p. 319 (edited by H. D. Bist, J. R. Durig and J. F. Sullivan). Elsevier, Amsterdam (1989).
G. M. Roberts, O. Lee, J. Calienni and M. Diem, *J. Am. Chem. Soc.* **110**, 1749 (1988).
L. Hecht, L. D. Barron and W. Hug, *Chem. Phys. Lett.* **158**, 341 (1989).
L. Hecht and L. D. Barron, *Appl. Spectrosc.* **44**, 438 (1990).
L. D. Barron, L. Hecht, W. Hug and M. J. Macintosh, *J. Am. Chem. Soc.* **111**, 8731 (1989).
L. D. Barron, A. R. Gargaro and Z. Q. Wen, *J. Chem. Soc., Chem. Comm.* 1034 (1990).
L. D. Barron, A. R. Gargaro, Z. Q. Wen, D. D. Nacnicol and C. Butters, *Tetrahedron: Asymmetry* **1**, 513 (1990).
L. D. Barron, A. R. Gargaro and Z. Q. Wen, *Carbohydr. Res.*, in press.
P. K. Bose, L. D. Barron and P. L. Polavarapu, *Chem. Phys. Lett.* **155**, 423 (1989).
P. K. Bose, P. L. Polavarapu, L. D. Barron and L. Hecht, *J. Phys. Chem.* **94**, 1734 (1990).
T. M. Black, P. K. Bose, P. L. Polavarapu, L. D. Barron and L. Hecht, *J. Am. Chem. Soc.* **112**, 1479 (1990).
P. L. Polavarapu, *J. Phys. Chem.* **94**, 8106 (1990).
M. Diem, P. L. Polavarapu, M. Oboodi and L. A. Nafie, *J. Am. Chem. Soc.* **104**, 3329 (1982).

[21] S. F. A. Kettle, E. Lugwisha, P. Vorderwisch and J. Eckert, *Spectrochim. Acta* **46A**, 921 (1990).
[22] M. Diem, *J. Am. Chem. Soc.* **110**, 6967 (1988).
[23] T. B. Freedman, A. C. Chernovitz, W. M. Zuk, M. G. Paterlini and L. A. Nafie, *J. Am. Chem. Soc.* **1** 6970 (1988).
[24] R. Hohmann, Doctoral Thesis, University of Toledo (1982).
[25] L. D. Barron, D. J. Cutler and J. F. Torrance, *J. Raman Spectrosc.* **18**, 281 (1987).
[26] W. Hug, in *Raman Spectroscopy*, p. 3 (edited by J. Lascombe and P. V. Huong). Wiley-Heyd Chichester (1982).
[27] L. D. Barron and A. D. Buckingham, *Molec. Phys.* **20**, 1111 (1971).
[28] L. D. Barron, *Molecular Light Scattering and Optical Activity*. Cambridge University Press, Cambri (1982).
[29] L. D. Barron, L. Hecht, A. R. Gargaro and W. Hug, *J. Raman Spectrosc.* **21**, 375 (1990).
[30] L. Hecht and L. A. Nafie, *Molec. Phys.* **72**, 441 (1991).
[31] R. D. Amos, *Chem. Phys. Lett.* **87**, 23 (1982).
[32] R. D. Amos and J. E. Rice, *CADPAC; The Cambridge Analytical Derivatives Package*. Issue 4 Cambridge (1987).
[33] J. S. Alper, H. Dothe and M. A. Lowe, *Chem. Phys. Lett.* **163**, 571 (1989).
[34] P. L. Polavarapu, *Chem. Phys. Lett.* **163**, 576 (1989).
[35] M. S. Lehman, T. F. Koetzle and W. C. Hamilton, *J. Am. Chem. Soc.* **94**, 2657 (1982).
[36] R. Bursi, F. J. Devlin and P. J. Stephens, *J. Am. Chem. Soc.* **112**, 9430 (1990).
[37] L. D. Barron, *J. Chem. Soc., Perkin II* 1790 (1977).
[38] W. Hug, A. Kamatari, K. Srinivasan, H.-J. Hansen and H.-R. Sliwka, *Chem. Phys. Lett.* **76**, 469 (198(
[39] L. D. Barron, L. Hecht and P. L. Polavarapu, *Chem. Phys. Lett.* **154**, 251 (1989).
[40] W. M. Zuk, T. B. Freedman and L. A. Nafie, *J. Phys. Chem.* **93**, 1171 (1989).
[41] H. J. Himmler and H. H. Eysel, *Spectrochim. Acta* **45A**, 1077 (1989).

JOURNAL OF RAMAN SPECTROSCOPY, VOL. 21, 375–379 (1990)

Vibrational Raman Optical Activity in Forward Scattering: *trans*-Pinane and β-Pinene

L. D. Barron,* L. Hecht and A. R. Gargaro
Chemistry Department, The University, Glasgow G12 8QQ, UK

W. Hug
Institut de Chimie Physique, Université de Fribourg, CH-1700 Fribourg, Switzerland

The first measurements of vibrational Raman optical activity (ROA) have been performed employing a forward scattering geometry. Forward-scattered ROA spectra of (+)-*trans*-pinane and (−)-*β*-pinene are presented as first examples. Comparison with the corresponding backward- and right-angle-scattered spectra confirmed that the bond polarizability theory of ROA is a good approximation for *trans*-pinane, and has identified unequivocally a large isotropic contribution to the ROA in *β*-pinene bands at 716 and 765 cm^{-1} ascribed to interactions between the olefinic methylene twist and a skeletal mode of the pinane structure. Unless large isotropic contributions are present, which is unusual, forward scattering is by far the least favourable of the ROA measurement strategies, which might explain the failure of recent attempts to observe ROA in coherent anti-Stokes Raman scattering.

ODUCTION

or breakthrough in Raman optical activity (ROA) nentation has been achieved recently by replacing ndard right-angle (90°) scattering geometry with scattering (180°) arrangement[1] which, in conjunc- ith a cooled charge-coupled device (CCD) detec- hould render the ROA method more widely able to stereochemical studies of chiral mol- .[1,2] Forward (0°) scattering ROA measurements e performed just as easily using the same optical onents (in a modified configuration), and this reports the first results.

ough ROA spectra measured in forward scat- are not expected to be as important for routine s as their backscattered counterparts, they do fundamental significance because they complete t of measurements necessary to extract the tensor ants responsible for observed ROA features, is necessary for an understanding of the mecha- responsible for the generation of ROA within l chiral molecules. This complete set of measure- comprises the ROA intensities in forward and ard scattering, together with the total ROA inten- olarized plus depolarized) in 90° scattering.[3–6] In he separate polarized and depolarized ROA inten- in 90° scattering, which can now be measured rou- [7] together with one or other of the forward or ard ROA intensities, provide similar information. ver, we shall see that the availability of the rd ROA intensity enables scattering mechanisms discussed with much greater confidence in certain nstances.

Another experimental strategy should be mentioned in this context. It has been shown that, by setting the transmission axis of the polaroid analyser in the 90° scattered beam at the 'magic angle' of $\pm\cos^{-1}(\sqrt{2}/\sqrt{3}) = \pm 35.26°$ to the vertical, the contribution from the electric dipole–electric quadrupole ROA mechanism vanishes so that pure electric dipole–magnetic dipole ROA spectra can be measured.[6,8] Magic angle ROA spectra are particularly favourable for comparisons with *ab initio* computed spectra[9] because the magnetic dipole and electric quadrupole contributions can sometimes reinforce and sometimes oppose each other, which can complicate the comparisons.

We present here the forward and backward ROA spectra of (+)-*trans*-pinane and (−)-*β*-pinene. Since polarized and depolarized 90° ROA spectra of both samples have been published previously,[10,11] and also the magic angle ROA spectrum of *β*-pinene,[8] we are now in a position to make some definitive pronouncements on ROA mechanisms in these molecules, especially with regard to the validity of the bond polarizability model and the importance of contributions from the isotropic part of the electric dipole–magnetic dipole scattering tensor products.

THEORY

We measure the ROA as the dimensionless circular intensity difference (CID):[12]

$$\Delta_\alpha = (I_\alpha^R - I_\alpha^L)/(I_\alpha^R + I_\alpha^L) \quad (1)$$

where I_α^R and I_α^L are the scattered intensities with linear α-polarization in right and left circularly polarized incident light. The CIDs, in terms of molecular property tensor invariants, for forward (0°), backward (180°) and polarized (x), depolarized (z) and magic angle

thor to whom correspondence should be addressed.

06/90/060375–05 $05.00

Received 1 December 1989
Accepted 21 February 1990

(*) right-angle (90°) scattering are[3,6,8,12]

$$\Delta(0^\circ) = \frac{8[45\alpha G' + \beta(G')^2 - \beta(A)^2]}{2c[45\alpha^2 + 7\beta(\alpha)^2]} \quad (2a)$$

$$\Delta(180^\circ) = \frac{48[\beta(G')^2 + \tfrac{1}{3}\beta(A)^2]}{2c[45\alpha^2 + 7\beta(\alpha)^2]} \quad (2b)$$

$$\Delta_x(90^\circ) = \frac{2[45\alpha G' + 7\beta(G')^2 + \beta(A)^2]}{c[45\alpha^2 + 7\beta(\alpha)^2]} \quad (2c)$$

$$\Delta_z(90^\circ) = \frac{12[\beta(G')^2 - \tfrac{1}{3}\beta(A)^2]}{6c\beta(\alpha)^2} \quad (2d)$$

$$\Delta_*(90^\circ) = \frac{(20/3)[9\alpha G' + 2\beta(G')^2]}{(10/3)c[9\alpha^2 + 2\beta(\alpha)^2]} \quad (2e)$$

where α and G' are the isotropic invariants of the polarizability tensor and the electric dipole–magnetic dipole optical activity tensor, and $\beta(\alpha)^2$, $\beta(G')^2$ and $\beta(A)^2$ represent the anisotropic invariants of the polarizability, electric dipole–magnetic dipole and electric dipole–electric quadrupole optical activity tensor products. [Common factors in the numerators and denominators of Eqns (2) have not been cancelled so that the relative sum and difference intensities can be directly compared.] Graphs for the dependence of these invariants on the scattering angle for various analyser orientations are presented in Ref. 6, where the virtues of different experimental strategies for the detection of ROA are discussed.

For the case of a molecule composed entirely of idealized axially symmetric bonds, the bond polarizability theory of ROA intensities[3] predicts the relations $\beta(G')^2 = \beta(A)^2$ together with $\alpha G' = 0$, in which case the CIDs in Eqns (2) reduce to

$$\Delta(0^\circ) = 0 \quad (3a)$$

$$\Delta(180^\circ) = \frac{64\beta(G')^2}{2c[45\alpha^2 + 7\beta(\alpha)^2]} \quad (3b)$$

$$\Delta_x(90^\circ) = \frac{16\beta(G')^2}{c[45\alpha^2 + 7\beta(\alpha)^2]} \quad (3c)$$

$$\Delta_z(90^\circ) = \frac{8\beta(G')^2}{6c\beta(\alpha)^2} \quad (3d)$$

$$\Delta_*(90^\circ) = \frac{(40/3)\beta(G')^2}{(10/3)c[9\alpha^2 + 2\beta(\alpha)^2]} \quad (3e)$$

Hence, within this approximation, the ROA intensity in backward scattering is four times that for polarized 90° scattering, which has recently been confirmed experimentally for *trans*-pinane.[1] This same sample also shows the predicted ratio of 2:1 for the polarized-to-depolarized ROA intensities in 90° scattering.[10] A crucial test is therefore to discover if *trans*-pinane shows zero ROA in forward scattering, which was one of the main purposes of this study.

In general, the bond polarizability theory results in Eqns (3) are expected to yield reasonable results for pure saturated hydrocarbons such as *trans*-pinane. However, they are not expected to hold for molecules that contain oxygen or sulphur heteroatoms because such molecules can show large deviations from the predicted ratio of 2:1 for the polarized-to-depolarized ROA intensities despite having axial symmetry in all the bonds.[13–15] Also, of course, they are not expect hold for molecules that contain non-axially symr bonds such as C=O or C=C,[10] a typical exa being β-pinene.[11]

EXPERIMENTAL

The ROA spectra were recorded using the Gla multi-channel instrument described in Ref. 7. Hov the intensified diode-array detector has now replaced with a cooled (unintensified) CCD det (Wright Instruments, Model AT1), which, as desc previously,[2] offers significant advantages for ROA owing to the increased quantum efficiency and th read-out noise, in addition to other factors.

The optical system employed for the backward- forward-scattered ROA measurements was simil that described by one of us some time ago,[16] but two minor modifications: the fibre-optic cross-se transformer was replaced with a simpler syste which the circular image of the backward- or forv scattered light was focused on the slit of the spe meter; and the Lyot calcite polarization scran (2 + 4 mm) was replaced with a thicker one (3 + 6 from Phillips Optical. Of course for the forw scattering measurements the assembly is turned ar through 180° so that the sample cell, Lyot polariz scrambler and collimating lens are now in front o diverting mirror.

The samples of (+)-*trans*-pinane and (−)-β-pi were purchased from Fluka and were studied as liquids distilled into quartz microfluorescence using a focused 600-mW argon-ion laser beam at 4 nm and a spectral resolution (full width at maximum intensity) of *ca.* 8 cm^{-1} with an acquisi time of 1 h.

Artefacts are generally greatly reduced in b scattered ROA measurements compared with 90° tering, and good reflection symmetry is seen in backscattered enantiomeric spectra of *trans*-pin shown in Ref. 1. We have found the same to be tru forward-scattered ROA measurements, and obtained good 'mirror-image' forward ROA spectra the two enantiomers of *trans*-pinane, although only of the (+)-enantiomer is shown here. Unfortunately, (+)-enantiomer of β-pinene is not available co mercially, so we were unable to obtain enantiom forward ROA spectra of β-pinene; however, from previous experience we are confident in the spectrum (−)-β-pinene shown here.

RESULTS AND DISCUSSION

trans-Pinane: the bond polarizability theory

Figure 1 shows the Raman circular intensity sum a difference spectra of (+)-*trans*-pinane in forward sc tering (top pair) and backward scattering (bottom p in the range *ca.* 630–1070 cm^{-1}. It is gratifying that results accord with the predictions of the bond polari bility theory as summarized in Eqns (2). This w expected in view of the previously observed behavio

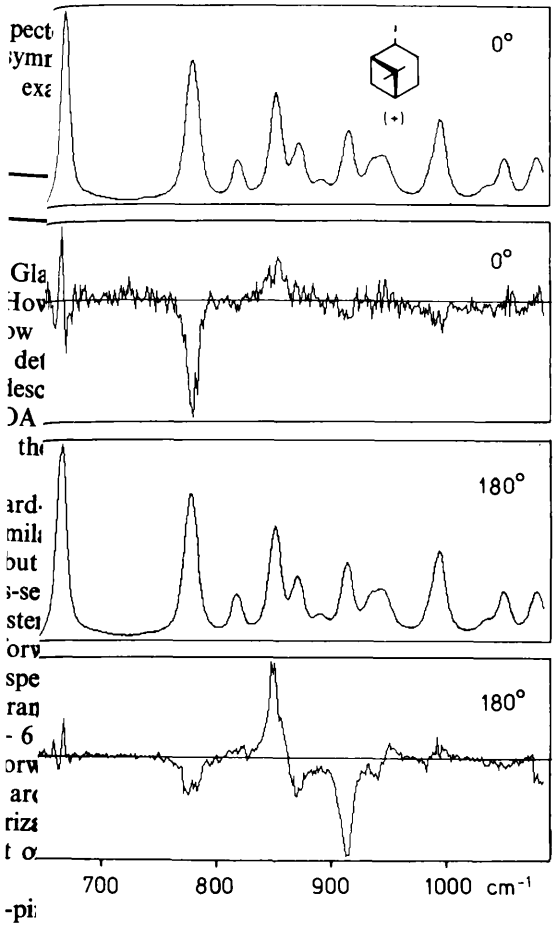

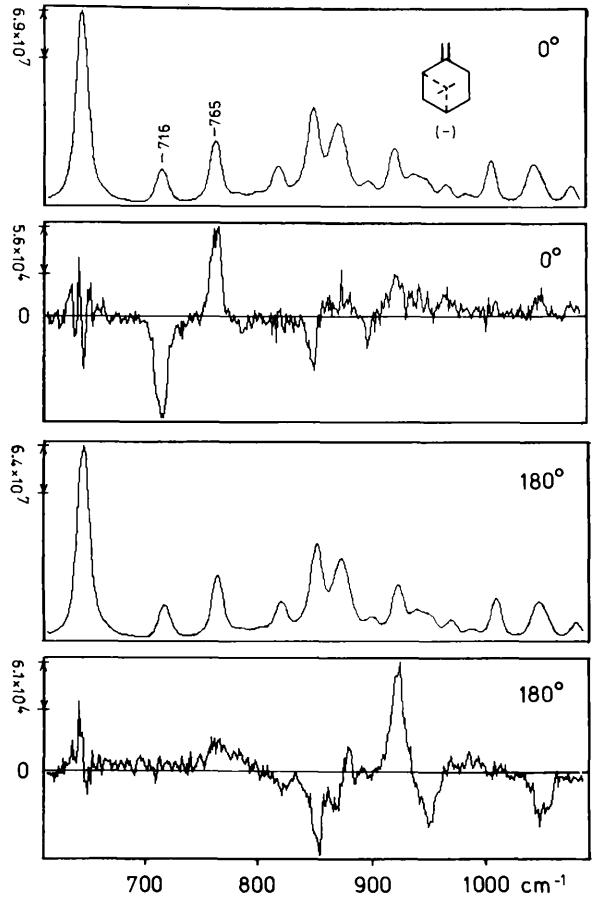

Figure 2. The forward-scattered (upper pair) and backward-scattered (lower pair) Raman circular intensity sum and difference spectra of neat (−)-β-pinene.

-pi
as 1. The forward-scattered (upper pair) and backward-
e d (lower pair) Raman circular intensity sum and difference
t 4 of neat (+)-*trans*-pinane. The intensity scale is arbitrary
t n counts).

ıisi

larized and depolarized 90° scattering.[10] First it
bd be noted that, as predicted by the denominators
° gs (2a) and (2b), the circular intensity sum spectra
in rtually identical in forward and backward scat-
pin However, as predicted by Eqn (3a) and the
trurator of Eqn (3b), the corresponding circular
ity difference spectra are dramatically different:
:trifrom the ROA band at 775 cm^{-1}, which is similar
ly th spectra with $\Delta(0°) \approx \Delta(180°) \approx -0.7 \times 10^{-3}$,
ly, a few small ROA features are seen in forward scat-
ct whereas in backward scattering the ROA is large
mmost identical in appearance with the ROA in 90°
n ring,[10] but much more intense,[1] again as predict-
unthe band at 775 cm^{-1} in the forward-scattered
spectrum is of particular interest because it prob-
originates in isotropic scattering associated with a
cteristic pinane-type skeletal mode and shows a
lation with the equivalent band in β-pinene (see
).

ene: isotropic scattering associated with the
ylene twist
sc

Pa Raman circular intensity sum and difference
t tra of (−)-β-pinene in the range *ca.* 630–1070 cm^{-1}
ris own in Fig. 2, with the forward- and backward-
ered spectra again at the top and bottom, respec-
vid. As expected, the forward and backward circular intensity sum spectra are virtually identical. The backward circular intensity difference spectrum is very similar to the corresponding depolarized 90° spectrum,[8,11] but the forward circular intensity difference spectrum is different from both. Most of the ROA features in the backward-scattered spectrum have either disappeared or become much reduced in the forward-scattered spectrum; however, a large ROA couplet with $\Delta(0°) \approx \pm 2 \times 10^{-3}$ appears in the bands at 716 and 765 cm^{-1} in forward scattering that is completely absent in backscattering. A similar couplet is seen in both the polarized[11] and magic angle[8] 90° ROA spectra, and its absence in the corresponding depolarized spectrum was explained by Barron and Escribano[11] in terms of a large electric quadrupole contribution associated with olefinic deformations, with $\beta(A)^2 \approx 3\beta(G')^2$ deduced from the numerator of Eqn (2d) and the assumption that the isotropic term $\alpha G'$ makes negligible contributions. The neglect of the isotropic term was justified at that time by the fact that it vanishes within the bond polarizability theory, and that there was no direct experimental evidence for significant isotropic contributions in other polarized ROA spectra. However, Barron and Escribano did emphasize that isotropic scattering could not be ruled out as the source of this ROA couplet and that measurements at other scattering angles are necessary to provide further experimental evidence to distinguish between the two possibilities. This was a wise proviso because, from

Eqns (2), the ROA measurements in forward and backward scattering presented here can only be reconciled with the earlier 90° measurements if this couplet originates in almost pure isotropic scattering. This conclusion is reinforced by the CID Δ values, which are predicted by Eqns (2a) and (2c) to have twice the value in forward scattering that they have in 90° polarized scattering if the mechanism is pure isotropic, which is what is found (within experimental error) if the $\Delta(0°)$ values given above are compared with $\Delta_x(90°) \approx \pm 1 \times 10^{-3}$ estimated from Fig. 1 in Ref. 11.

It is easy to understand qualitatively how the isotropic ROA couplet might be generated in the 716 and 765 cm^{-1} bands. Hecht and Barron[8] suggested that the olefinic methylene twist makes a significant contribution to the Raman band at 716 cm^{-1}, and since the Raman band at 765 cm^{-1} is one of a set of well characterized pinane-type skeletal modes, they ascribed the origin of this interesting ROA couplet to interactions between this twist and the skeletal mode. The methylene twist transforms as A_u in the D_{2h} point group of ethene itself, and as A_2 in a structure of C_{2v} symmetry, both of which irreducible representations are spanned by the tensor components G'_{xx}, G'_{yy} and G'_{zz}. Hence a fundamental Raman scattering transition associated with the methylene twist is allowed through G', the isotropic part of the axial electric dipole–magnetic dipole optical activity tensor, even in the parent structure of highest symmetry (D_{2h}) and so might be expected to show significant isotropic ROA if the effective symmetry of the olefinic group is reduced to that of a chiral point group as in β-pinene in which α, the isotropic part of the polar polarizability tensor, can also contribute to Raman scattering in the methylene twist. This condition (a Raman transition allowed through G' in a high-symmetry parent structure but only allowed through α owing to chiral perturbations) is a particularly favourable experimental situation because large ROA could be generated in association with a weak Raman band; this is analogous to the favourable situation in conventional electronic circular dichroism studies where a magnetic dipole-allowed transition is present in a high-symmetry chromophore and the parallel electric dipole transition is induced by the chiral environment so that the circular dichroism is associated with a weak absorption band, the classic example being the $\pi^* \leftarrow n$ transition in the carbonyl chromophore.[3,17]

The Raman band in *trans*-pinane at 775 cm^{-1} has similar origins to that in β-pinene at 765 cm^{-1}, namely the pinane-type skeletal mode mentioned above. Hence it is gratifying that the associated isotropic forward ROA in this mode in (+)-*trans*-pinane has the opposite sign to that in (−)-β-pinene, since the pinane-type skeletons have opposite absolute configurations in the two molecules.

CONCLUSIONS

The results for *trans*-pinane reinforce the earlier su tion that the bond polarizability theory of ROA reasonable approximation for pure saturated hydr bons. The small effects observed in its forward spectrum probably originate in isotropic scattering.

The existence of large isotropic ROA contributio β-pinene seems unequivocal. It also seems reaso that they are associated with the methylene twis which case we would expect to find significant isot ROA in twist and torsion modes of other molecu the mode transforms the same as the isotropic op activity tensor invariant G' in a parent structur higher symmetry.

This study is also of interest in connection with gestions that coherent Raman techniques migh favourable for ROA measurements.[18–21] The reported attempt at observation is that of Schneid *al.*,[22] who failed to detect any ROA in a polariza coherent anti-Stokes Raman (CARS) experiment or 1002 cm^{-1} phenyl breathing mode of (+)- and (- phenylethylamine. The CARS experiment essent measures ROA in forward scattering, but we demonstrated that, unless there is a large isotropic tribution, which is unusual, forward scattering is u vourable for incoherent ROA measurements so would expect CARS ROA measurements to be simil unfavourable. Indeed, it has been shown theoretic that coherent ROA vanishes within the bond polar bility (two-group) model.[18] We therefore suggest future attempts to observe CARS ROA should con trate initially on the 716 and 765 cm^{-1} bands ir pinene, which are highly favourable on account of large isotropic contribution.

Acknowledgements

We thank the Science and Engineering Research Council fc Research Studentship for A.R.G. and for a Research Grant, Wolfson Foundation for a Research Grant, the Deutsche Forschu gemeinschaft for a Postdoctoral Scholarship (III02-He 1588/1-1) L.H. and Prof. P. L. Polavarapu for helpful comments on the ma script.

Note added in proof

After this article went to press, we were reminded of some highly r vant earlier work. Specifically, B. A. Garetz pointed out in *Op Commun.* **49**, 65 (1984) that the large ROA observed by M. Klein M. Maier in forward *stimulated* Raman scattering in α-quartz, rep ed in *Optics Commun.* **44**, 411 (1983), could be due to isotropic scattering. See also M. Klein, M. Maier and W. Prettl, *Phys. Rev.* **28**, 6008 (1983).

REFERENCES

1. L. Hecht, L. D. Barron and W. Hug, *Chem. Phys. Lett.* **158**, 341 (1989).
2. L. D. Barron, L. Hecht, W. Hug and M. J. MacIntosh, *J. Am. Chem. Soc.* **111**, 8731 (1989).
3. L. D. Barron, *Molecular Light Scattering and Optical Activit* Cambridge University Press, Cambridge (1982).
4. D. L. Andrews, *J. Chem. Phys.* **72**, 4141 (1980).
5. J. R. Escribano, *Chem. Phys. Lett.* **121**, 191 (1985).

—ɕht and L. D. Barron, *Appl. Spectrosc.* in press.
—) Barron, D. J. Cutler and J. F. Torrance, *J. Raman Spec-*
:18, 281 (1987).
ɕht and L. D. Barron, *Spectrochim. Acta, Part A* **45**, 671
su89).
)A(Bose, P. L. Polavarapu, L. D. Barron and L. Hecht, *J.*
ydr *Chem.* **94**, 1734 (1990).
d) Barron, J. R. Escribano and J. F. Torrance, *Mol. Phys.*
653 (1986).
ng.) Barron and J. R. Escribano, *Chem. Phys. Lett.* **126**, 461
ıtio86).
ısor). Barron and A. D. Buckingham, *Mol. Phys.* **20**, 1111
twis71).
). Barron and P. L. Polavarapu, *Mol. Phys.* **65**, 659 (1988).
sot). Barron, L. Hecht and S. M. Blyth, *Spectrochim. Acta,*
ecu *A* **45**, 375 (1989).
op). Barron, L. Hecht and P. L. Polavarapu, *Chem. Phys. Lett.*
ctur 251 (1989).
16. W. Hug, in *Raman Spectroscopy*, edited by J. Lascombe and P. V. Huong, p. 3. Wiley–Heyden, Chichester (1982).
17. S. F. Mason, *Molecular Optical Activity and the Chiral Discriminations*, Cambridge University Press, Cambridge (1982).
18. J. O. Bjarnason, H. C. Anderson and B. S. Hudson, *J. Chem. Phys.* **72**, 4132 (1980).
19. J. L. Oudar, C. Minot and B. A. Garetz, *J. Chem. Phys.* **76**, 2227 (1982).
20. S. A. Akhmanov, V. F. Kamalov and N. I. Koroteev, in *Laser Scattering Spectroscopy of Biological Objects*, edited by J. Štěpánek, P. Anzenbacher and B. Sedláček, p. 67. Elsevier, Amsterdam (1987).
21. R. Brakel and F. W. Schneider, in *Advances in Non-Linear Spectroscopy*, edited by R. J. H. Clark and R. E. Hester, p. 149. Wiley, Chichester (1988).
22. F. W. Schneider, R. Brakel and H. Spiegel, *Ber. Bunsenges. Phys. Chem.* **93**, 304 (1989).

ıith
ıigh
ıe
ıeid
ıriza
t or
1 (–
sent
ve l
pic
is u
so
ɜimil
retic
ɔolaı
est
con
ls ir
ıt of

ıcil fc
rant,
ɔrschu
38/1-1)
the m

ighly r
in *Op*
Klein
tz, repi
tropic
ɔs. *Rev.*

Activi

OYAL SOCIETY
OF
HEMISTRY

Chemical Communications

Reprinted From

J. Chem. Soc., Chemical Communications.

Issue 15 1990

brational Raman Optical Activity of Peptides and Proteins

urence D. Barron,* Angelo R. Gargaro, and Zai Q. Wen
emistry Department, The University, Glasgow G12 8QQ, UK

Vibrational Raman Optical Activity of Peptides and Proteins

Laurence D. Barron,* Angelo R. Gargaro, and Zai Q. Wen

Chemistry Department, The University, Glasgow G12 8QQ, UK

Vibrational Raman optical activity spectra in the range 1100—1500 cm^{-1} of aqueous solutions of L-alanyl-L-alanine, D-alanyl-D-alanine, lysozyme, and α-chymotrypsin show features originating in coupled C_α–H and N–H deformations of the peptide backbone and appear to be sensitive to the details of the secondary conformation.

Vibrational Raman optical activity (ROA) measurements on chiral molecules can provide a wealth of stereochemical information because a vibrational spectrum contains bands associated with every part of the molecular framework.[1—3] ROA is expected to be particularly valuable in studies of biologically significant molecules. However, owing to its greater sensitivity, the complementary technique of vibrational circular dichroism (VCD) has so far set the pace in this area.[4] However, a recent dramatic advance in ROA instrumentation based on the use of a backscattering geometry[5,6] (in place of the usual 90° scattering arrangement) together with a cooled charge coupled device (CCD) detector[7] has now provided sufficient sensitivity to render biologically significant molecules in aqueous solution accessible to ROA studies. This communication reports the first ROA spectra of peptides and proteins.

The peptide and protein samples were studied as near saturated solutions in water contained in quartz microfluorescence cells, and ROA measurements were made using a focused 500 mW argon-ion laser beam at 488.0 nm and spectral resolution (FWHH) of ~8 cm^{-1}.

Figure 1 shows the backscattered Raman and ROA spectra of L-alanyl-L-alanine and D-alanyl-D-alanine solutions acquired in 4 h. It can be seen that there is excellent reflection symmetry between the enantiomeric spectra. Interpretation of these spectra is aided considerably by the assignment work of Diem *et al.* using conventional Raman measurements[8,9] together with VCD,[10] and by our recent experimental and *ab initio* theoretical ROA work on alanine.[11] This report concentrates on a few ROA features that appear to be characteristic of the peptide conformation. The large couplet in the Raman bands at 1340 and 1372 cm^{-1} is also shown by

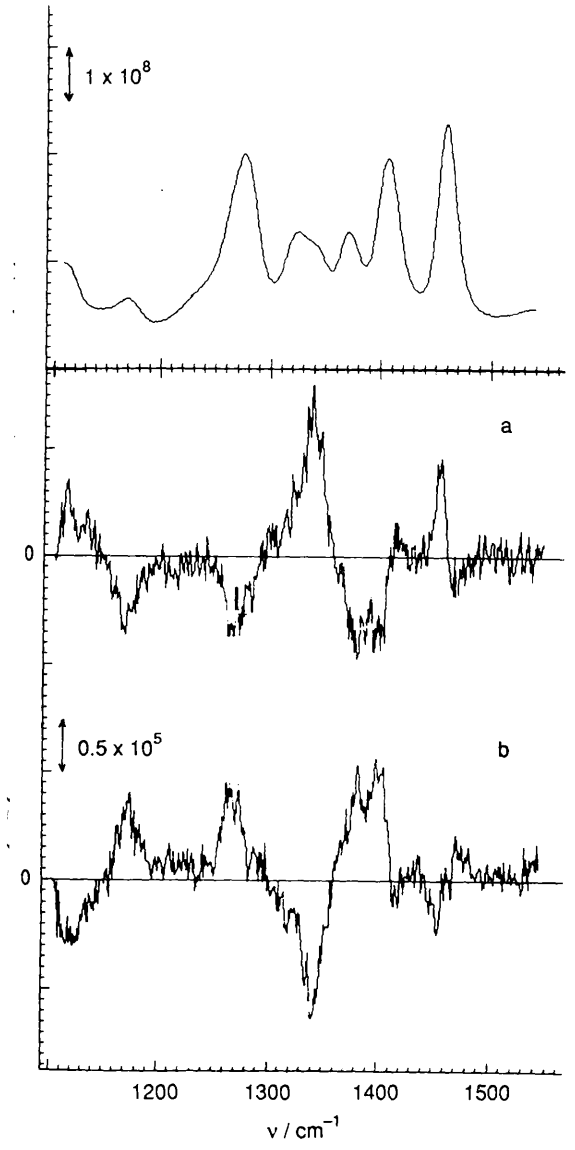

re 1. The backscattered Raman ($I^R + I^L$) and ROA ($I^R - I^L$) tra of (a) L-alanyl-L-alanine and (b) D-alanyl-D-alanine in water. intensity scales (in electron counts) are arbitrary.

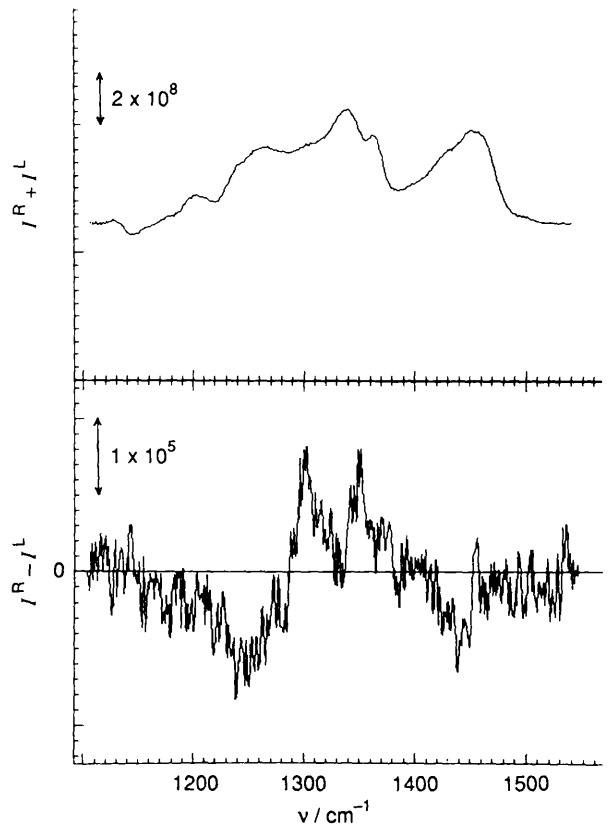

Figure 2. The backscattered Raman and ROA spectra of lysozyme in water.

ıine,
ıtions

——ine,[11] where it is known that the lower and higher ; nearquency component bands originate in a methine C_α–H ofluorrmation and the symmetric methyl deformation, respectısing ly. However, interaction with the symmetric methyl de- and mation is probably not the main source of ROA intensity in 1340 cm^{-1} C_α–H band because a positive feature of similar spectrnsity appears at the same frequency in the ROA spectrum lutionhe L-L-L-alanyl tripeptide ROA spectrum (not shown) with lectionuch reduced negative feature in the methyl symmetric ıtion ormation; also a large positive feature is seen at slightly vork or frequency in the ROA spectrum of L-polyglutamic acid ıents[8,9] shown) which contains no methyl groups. The next band, :al and325 cm^{-1}, which shows ROA of the same sign as that at report0 cm^{-1} (but weaker) is probably related to one in alanine at to bently lower frequency with similar ROA and which is known :ouplerigınate in another C_α–H deformation.[11] The band at)wn by79 cm^{-1} showing ROA of opposite sign to that in the 1325 1340 cm^{-1} bands is conventionally assigned to the 'amide III' vibration, which is supposed to consist mainly of the N–H deformation.[12] However, Diem *et al.*[8—10] have shown that in fact this band, together with those at 1325 and 1340 cm^{-1}, involves much more mixing between the C_α–H and the N–H deformations than previously supposed, which explains the well known geometric sensitivity of the amide III band.

Figures 2 and 3 show the backscattered Raman and ROA spectra of lysozyme and α-chymotrypsin solutions, the first being run for 16 h and the second for 13 h. The dominant feature common to both ROA spectra is a broad couplet, negative on the lower frequency side and positive at higher frequency, centred at ~ 1275 cm^{-1}, which is within the conventional amide III region. However, a major difference between the two protein ROA spectra appears to the high frequency side of this broad couplet, where α-chymotrypsin shows a second couplet centred at ~1320 cm^{-1} that is positive at lower frequency and negative at higher frequency. The lysozyme ROA drops to zero rapidly towards 1320 cm^{-1} and then becomes positive again suggesting a similar couplet to that in α-chymotrypsin but with opposite sign. Extrapolating from the peptide results discussed above, we tentatively propose that these major protein ROA features originate in coupled C_α–H and N–H deformations from the peptide backbone and so represent a superposition of ROA bands from the various types of secondary backbone conformations, being particularly sensitive to the range of angles φ around the different C_α–N bonds present in the particular protein. It is intriguing that the region from ~1300 to 1380 cm^{-1} where the ROA spectra of the two proteins differ significantly is the region where 'amide III' modes characteristic of reverse turns in polypeptide chains are expected to be observed.[13]

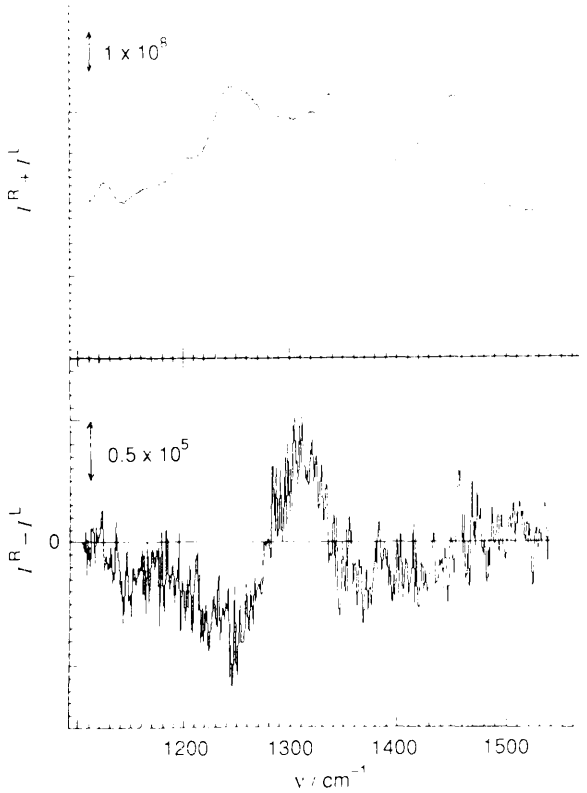

Figure 3. The backscattered Raman and ROA spectra of α-chymotrypsin in water

The importance of the preliminary results presented here is that they demonstrate that it is now possible to obtain ROA spectra of biological molecules in aqueous media and that the spectra appear to be sensitive to important conformational features. For the same reasons that have led conventional Raman spectroscopy to find many applications in biochemistry (water is a good solvent for Raman studies, complete vibrational spectrum is accessible, resonan enhancement enable sites of biological function to be prob directly, *etc.*[14]), ROA is now expected to become a power new method in biochemical spectroscopy.

We thank the SERC and the Wolfson Foundation Research Grants, the SERC for a Research Studentship (A. R. G.), Drs. A. Cooper and G. E. Tranter for discussi and the Wellcome Research Laboratories for supply samples.

Received, 17th April 1990; Com. 0001666G

References

1 L. D. Barron, 'Molecular Light Scattering and Optical Activi Cambridge University Press, Cambridge, 1982.
2 L. D. Barron, in 'Vibrational Spectra and Structure,' eds. H. Bist, J. R. Durig, and J. F. Sullivan, Elsevier, Amsterdam, 19 vol. 17B, p. 345.
3 L. A. Nafie and C. G. Zimba, 'Biological Applications of Ran Spectroscopy,' ed. T. G. Spiro, Wiley, New York, 1987, vol p. 307.
4 P. Pancoska, S. C. Yasui, and T. A. Keiderling, *Biochemis* 1989, **28**, 5917.
5 L. Hecht, L. D. Barron, and W. Hug, *Chem. Phys. Lett.*, 19 **158**, 341.
6 W. Hug, in 'Raman Spectroscopy,' eds. J. Lascombe and P. Huong, Wiley-Heyden, Chichester, 1982, p. 3.
7 L. D. Barron, L. Hecht, W. Hug, and M. J. MacIntosh, *J. A Chem. Soc.*, 1989, **1111**, 8731.
8 M. R. Oboodi, C. Alva, and M. Diem, *J. Phys. Chem.*, 1984, 501.
9 M. Diem, M. R. Oboodi, and C. Alva, *Biopolymers*, 1984, 1917.
10 G. M. Roberts, O. Lee, J. Calienni, and M. Diem, *J. Am. Ch Soc.*, 1988, **110**, 1749.
11 L. D. Barron, A. R. Gargaro, L. Hecht, and P. L. Polavarapu be published.
12 T. Miyazawa, T. Shimanouchi, and S. I. Mizushima, *J. Ch Phys.*, 1958, **29**, 611.
13 S. Krimm, in 'Biological Applications of Raman Spectrosco ed. T. G. Spiro, Wiley, New York, 1987, vol. 1, p. 1.
14 T. G. Spiro, *Chem. B.*, 1989, **25** (6), 602.